THESIS

RADIATION DOSES AROUND THE FUKUSHIMA DAI-ICHI NUCLEAR POWER PLANT: MEASUREMENTS AND NOVEL METHODS OF ANALYSIS

Submitted by

Peter James Seel

Department of Environmental and Radiological Health Sciences

In partial fulfillment of the requirements

For the Degree of Master of Science

Colorado State University

Fort Collins, Colorado

Fall 2018

Master's Committee:

Advisor: Ralf Sudowe

Alexander Brandl
Charles W. Miller

ABSTRACT

RADIATION DOSES AROUND THE FUKUSHIMA DAI-ICHI NUCLEAR POWER PLANT: MEASUREMENTS AND NOVEL METHODS OF ANALYSIS

The nuclear accident which occurred at the Fukushima Dai-Ichi Nuclear Power Plant in March of 2011 released an estimated 940 petabecquerels (PBq) of I-131 equivalent radioactive emissions, of which over 32 PBq were the longer-lived isotopes Cesium-134 and Cesium-137 (Half-lives: 2.06 years, and 30.01 years). Accurate means and methods of tracking the dose rates resulting from the deposition of these two isotopes are critical to understanding when former residents can move back into the area and the remaining potential health risks.

Remote sensing stations, vehicle surveys, and airborne surveys were all analyzed and compared for their efficacy and utility in dose rate tracking. Remote stations were found to be useful for long-term temporal trends, but lack validity in generalizing beyond the immediate area of each site. Analysis of data provided by these stations showed a statistically significant drop in dose rate below that expected from radioactive decay alone. This implies that radioisotopes are moving out of the vicinity of stations, likely through environmental means. Vehicle surveys provide a middle ground of spatial resolution and frequency of data collection, and dose correction factor of 1.31 from car dose rate to ambient dose equivalent rate was modeled based on conducted vehicle surveys for field use by non-experts. Utilizing GIS analytical techniques, elevation and slope were found to be statistically influential factors in dose rate changes. Importantly, different types of environments were stratified and compared to show the relative loss of radiation within them, confirming that most forests retain radioisotopes more than the median level for the region, while urban area and bare land dose rates decrease more quickly. The GIS methods tested will be useful in analyzing further surveys results and could be used to plan future research and compare to other measurement types.

ACKNOWLEDGEMENTS

First, I would like to thank my thesis advisor, Dr. Ralf Sudowe, and my thesis committee members, Dr. Alexander Brandl and Dr. C.W. Miller, for staying alongside me as I completed this thesis. Their support has meant much in completing this thesis, and even more so for making it through the courses and rigors of this program. Dr. Sudowe accepted my peculiar proposal from an equally peculiar student and has supported my research decisions through the creation of this thesis. Drs. Brandl and Miller were some of my favorite professors during my tenure as a student at CSU and having their knowledge and assistance has been extremely valuable as a writer, scholar, and future professional. I would also like to thank all of the Geospatial Centroid, especially Sophia Linn, for their assistance, time, and expertise in GIS.

I would also like to offer my thanks to the Matsuo Laboratory at the University of Tokyo's School of Art and Sciences including Dr. Motoyuki Matsuo, Dr. Katsumi Shozugawa, and Dr. Mayumi Hori. Not only did I receive the utmost hospitality from them while searching for housing and during my stay, but I found a lab group which helped challenge me in my research pursuits and grow professionally. I was given extra time to honeymoon with my wife, two excursions to Fukushima during a busy summer term, and a significant portion of time with extremely hard-working individuals. I cannot overstate how meaningful and fulfilling of an opportunity it was to study in Tokyo, researching a critical concern of the Japanese people, who all offered me nothing short of complete care and respect. Thank you as well to Dr. Thomas Johnson for offering me the opportunity in the first place, one I never would have considered without his blunt presentation of the possibilities facilitated my decision.

Most importantly, I would like to thank my wife Savanna for sticking by my side through all the trials and tribulations of life. Even as I struggled with the perfidious precipice of procrastination, she offered me the love and support I have needed and used through this graduate program and the creation of this thesis. I will be by your side, as you are by mine. Thank you.

TABLE OF CONTENTS

1 Introduction

"Radiation" exists for the lay member of society as one of the most threatening and poorly understood topics in science. Insufficient information about what the benefits and hazards of ionizing radiation, as well as what is entailed in its use, seem to be the likely cause of this. A 2016 survey by the Nuclear Energy Institute (NEI) illustrated that increasing individual knowledge about nuclear power, and radiation risks by association, eases anxiety about nuclear energy generation (NEI, 2016). Furthermore, this survey and additional studies in Japan show that proximity to nuclear power plants increases comfort. As such, providing methods and means to make ionizing radiation more understandable in terms of how people may be exposed, and how that exposure relates to the environment, is essential to obtain and maintain public trust. These principles hold for any use of radioactive materials or devices, but the purpose of this research is to provide a greater understanding of the best means of measuring radiation around the Fukushima Dai-Ichi Nuclear Power Plant (FDNPP), as well as of the environment factors which influence the change in dose rates. A significant goal of research into the environmental characteristics around Fukushima is providing accurate models, which would describe when former residents of the exclusion zone would be able to return to the region.

On March 11, 2011, a magnitude 9.1 earthquake struck 70 km off the Northeast region (*Tōhoku*) of Japan. The earthquake occurred at 14:46 local time, and the ground rose by approximately 6 m along a large section of the fault, creating a major tsunami. Within a half hour, surge waters devastated local communities with initial impact heights up to approximately 7 meters and run-up heights reaching 40.1 meters. 24,596 people were killed, injured, or went missing based on National Police Agency of Japan statistics from December 8th, 2017. Hundreds of thousands of buildings were completely or partially destroyed by the flood waters. Compounding these tragic damages and their human toll was the accident which befell the FDNPP. (NPA, 2018)

The boiling water reactors (BWR's) operated at the FDNPP utilized the Mark I containment design, one of the earliest reactor designs, which was developed by General Electric. Mark I reactors are contained within a drywall of concrete that resembles an inverted light bulb, with the reactor in the center and piping leading to the donut shaped "wet well" suppression chamber below (Fig. 1.1).

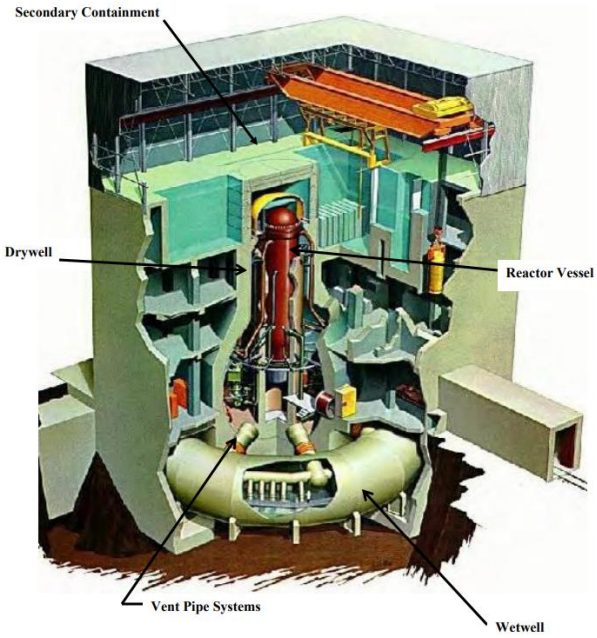

Figure 1.1: Cross Section of a Mark I Reactor (NRC, 2011)

The FDNPP housed five out of the eight Mark I reactors still in use in Japan, among only 37 in use across the globe (GE, 2011). Despite having a robust safety system, the effects of the earthquake combined with the tsunami incapacitated too many systems. Most important was the damage that occurred to the backup diesel generators providing the energy to the cooling systems supplying the reactor. BWR's are light water reactors which operate in manner similar to how electricity is generated in other types of electrical plants. A heat source evaporates water to run a steam turbine-generator. Steam is then condensed back into liquid water through heat exchange and the water is returned towards the reactor to continue the process. Nuclear power is unique in that the fuel continues to release energy even if the plant is shut off. Nuclear fission provides the large amount of energy necessary to boil enough water for power generation, and this occurs orders of magnitude lower when the reactor is not fully running. The radioactive decay,

e.g. alpha and beta decay, of the used fuel still generate a significant amount of heat given the density of nuclear fuel. In terms of plant safety, the cooling process is the most essential, as it mitigates the innate heat build-up inside the reactor. With the earthquake and tsunami damaging the existing power infrastructure, and without back-up generators, there was only battery power left to supply the cooling pumps. Unit 1's battery had insufficient charge within 4 hours after the earthquake, and both Unit 2 and 3 were down by March 14th.

Without circulation, the water within the system quickly turned to steam, and as a result the pressure within the containment began to rise (Braun, 2011). Simultaneously, the fuel rods in the reactor were exposed due to the decrease in water level, and the zirconium used in the cladding alloy for the rods interacted with the steam, creating hydrogen gas:

$$Zr + 2H_2O \rightarrow ZrO_2 + 2H_2 + Energy$$

This process is exothermic and further increased the temperature in the reactor markedly, with each of the units reaching at least 3000℃ (Tanabe, 2012). Xenon (Boiling: -108℃), iodine (Boiling: 184℃), cesium (Boiling: 671℃), and tellurium (Boiling: 988°C) became or were airborne and moved throughout the drywell. While much of the heavier elements like uranium (Boiling: 4131℃) and plutonium (3228℃) did not boil, they did melt down when the cores were without any liquid water for at least several hours. Water was pumped into the reactor to mitigate the temperature, which prevented the release of more isotopes. However, with the steam, hydrogen releases, and heat expansion, the pressure within the reactor containment vessel reached upwards of 8 bar, while the operational limit is listed as 5 bar. This necessitated venting excess gas into the service floors of each unit. Venting released all the noble gas emissions from the core and some of the aerosolized cesium and iodine. Through some unknown mechanism, the hydrogen gas in units 1 and 3 both ignited, leading to explosions on the service floors. In unit 2, the hydrogen caught fire in the reactor containment itself. Units 2 and 3 are thought to account for 80% of total releases, with unit 1 comprising the other 20%. These explosions resulted in additional sudden releases of radioactive materials from the reactor units. Predominantly, the plant releases traveled

over the North Pacific Ocean, depositing 80% of the total atmospheric emissions here (Povinec, Hirose, & Aoyama, 2013). The other 20% of the disseminated radionuclides migrated northwest from the FDNPP, and that initial plume distribution remains visible with contemporary surveys (Fig. 1.2).

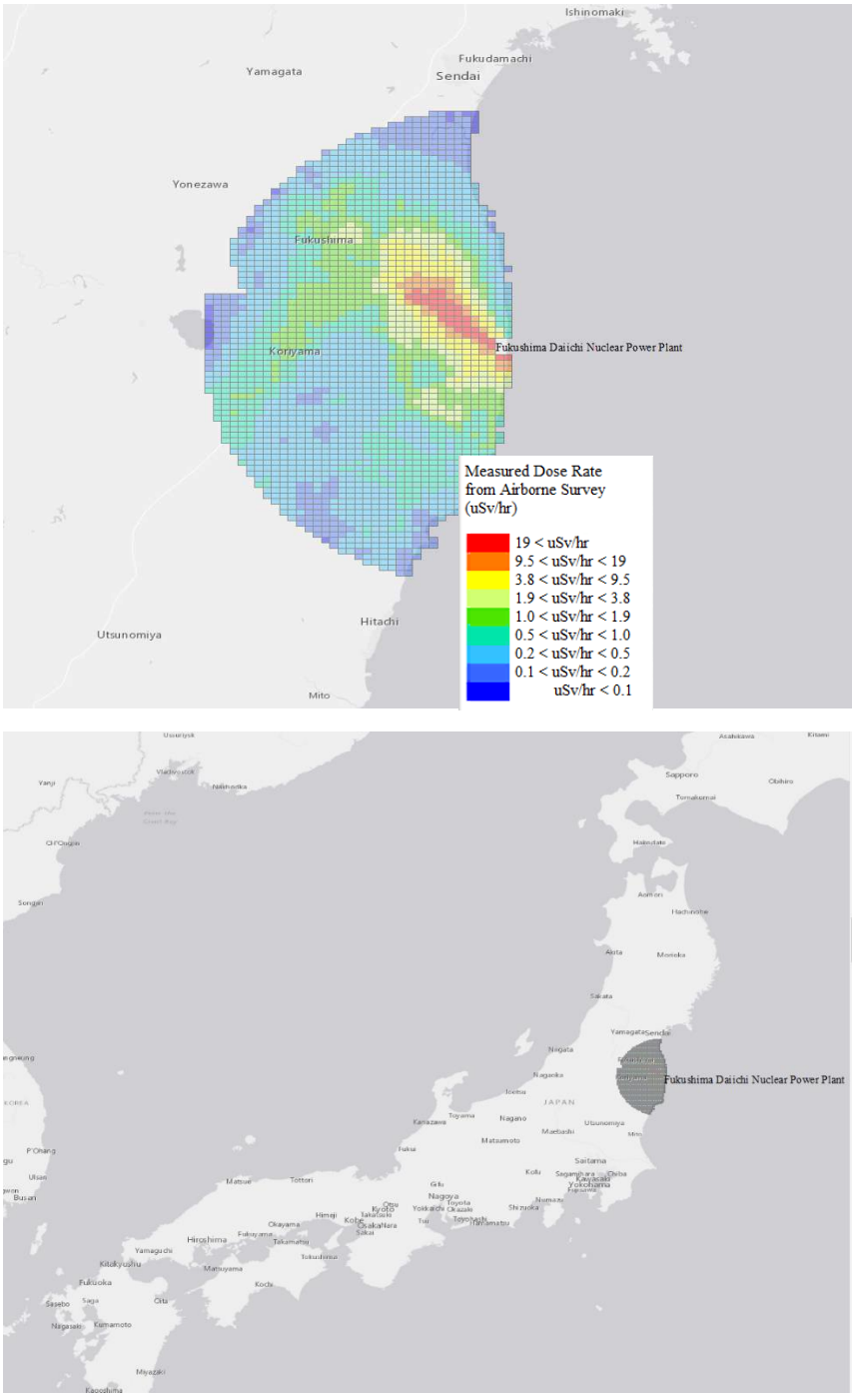

Figure 1.2: Plume Distribution around FDNPP and Location on the Island of Honshu.

In total, 2012 estimates from TEPCO, the company which manages the NPP, estimated 940 PBq ($940x10^{15}$ disintegrations per second) of I-131 equivalent released (this standardizes the relative activities of the different isotopes). A further 500 PBq of noble gases were released, but short half-lives and no biological activity makes them only a target for plume tracking, with little public health concern. Of the 940 PBq of I-131 equivalent, it is estimated that 17.5 PBq of Cs-134 and 15.3 PBq of Cs-137 were released atmospherically. Total releases in all mediums are estimated at 168 and 156 PBq for each isotope, respectively. Of the isotopes released in significant quantities, only the cesium isotopes remain, since Cs-134 has a 2.065 year half-life and Cs-137 has a 30.08 year half-life. Nearly all other dominant released isotopes, I-131 (8.0 day half-life), I-133 (20.8 hour half-life), Te-132 (3.2 day half-life), Te-129m (33.6 day half-life), and Xe-133 (5.25 day half-life) have decayed to levels below the minimum detectable activity. The only exceptions are Kr-85 (10.25 year half-life), a noble gas estimated at 44 PBq of release, and H-3 or tritium (12.1 year half-life) which is a continuing water contaminant. (Steinhauser, Brandl, & Johnson, 2014)

Many environmental and public health concerns have arisen since the accident occurred. Due to the tandem effects of the natural disasters and the radioactive releases, an estimated 154,000 residents were evacuated and initially unable to return to their homes. After several re-evaluations of risk and the spread of contamination, an exclusion zone was established and progressively expanded to 20 km around the FDNPP. This exclusion zone has been the focus of subsequent decontamination efforts. Only the nearby town of Futaba and the plant itself are fully restricted for access, but Okuma and Namie, to the south and northwest respectively, are still contaminated, resulting in dose rates up to 17 μSv/h. Due to radioactive decay, environmental movement, and decontamination efforts, certain residential areas are being opened (Fig. 1.3). Further, before the 2020 Tokyo Olympics, the government is attempting to reopen the train line which runs through the exclusion zone.

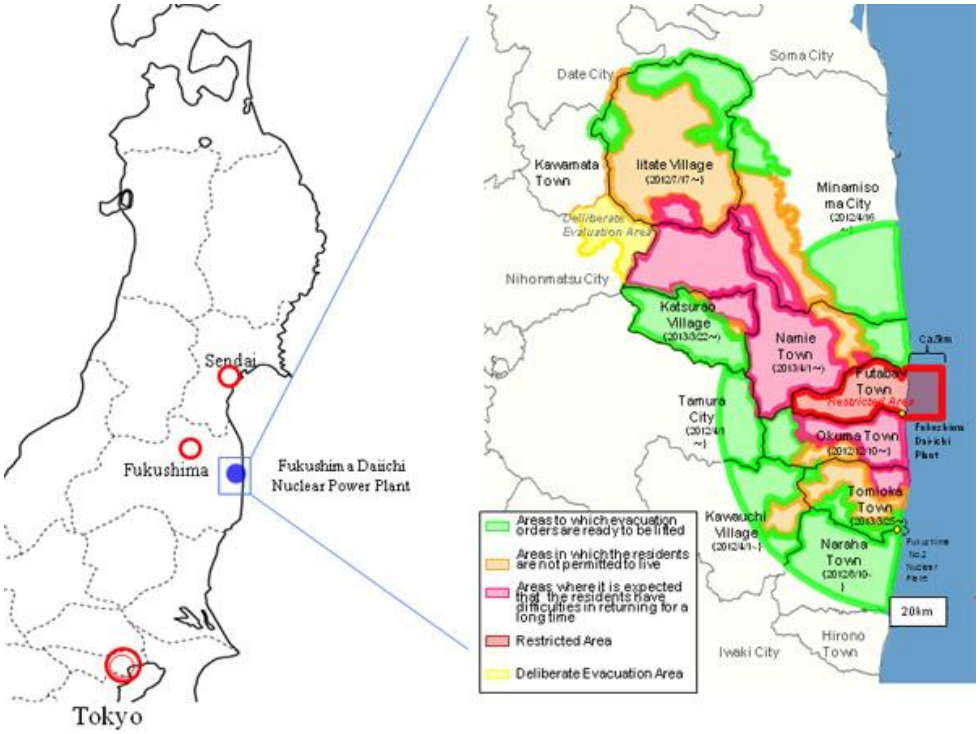

Figure 1.3: Evacuation Zones around the FDNPP (Reconstruction Agency, n.d.)

Initially, the primary radionuclides of concern were I-131 and I-133, since they were released in significant quantities and have a short half-life, thereby posing a greater risk of exposure around the time of evacuation. Potassium iodide tablets were considered for distribution, since iodine poses a risk for thyroid exposure, and stable iodine competes with radioactive iodine for biological incorporation. However, it is estimated that little public exposure occurred during the evacuation (Hasegawa et al., 2015). Unlike in Chernobyl, there were no casualties at the NPP from radiation induced injuries. Since the noble gases dissipated quickly, the only remaining contaminants of primary concern were Cs-134/137. These radionuclides have since then been the focus of decontamination efforts and research, due to the longer half-life and significant quantities involved. As a result of the widespread dispersion across the region, there are many avenues of terrestrial and aquatic movement of radioisotopes, all eventually leading to the ocean as in Fig. 1.4:

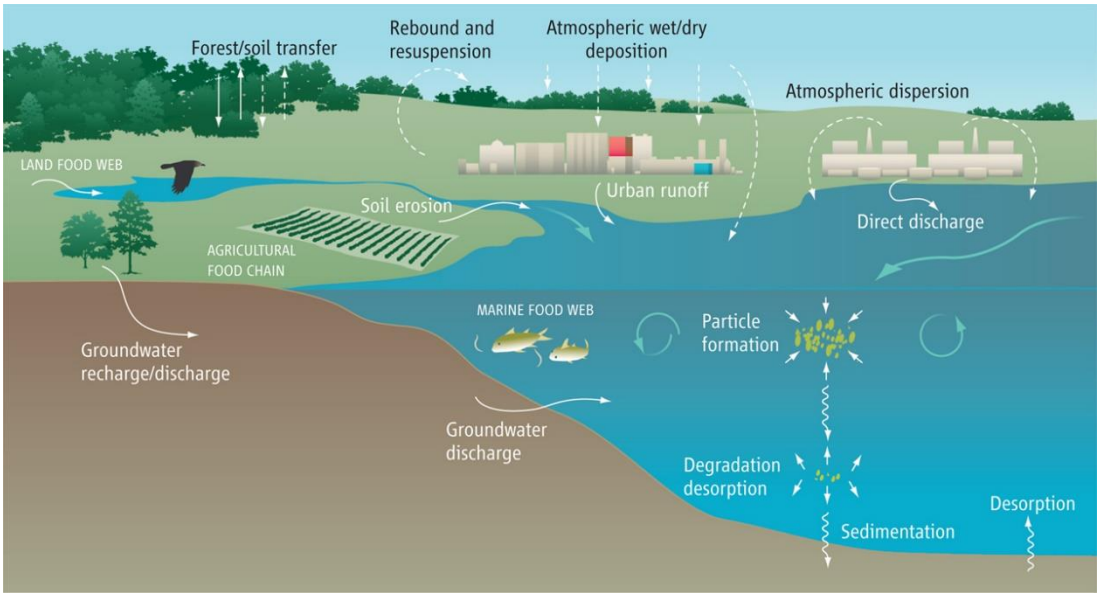

Figure 1.4: Environmental Mechanisms of Particle Movement (Yoshida & Kanda, 2012)

Cesium, being an alkali metal, is easily soluble and has the potential to compete with potassium in the ecosystem. It will be absorbed by plants as well as incorporated into tissue in animals, especially soft tissues such as muscle. This poses challenges for the prediction of environmental mobility, as its presence in organic vs. inorganic phases determines its solubility in water, retention in plants, and deposition in soil layers.

Considering that the Cs-137 will not naturally decay below operational detection limits for ten half-lives (~300 years), finding and confirming methods that will enable accurate surveying and modeling of cesium movement are essential. Not only do such efforts contribute to the literature of radioecology and radiochemistry, but they allow for pertinent and critically needed information to be conveyed in a timely manner to former residents. By developing a better understanding of the environmental movement and persistence of radiocesium around the Fukushima prefecture and beyond, scientists are helping to build the framework that will allow people to return to their former towns. As such, this research is focused on the evaluation of different means of environmental monitoring for radiocesium to predict dose rates and augment means of modeling, through remote sensing, car surveys, and airborne surveys.

2 Literature Review

The Fukushima province has been extensively studied since the accident occurred, with research delving into various means of tracking radiation dose rates across the affected region. Given this study's focus on methods of accurate dose evaluation, literature pertaining to the dominant means of measuring and tracking radiation was reviewed. Of particular interest are studies which utilize the same techniques implemented for this research, including vehicle-based surveys, remote sensing, and GIS mapping and analysis.

2.1 Vehicle Surveys

A predominant amount of the spatial radiation assessments around the FDNPP has been conducted through vehicle surveys. This is due to the relative ease with which vehicle measurements can be gathered and their utility for widely trafficked areas. Two of the largest contributors to these studies were the Japanese Atomic Energy Agency (JAEA) and researchers from Kyoto University. Vehicle based surveys are best conducted in areas where there is another dataset to reference against, allowing to correct the measurements for the inevitable variability of vehicular travel. They have been used to accurately determine the dose rate along roads and can show variability by environment type (Andoh et al., 2015). These studies utilized the Kyoto University Radiation Mapping (KURAMA) and KURAMA-II systems in conjunction with JAEA air survey results for cross-checking. These surveys were conducted in both areas with greater population (Fukushima, Sendai) as well as within the exclusion zone (Ishihara, 2014; Wainwright, Seki, Chen, & Saito, 2017; Wainwright, Seki, Mikami, & Saito, 2018).

Further, the characteristics of radiation interactions with detectors inside of vehicles have been quantitatively analyzed (Takahara, Watanabe, Hirouchi, Iijima, & Munakata, 2018). This is an important aspect of conducting vehicle borne measurements. Nearly every major vehicle-borne survey, including those presented in this research, had detectors placed inside of the vehicle. While comparisons with

measurements taken outside the vehicle to fit car data to ambient dose equivalent rates were done, greater accuracy in modeling is essential.

2.2 Soil Sampling

Another common assessment technique is based on the survey of collected soil. Soil studies have been used in both spatial and environmental composition studies. Acquisition of spatial data involved the extensive collection of samples from across the Tohoku and even Kanto regions, allowing for the development of maps comparable to those obtained from airborne surveys (Saito et al., 2015). Soil studies illustrate the same patterns as all other types of mapping and are able to provide even more information about environment characteristics like the composition of soil types, the methods of cesium deposition, and, with repeated sampling, changes in soil contamination over time. Cesium is known to have a heterogeneous distribution through the soil, as a result of the production of water-soluble radiocesium and a "hot" counterpart which sorbs irreversibly to soil and rock (Tanaka et al., 2013). This helps explain the mixed results that have been obtained regarding the importance of water erosivity on radiocesium movement. Quantifiable amounts of contaminated sediment have been measured across the region, but the amount of contamination measured reduced over time (Evrard et al., 2016). Much of this has been due to the impact of cyclones relative to typical precipitation, as they contribute about 40% of the yearly erosivity (Laceby et al., 2016). Since the amount of contaminated sediment measured is seen as decreasing over time, alluvial deposits of soil/sediment onto land are no longer a pressing concern. As such, determining the location of cesium within terrestrial soil environments, and quantifying the amount of soil deposition into the ocean take precedence. While cesium has been found throughout the soil column, the first five centimeters contain the majority of measurable cesium (Konoplev et al., 2016).

2.3 GIS Analyses

GIS mapping of data has been used in many studies in the region around the Fukushima NPP. Most vehicle studies include GIS data, visualized in Google Earth or Google Maps, to ensure that dose rates are

tracked along the route driven (Andoh et al., 2015). Soil surveys are often mapped to show regions where collections occurred and to show changes in environment type over space (Saito et al., 2015). Recent research has attempted to integrate a variety of survey sources into one analytical framework through the use of Bayesian statistics (Wainwright et al., 2017). The results show that statistical "stitching" of data is a feasible means to account for the varying spatial resolutions of different survey types. When put into practice, it was found that these techniques were appropriate for measuring dose rate changes across the Fukushima region, with some capacity to differentiate dose rate changes by environment type (Wainwright et al., 2018).

Little research was, however, found that utilized data from the remote sensing stations that the Japanese Nuclear Regulatory Agency has placed around the FDNPP. It was not the focus of studies found in the course of this literature review. For vehicle surveys, research did not often focus on the attenuation of measurements of vehicle data or how to correct for that impact. Some combined airborne dose rate surveys as comparisons, but often it is linked with a collection of vehicle surveys (Wainwright et al., 2018). In GIS data, there does not seem to be research showing integration with other environmental factors which may play a role. Literature either focuses on soil studies, which are mapped but not linked with other factors, or environmental characterization as an aspect of dose measurement, focused only on mean deviations (Saito et al., 2015; Wainwright et al., 2018). These gaps in the literature are the focus of the research conducted, aiming to include remote sensing data, vehicle-survey dose rate corrections, and integrate analysis of environmental factors and dose rate change through GIS analysis of airborne surveys.

3 Methods

The research conducted for this thesis was completed in three sections: Remote Sensing, Vehicle-Borne Surveys, and Airborne GIS analysis.

3.1 Remote Sensing

Remote sensing data were obtained from several sources. The primary source of data was the Japanese Nuclear Regulatory Agency (NRA), which provides information from remote monitoring stations across the Fukushima area. These stations are built by Fuji Electric and consist of silicon semi-conductor detectors, powered locally by solar panels and include a display for the ambient dose rate. An image for a detector can be found in Fig. 3.1:

Figure 3.1.1: Fuji Electric Remote Sensing Station. This station was outside of the Okuma town administrative office.

These stations record the location name, time, date, radiation dose rate (measured in μSv per hr), and GPS coordinates every ten minutes. All this information is available for download in CSV format from the NRA website (http://radioactivity.nsr.go.jp/map/ja/index.html), and the real-time CSV are linked on the right side of the page as seen in Fig. 3.1.2:

Figure 3.1.2: Real-Time Measurements Page with Download Link visible on the Right Side. This page is not available on the English language webpage.

All helpful information is only accessible through Japanese language web pages, and Google Chrome's built in translate function was utilized to navigate the websites. For ease of data management, structured temporal sampling was utilized, where a specific set of hours was sampled for analysis. In the Futaba and

Okuma data sets, data points between 8:00 and 17:00 were downloaded for each sampled day, as seen in Fig. 3.1.3:

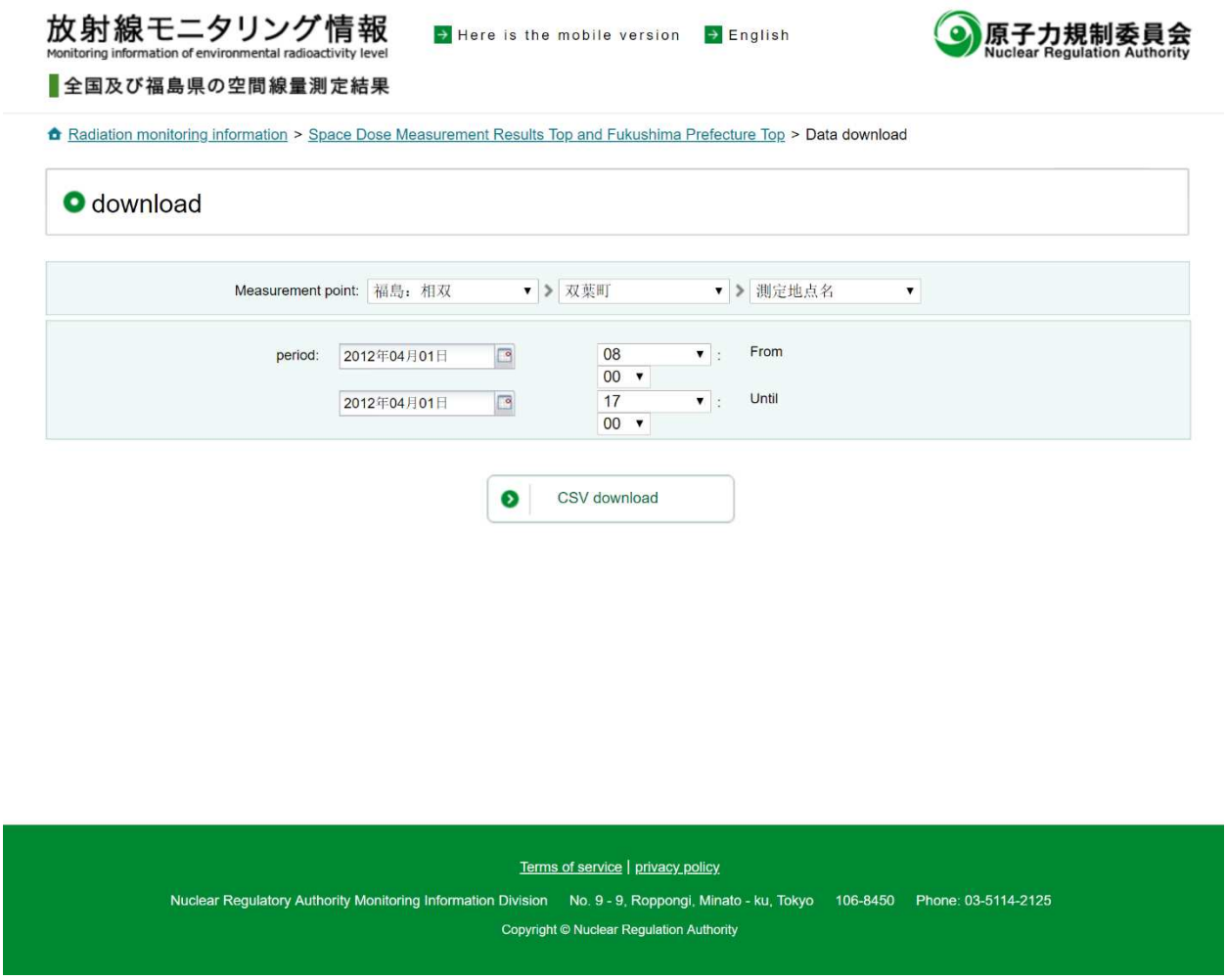

Figure 3.1.3: CSV Download for Futaba Town on April 1st, 2012 from 8:00 to 17:00. This was the time period used for both the Okuma and Futaba and this done for each day that was used in analysis.

This abridged time frame was originally selected to ease computation time and data management and was found to be statistically similar to the entire day's data.

Due to damage from the tsunami, measurements from 2011 were difficult to find, and so only remote sensing data taken from April 1st, 2012 onwards was considered. Only a limited number of stations were present in each town on the first date, therefore every station in each town was used in the 2012 data. Additional stations were constructed each year, but they were excluded from analysis. GPS locations for the Okuma, Futaba, and Namie sites may be found in Appendix A. In Microsoft Office Excel, station data

was linked by GPS coordinates from 2012 through 2017, with April 1st of that year used as a sample. Average dose rates were found for each station, each year. Some statistical tests, such as T-tests, were completed using R native tests without additional packages.

Precipitation data for the Namie weather station (37.491667, 140.965000) were obtained from the Japan Meteorological Agency (https://www.data.jma.go.jp/obd/stats/etrn/index.php), also on Japanese language webpages as seen in Fig 3.1.4:

月	降水量(mm)				気温(℃)					風向・風速(m/s)					日照時間(h)	雪(cm)		
	合計	日最大	最大 1時間	最大 10分間	平均 日平均	平均 日最高	平均 日最低	最高	最低	平均風速	最大風速 風速	最大風速 風向	最大瞬間風速 風速	最大瞬間風速 風向		降雪の合計	日降雪の最大	最深積雪
1	20.0	12.5	5.0	1.0	1.9	8.4	−5.6	15.4	−10.1	2.2	11.5	西南西	24.5	西	189.9	///	///	///
2	164.5	90.5	12.0	2.5	1.5	6.9	−4.5	16.9	−12.4	2.4	10.1	西北西	22.3	西	159.1	///	///	///
3	128.5	46.5	8.5	3.0	5.7	11.2	0.3	24.2	−7.4	2.5	11.6	西北西	25.8	西	168.5	///	///	///
4	133.5	88.5	23.0	4.5	10.3	17.2	2.2	25.0	−4.1	2.2	10.1	西	20.0	西	244.5	///	///	///
5	134.5	58.5	14.0	13.5	15.8	22.5	8.4	30.1	0.7	2.1	13.0	西	23.9	西	236.3	///	///	///
6	255.0	50.0	18.0	6.0	19.7	24.5	15.3	30.1	9.9	1.6	8.5	西南西	16.9	西	135.5	///	///	///
7	159.5	38.0	11.5	6.5	23.2	28.5	18.7	34.3	14.5	1.5	9.2	北北西	16.8	北	166.2	///	///	///
8	214.5	84.5	12.5	7.0	23.9	29.0	20.4	36.5	17.4	1.4	7.4	南南東	15.6	南南東	145.0	///	///	///
9	81.0	43.0	16.5	10.5	18.9	25.1	13.3	31.3	8.0	1.5	5.3	北北西	11.1	南南西	163.2	///	///	///
10	328.5	123.5	37.0	11.0	14.4	20.9	8.2	27.9	1.1	1.6	12.3	北北西	22.5	北北西	165.7	///	///	///
11	100.0	32.5	6.5	2.0	9.7	15.6	3.6	21.7	−3.0	1.9	11.1	西	22.9	西南西	140.8	///	///	///
12	58.5	17.0	6.0	3.0	3.1	9.1	−3.0	17.6	−8.5	2.2	11.7	西	23.4	西	175.7)	///	///	///

Figure 3.1.4: Tabular Weather data from the Namie Weather Station from the Japan Meteorological Agency website. The data includes temperatures, precipitation, and wind data by month. No snow data were available at this station.

While there is only one weather station for the entire town, all the remote monitoring stations were utilized for the dose rate calculation, under the assumption that the local weather patterns would not differ substantially within one township. Due to monthly averages of rainfall, the Namie dose rate data were computed monthly, using the averaged dose rate of the first of each month to measure changes from the previous month (i.e., March 1st represented the final dose rate after February), and correlated those

changes with precipitation. Due to a lack of temperature data accompanying the precipitation, there is no distinction that may be made between snow or rain. Monthly mean and maximum wind speed data were also available from this same data set and used for analytical purposes.

3.2 Vehicle-Bourne Survey

All the surveys utilized a Geiger-Mueller detector with built-in GPS trackers. In each survey, the GM detector was placed on the dashboard of the vehicle facing forward. The surveys also used a Sekiya TCS 172 NaI Scintillation detector placed facing forward on the central console. The TCS also had an attached GPS module to record location data. These surveys were conducted using a Subaru model 2008 Forester XT.

Figure 3.2.1: Detector Set-up for a Vehicle Survey. The GM detector is visible above the driver's side dashboard, while the TCS detector is visible at the bottom.

On the August 4th, 2017 survey, a BNC Model 940 was used for comparison against the other probes, and also had an attached GPS module.

The following vehicle surveys were conducted and analyzed:

Table 3.1: Vehicle Surveys Conducted

Survey Number	Date Conducted
1	2014-09-15
2	2014-10-18
3	2016-03-01
4	2017-05-20
5	2017-08-04

To provide a baseline of analysis, the car dose rates were compared to remote monitoring stations. A station had to be within 100 m to be considered usable for a dose comparison. The list of compared stations can be found in Appendix A for each survey. While each survey followed a different route, route variability was not a major factor since station comparisons were the analytical focus.

Every map created using the vehicle-borne data was made from imported CSV files in Google Maps. Remote station distances from vehicle data were measured using the built-in Ruler tool, with distance in meters and lat./long. data collected for analysis.

For the final analysis with the August 4th, 2017 survey, the data were compared to both the Eleventh and First (Decay-corrected) Airborne surveys. This was done by joining the vehicle to the airborne data, spatially, in ArcMap 10.5.1, a licensed GIS software produced by Esri. Results were then narrowed to distances less than 1 m away.

3.3 Airborne Analysis

Airborne Surveys were conducted by the Japanese NRA using helicopters equipped with NaI scintillation detectors (http://radioactivity.nsr.go.jp/ja/list/362/list-1.html). These data could be attained in both KMZ and CSV format, but the CSV was used for the analytical approach. The helicopters flew at approximately 300 m above the ground and measurements are converted into air dose rates at 1 m above the surface, recording results every second. Two different surveys were used for comparison of temporal patterns: the first airborne survey, which was conducted from April 6th through April 19th, 2011, and the eleventh

airborne survey, whose measurements were taken from September 14th through November 16th, 2016. These data were imported into ArcMap 10.5.1. Environmental classification data produced by the Japanese Aerospace Exploration Agency (JAXA), through their Advanced Land Observing Satellite, were integrated into the dataset (http://www.eorc.jaxa.jp/ALOS/lulc/lulc_jindex.htm#4). These data are available as Geotiffs from a KMZ file which indexes links to each file by latitude and longitude boundaries as seen in Figures 3.3.1 and 3.3.2:

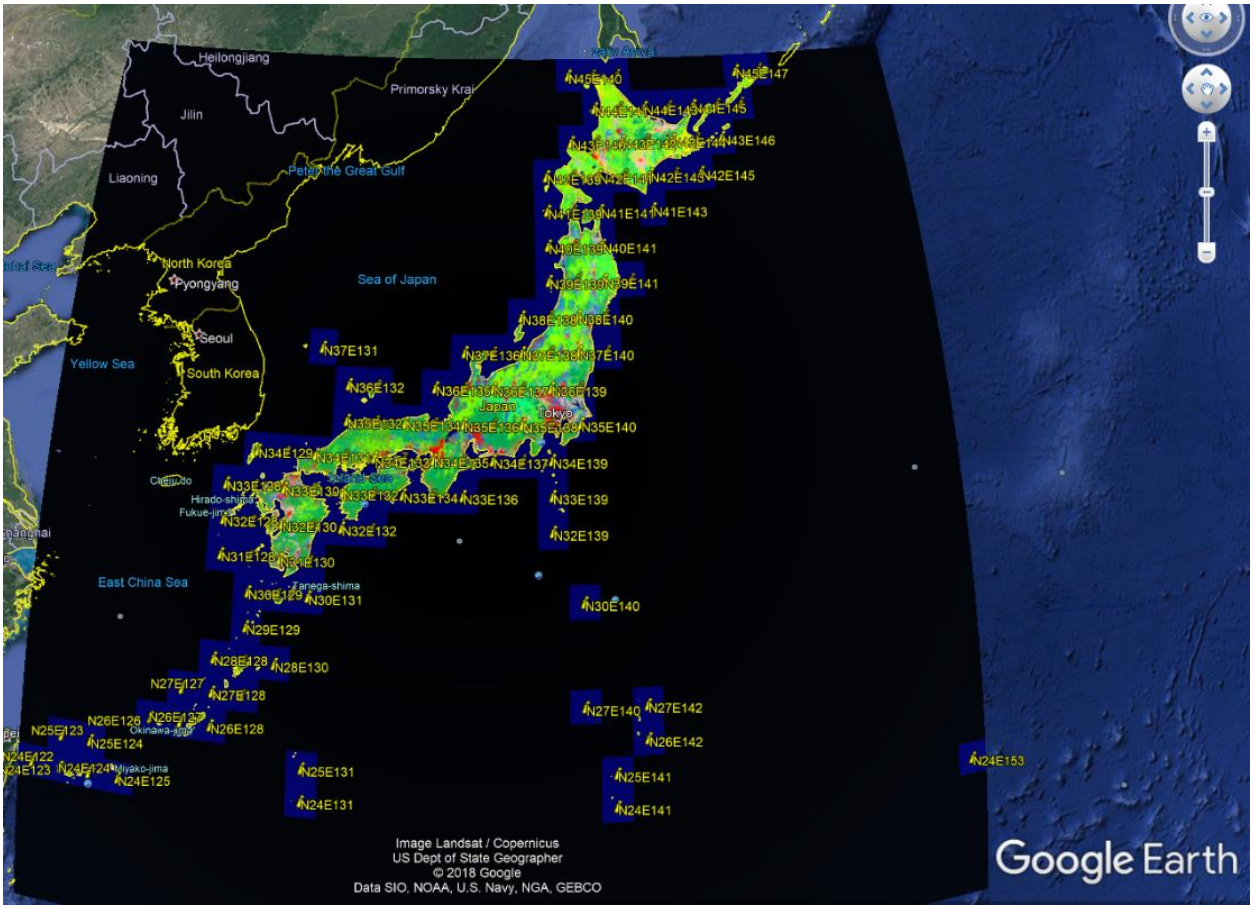

Figure 3.3.1: Geotiff database displayed in Google Earth for the entire Japanese Region. This was the entire dataset provided by JAXA and each region was linked to the physical region.

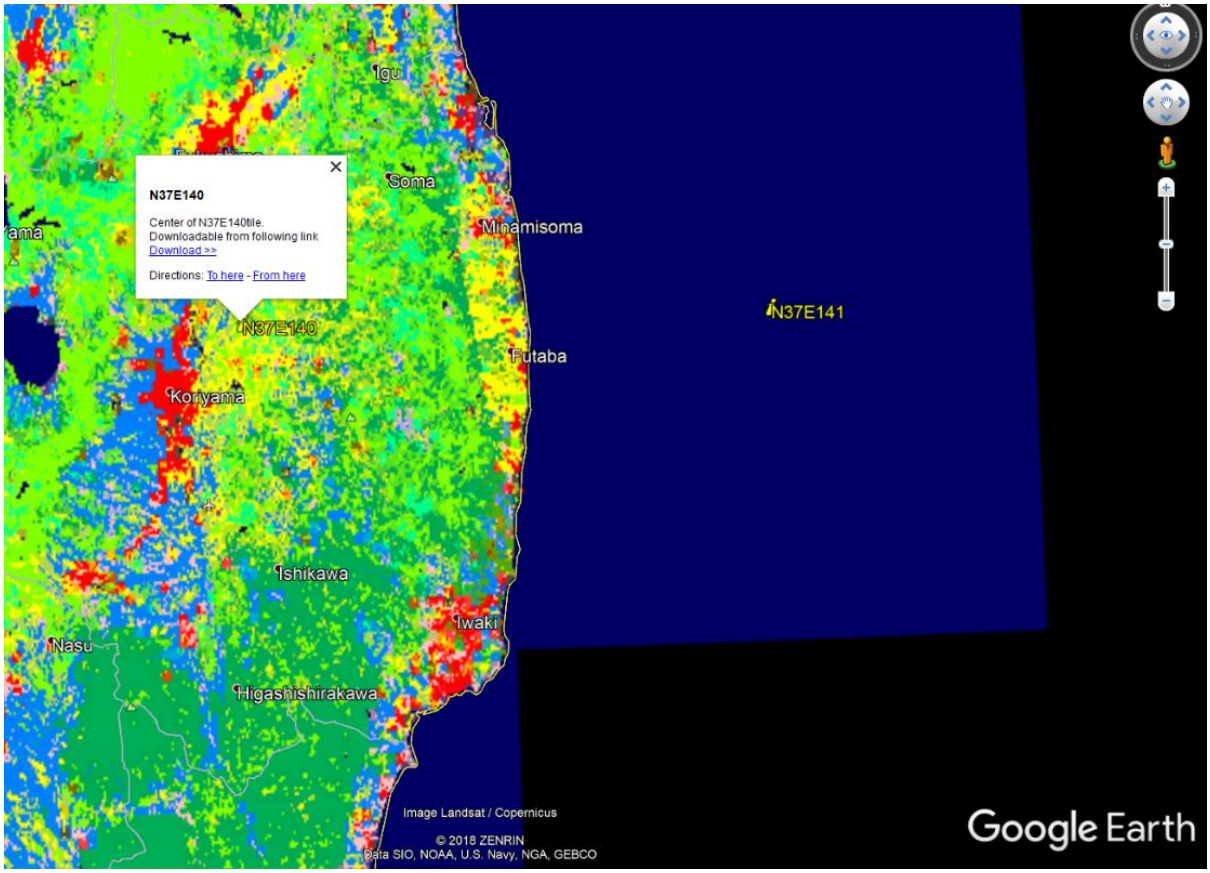

Figure 3.3.2: The Geotiff database overlooking Fukushima. Comprising N37E140 and N37E141, these data were used for the environmental analysis.

Version 18.03, produced in March 2018, utilized averaged environmental data from 2014-2016, while Version 16.09, produced in September 2016, used 2005-2011 data. It is built with a mixture of satellite imagery, classification algorithms, and personal observations as a 10x10 m^2 mesh and each pixel given a number to classify the type of flora present. The environmental classification is defined as:

- # 0: Unclassified (unknown)
- # 1: Water area (water)
- # 2: City (urban)
- # 3: Paddy field (rice paddy)
- # 4: Upland (crop)
- # 5: Grassland (grass)
- # 6: Deciduous hardwood (DBF)
- # 7: Deciduous softwood (DNF)

- # 8: Evergreen broad-leaved tree (EBF)
- # 9: Evergreen conifers (ENF)
- # 10: bare land (bareland)
- # 255: No data (nodata)

Further, elevation, slope, and aspect data were retrieved from Google Earth Engine. All data were integrated with the following method:

1. Define the region of interest (ROI), most likely by importing the base KML's for the airborne data (or other data) to establish where subset of data will be.
2. Under the Catalog tab (right side of ArcMap), link to the folder with the desired data set.
3. Drag the CSV from the catalog tab into the Table of Contents.
4. Right click on the CSV file and select Display XY Data
    a. Place the longitude as X field, Latitude as Y field
5. Export CSV data by right-clicking on the layer and export into a shapefile.
6. With a shapefile, a specific region can be selected which can then be saved as a separate shapefile to create a smaller subset of the total data for analysis.
7. Create a new simple vector polygon using the draw toolbar that conforms to the same of the ROI. This is the bounding box. Using the drop-down menu under Draw, convert drawing to shape feature.
8. Use the method in Appendix B to generate topographic data for the ROI and then import these .tif files into the ArcMap file.
9. Once Spatial Analyst tools are activated, use the Extract Value to Point to combine the CSV shape data with the JAXA classification data, then all the other .tif files to create one combined file for analysis. After each combination:
    a. Open attribute table.
    b. Add a new field, under table options, with a unique name. It will appear at the end next to the RASTERVALU column.

c. Use Field Calculator to copy RASTERVALU points into new column by double clicking RASTERVALU in the left box.

d. Delete the RASTERVALU column to allow another extraction since there cannot be two columns with the same name, and the software will not name it anything else.

e. Repeat for next extraction.

10. When finished, using Excel, open the final extracted shapefile's .dbf by looking under all files. **Save as an excel file before making any edits**. The column headers will need to be edited to be the same size. Any changes made to the .dbf will likely break the file.

All other data manipulation or statistical tests were conducted using either Excel or R.

4 Results

4.1 Remote Sensing:

4.1.1 Okuma

Due to its accessibility, Okuma was chosen as the first location to verify the effectiveness of remote sensing as a technique for dose rate tracking over time. The first 15 stations present in 2012 were used, and data from 2012 through 2017 were used. The results for the monitoring station in Okuma are shown in Table 4.1.1. Uncertainty estimates nor either standard deviation or error were not provided in the data. The values listed under each year correspond to the average dose rate recorded on April 1st of each given year:

Table 4.1.1: Okuma Remote Monitoring Data 2012-2017. These raw data points show the station variation both from the initial time point in 2012 across the town, and over the succeeding five years as the dose rates decrease.

Dose Rate in µSv/h						
Station	**2012**	**2013**	**2014**	**2015**	**2016**	**2017**
1	0.29	0.22	0.15	4.12	3.53	2.68
2	5.43	3.73	2.71	2.09	1.72	1.37
3	0.60	0.46	0.25	0.18	0.15	0.12
4	0.81	0.57	0.25	0.20	0.17	0.13
5	4.58	3.31	2.24	1.81	1.51	1.20
6	26.11	18.52	13.26	10.11	8.53	6.46
7	4.42	N/A	2.40	1.55	1.25	0.95
8	21.56	15.12	10.63	7.69	6.57	5.00
9	7.22	5.52	3.77	2.86	2.47	1.98
10	13.17	9.84	7.61	6.07	5.04	4.09
11	3.90	2.83	2.01	1.77	1.16	0.50
12	3.02	0.81	0.28	0.25	0.21	0.18
13	4.25	2.60	2.06	1.48	1.21	0.95
14	12.46	8.93	7.15	5.54	4.94	4.12
15	5.31	3.95	3.07	2.41	2.09	1.65
16	30.54	23.73	18.46	13.72	11.31	9.13
17	8.17	5.20	3.69	2.86	2.38	1.88
18	41.31	29.99	23.90	16.96	13.34	10.24

To facilitate analysis, the dose rates were converted to fractional values. These data are presented in Table 4.1.2. The first station was excluded from analysis since measured dose rates spiked through some unidentified outside means of contamination, and severely distorted the dose rate reduction. Since data for 2011 were not readily available, 2012 was set as the base dose rate. It should be noted, that for all fractional data, the reference date will be more than a year after the disaster since the first selected value was on April 1st, 2012. Dose rates immediately after the disaster could be reconstructed, but future predictions are more important to address current issues:

Table 4.1.2: Fractional Okuma Data 2012-2017

Fractional Dose Rates						
Station	**2012**	**2013**	**2014**	**2015**	**2016**	**2017**
1 (Excluded)	1	0.77	0.52	14.20	12.16	9.22
2	1	0.69	0.50	0.38	0.32	0.25
3	1	0.76	0.43	0.30	0.25	0.21
4	1	0.71	0.31	0.25	0.20	0.17
5	1	0.72	0.49	0.39	0.33	0.26
6	1	0.71	0.51	0.39	0.33	0.25
7	1	NA	0.54	0.35	0.28	0.21
8	1	0.70	0.49	0.36	0.30	0.23
9	1	0.76	0.52	0.40	0.34	0.27
10	1	0.75	0.58	0.46	0.38	0.31
11	1	0.73	0.51	0.45	0.30	0.13
12	1	0.27	0.09	0.08	0.07	0.06
13	1	0.61	0.49	0.35	0.29	0.22
14	1	0.72	0.57	0.44	0.40	0.33
15	1	0.74	0.58	0.46	0.39	0.31
16	1	0.78	0.60	0.45	0.37	0.30
17	1	0.64	0.45	0.35	0.29	0.23
18	1	0.73	0.58	0.41	0.32	0.25
Average	1	0.69	0.48	0.37	0.30	0.23

The temporal decrease in radiation dose rate can be compared to an “ideal” decrease based purely on the radioactive decay of a mixed Cs-137/134 source term resulting from the FDNPP releases. This ”ideal curve” is based on an analysis carried out by JAEA (Satoh et al., 2014)**.** This resulting theoretical

decrease is described in Table 4.1.3. A graphical representation of the temporal reduction in dose rate according to the "ideal decay" model is show in Figure 4.1.1.

Table 4.1.3: Ideal Decay Fractions. These points are the fractions of cesium atoms left at a given point in time for both isotopes of interest in Fukushima, the ratio of them together, and the ideal physical decay of dose rate based on relative activities.

Elapsed year	134Cs(A)	137Cs(B)	ratio (A/B)	Ideal decay of air dose rate
0.0	1.00	1.00	1.00	1.00
0.5	0.85	0.99	0.85	0.92
1.0	0.71	0.98	0.73	0.85
2.0	0.51	0.96	0.53	0.72
3.0	0.36	0.93	0.39	0.62
4.0	0.26	0.91	0.29	0.55
5.0	0.19	0.89	0.21	0.48
10.0	0.03	0.79	0.04	0.31
20.0	0.00	0.63	0.00	0.21
30.0	0.00	0.50	0.00	0.17

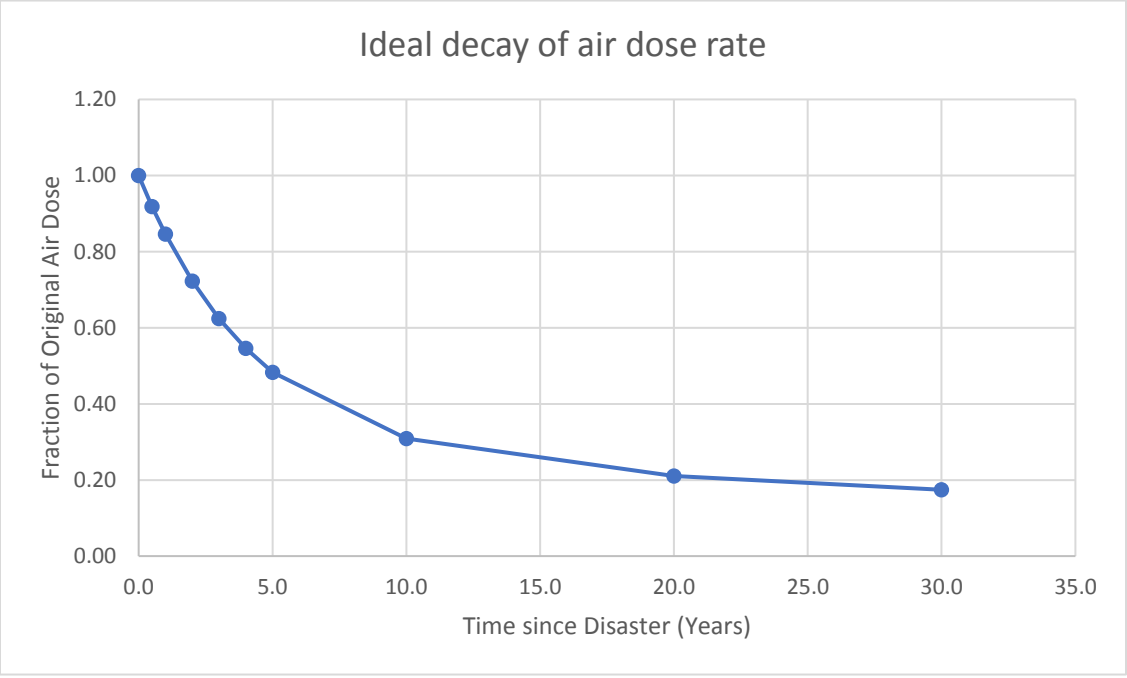

Figure 4.1.1: Ideal Decay Model 30-Year. This is the graphical representation of the final column of Table 4.1.3 and shows the variable decrease in dose through "all" half-lives of Cs-134 (20.65 years) and the first half-life of Cs-137.

Given that all the remote sensing data were recorded from 2012 through 2017, a subset of the original ideal decay data corresponding to the first 6 years after release is shown in Figure 4.1.2 to better relate these data to the station data.

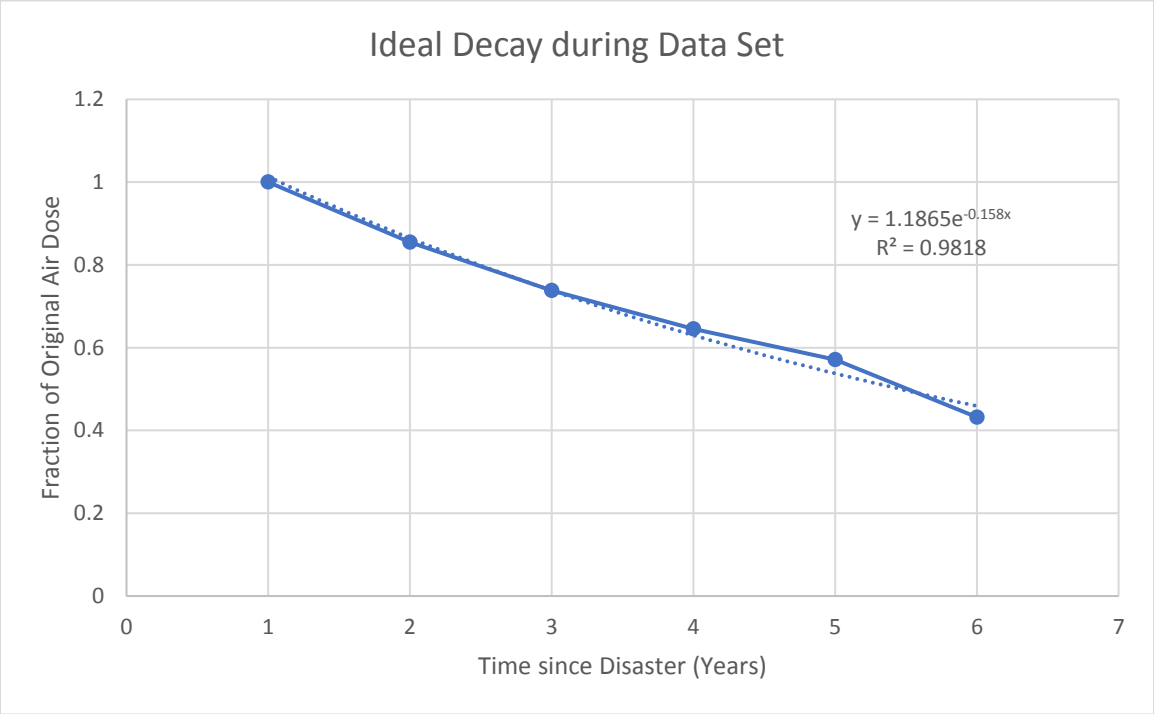

Figure 4.1.2: Ideal Decay Model 6-Year. This portion of the total curve is representative of the data collected from the stations, conforming to the period from 2012-2017.

With the ability the compare the ideal decay curve to the Okuma station data, it is possible to look for deviations in the monitoring data against expected physical decay patterns. Fig. 4.1.3 has each station separately plotted versus the ideal decay curve whereas Fig. 4.1.4 has all the stations (except station 1) plotted as collective data points.

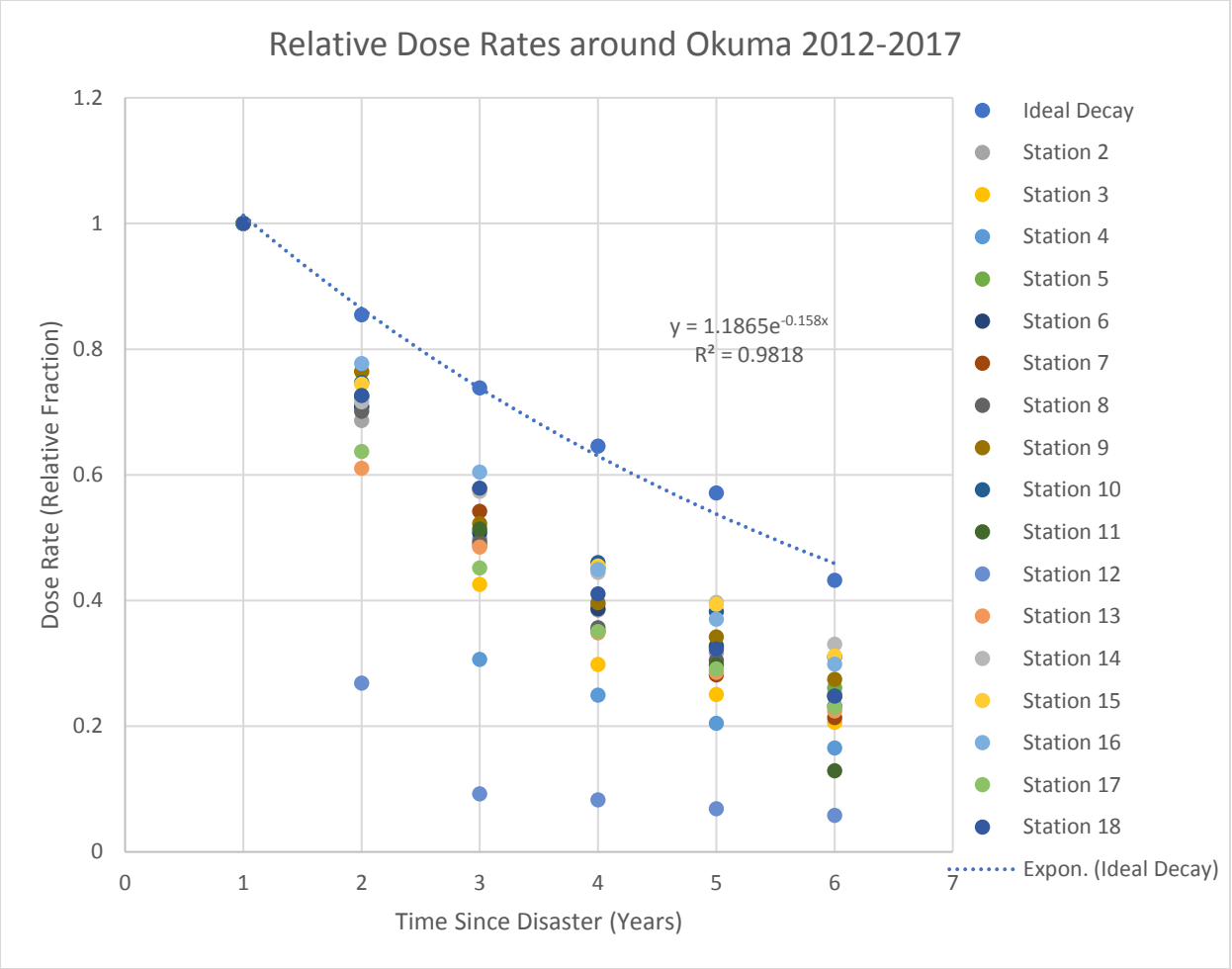

Figure 4.1.3: Fractional Dose Rates in Okuma, Ideal and all* Stations, 2012-2017. Station 1 was excluded for deviation but all the other stations are present in graphical form, compared with the ideal decay curve. Significant decreases in dose rate are noticeable in the stations versus the ideal curve.

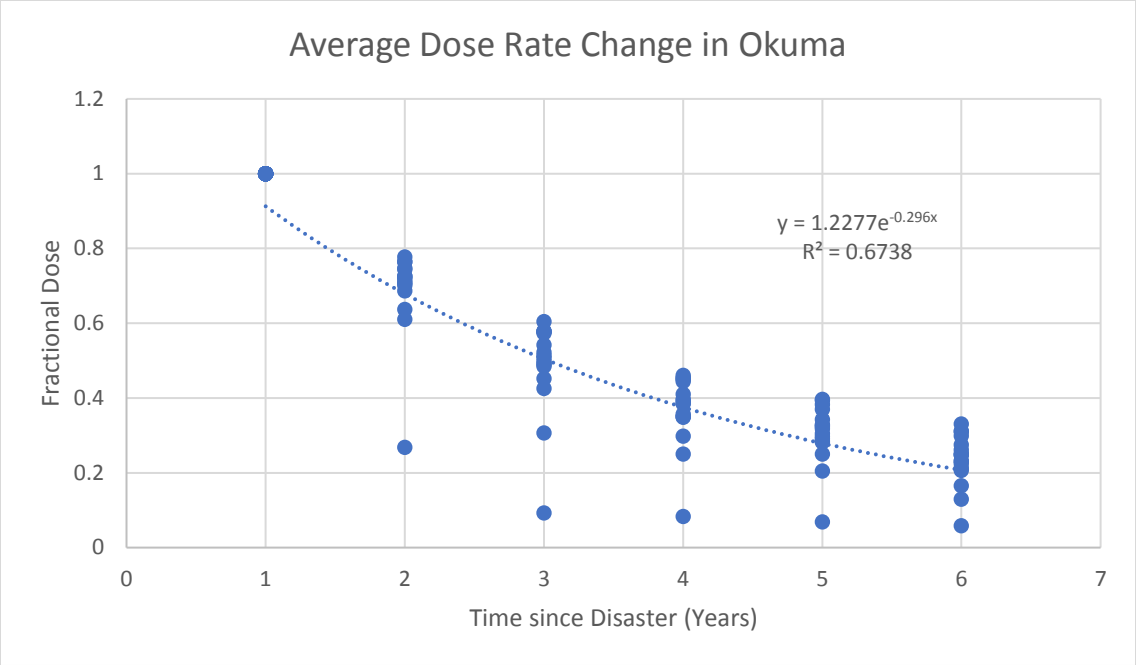

Figure 4.1.4: Average Dose Rate Change for Okuma Stations, 2012-2017. All station data was graphed as one data set and a combined exponential curve fitted through the center of station data.

A key finding in these charts is deviation between the measured average and the ideal curve. Based on the measurements, the actual dose rate is 0.2 lower than would be expected if decay was the only factor. This speaks to other means by which radiation is leaving the area.

4.1.2 Futaba

The town of Futaba has very similar data, just with more stations. The variety between each station can be visualized by year in Fig. 4.1.5:

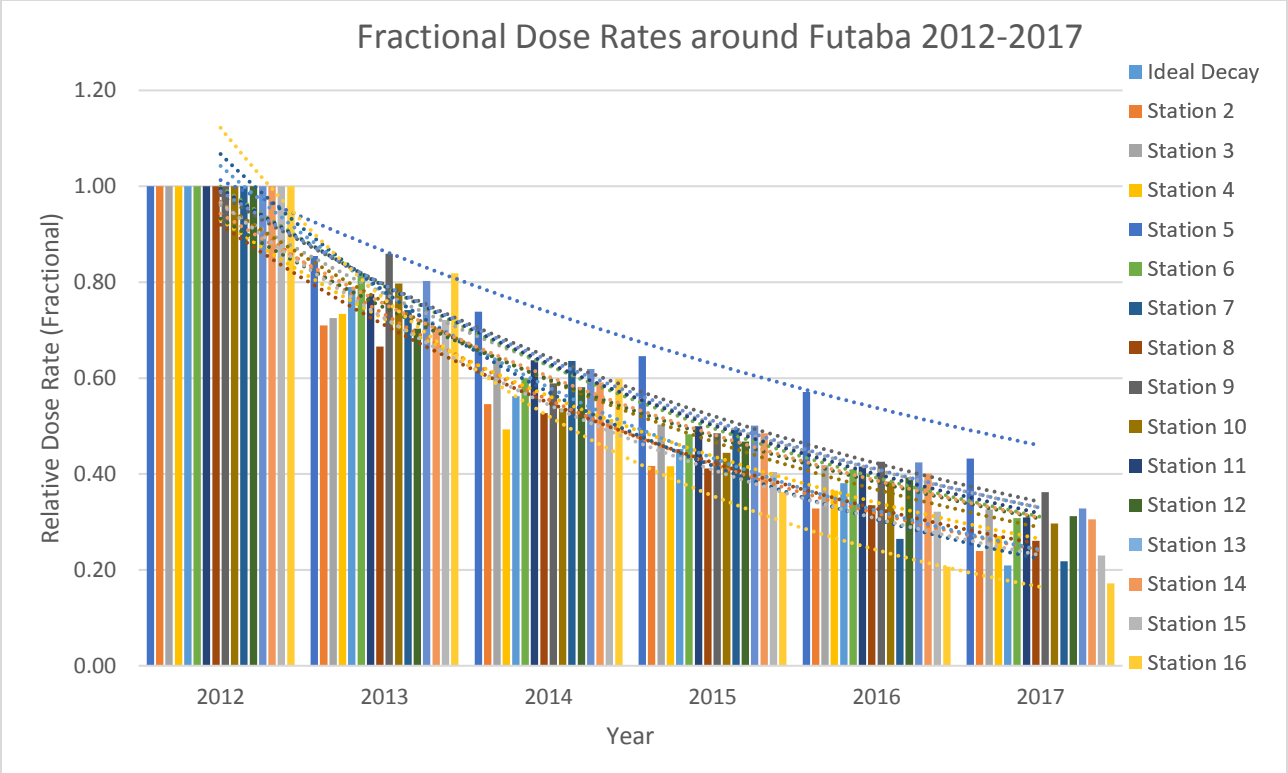

Figure 4.1.5: Fractional Dose in Futaba, Ideal and All Station, 2012-2017. This chart displays the same information as the Okuma chart in a bar graphical format, allowing for greater visualization of the station and yearly variation in dose rates. While all the exponential equations are plotted, only the equations for the first 8 are displayed for visual clarity.

The first bar are the ideal decay model, but all the others are the various stations around Futaba, illustrating the potential variation amongst each location in both equation (for the first eight stations) and yearly fluctuations based on the data in Table 4.1.4:

Table 4.1.4: Fractional Futaba Data. This data is also based on dose rate measurements in μSv/hr compared to the first station measurement on April 1st, 2012.

Fractional						
Station	**2012**	**2013**	**2014**	**2015**	**2016**	**2017**
Ideal Curve	1.00	0.85	0.74	0.65	0.57	0.43
1 (excluded)	1.00	0.78	0.63	N/A	3.62	2.86
2	1.00	0.71	0.55	0.42	0.33	0.24
3	1.00	0.72	0.64	0.50	0.42	0.33
4	1.00	0.73	0.49	0.42	0.37	0.27
5	1.00	0.79	0.56	0.45	0.38	0.21
6	1.00	0.82	0.60	0.48	0.41	0.31

7	1.00	0.78	0.64	0.50	0.42	0.31
8	1.00	0.67	0.53	0.41	0.33	0.26
9	1.00	0.86	0.59	0.48	0.43	0.36
10	1.00	0.80	0.54	0.44	0.38	0.30
11	1.00	0.74	0.64	0.50	0.26	0.22
12	1.00	0.70	0.58	0.47	0.39	0.31
13	1.00	0.80	0.62	0.50	0.42	0.33
14	1.00	0.70	0.59	0.49	0.40	0.31
15	1.00	0.72	0.51	0.40	0.32	0.23
16	1.00	0.82	0.60	0.36	0.21	0.17
Average	1.00	0.76	0.59	0.47	0.38	0.29

Figure 4.1.6 then graphically displays all the station data with a central exponential equation, which has a shallower slope than in Okuma.

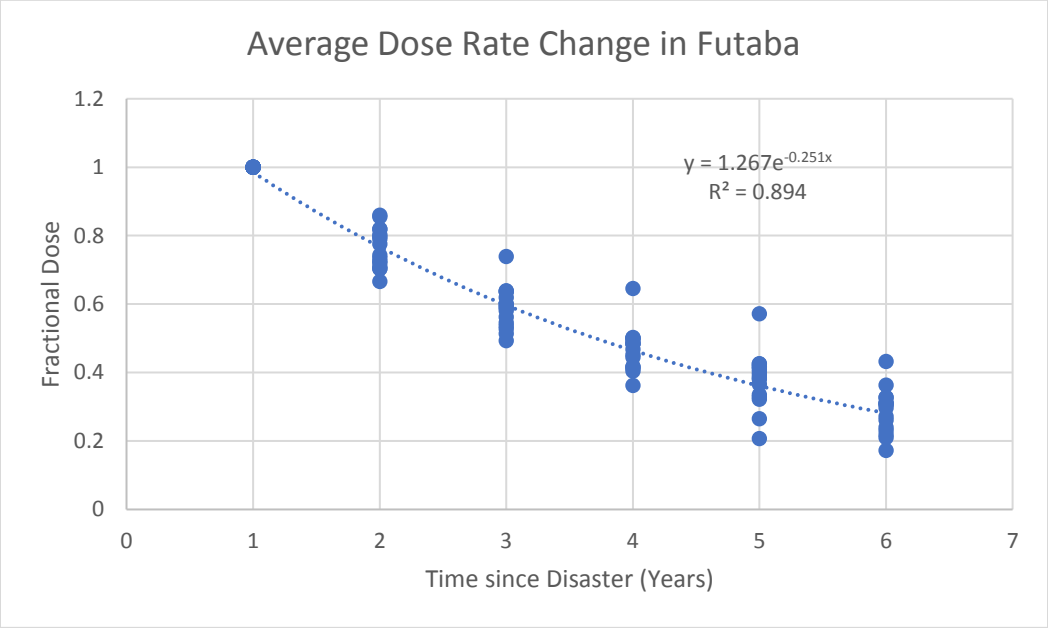

Figure 4.1.6: Average Dose Rate Change in Futaba 2012-2017. Again, the station data points excluding the first station were graphed as one data set with a central exponential equation. The dose rate around Futaba decreased at a lower rate than in Okuma.

As with Okuma, the rate at which radiation measurements are decreasing is higher than would be expected if radioactive decay was the only factor. The difference in Futaba is about half as much (10% vs. 20%) difference, but still noticeable.

To understand the significance of the differences between measured and theoretical, the data sets can be tested. Using a Shapiro-Wilks Test:

- P-value = 0.740 for Futaba data
- P-value = 0.563 for Okuma data
- Both sets are normally distributed

Looking for differences then between the station data and theory, a paired t-test is appropriate given normalcy and the need to distinguish differences:

- P-value = 0.01378 for Futaba data versus theoretical decay
- P-value = 0.00613 for Okuma data versus theoretical decay
- Both are statistically significant (α=0.05 for Futaba, and α=0.01 for Okuma) in their deviation, showing that environmental movement is playing a demonstrable role.

4.1.3 Namie

Considering data from Namie, the analysis now becomes more granular, with data points every month as seen in Table 4.1.5 and graphically in Fig. 4.1.7:

Table 4.1.5: Namie Monthly Dose Rate Statistics and Climate Data. The weather data is from the Namie Weather Station with the dose statistics calculated from all of the station within the town area.

Date	Years Since Accident	Precipitation (mm)	Average Wind Speed (m/s)	Max Wind Speed (m/s)	Average dose (uSv/hr)	Standard Deviation	Fractional Dose	Deviation Error from Year	Difference from Next Month
Jan-14	2.83	20	2.2	11.5	2.20	3.10	1.06	0.14	-0.08
Feb-14	2.92	164.5	2.4	10.1	2.03	2.90	0.98	0.07	0.02
Mar-14	3.00	128.5	2.5	11.6	2.07	2.90	1.00	0.07	-0.06
Apr-14	3.08	133.5	2.2	10.1	1.95	2.78	0.94	0.02	0.04
May-14	3.17	134.5	2.1	13	2.03	2.87	0.98	0.05	-0.06
Jun-14	3.25	255	1.6	8.5	1.90	2.71	0.92	0.00	0.01
Jul-14	3.33	159.5	1.5	9.2	1.92	2.73	0.93	0.00	-0.04
Aug-14	3.42	214.5	1.4	7.4	1.84	2.63	0.89	0.03	0.01
Sep-14	3.50	81	1.5	5.3	1.86	2.66	0.90	0.02	-0.06
Oct-14	3.58	328.5	1.6	12.3	1.74	2.53	0.84	0.07	-0.05
Nov-14	3.67	100	1.9	11.1	1.64	2.44	0.79	0.10	0.00
Dec-14	3.75	58.5	2.2	11.7	1.65	2.41	0.80	0.11	-0.21
Jan-15	3.83	75.5	2.2	10.3	1.21	1.71	0.58	0.21	0.20
Feb-15	3.92	44.5	2.5	10.7	1.62	2.34	0.78	0.07	0.00
Mar-15	4.00	167.5	2.5	13.8	1.61	2.36	0.78	0.08	0.02
Apr-15	4.08	113	2	9.6	1.65	2.39	0.80	0.10	-0.01
May-15	4.17	51.5	2.1	7.8	1.63	2.37	0.79	0.08	-0.06
Jun-15	4.25	111.5	1.9	9	1.51	2.21	0.73	0.01	0.04
Jul-15	4.33	190.5	1.4	6.4	1.59	2.29	0.77	0.05	-0.07
Aug-15	4.42	220	1.5	5.8	1.45	2.12	0.70	0.03	0.00
Sep-15	4.50	419	1.6	7.9	1.45	2.15	0.70	0.01	0.00
Oct-15	4.58	3.5	2.1	11.8	1.45	2.17	0.70	0.01	-0.05
Nov-15	4.67	190	1.6	11.4	1.34	2.06	0.65	0.06	-0.03
Dec-15	4.75	46	1.9	11.1	1.28	2.02	0.62	0.07	-0.12
Jan-16	4.83	89.5	2.2	10.8	1.03	1.73	0.50	0.06	0.06

Feb-16	4.92	21.5	2.3	9.8	1.15	1.98	0.55	0.08	-0.01
Mar-16	5.00	28	2	9.1	1.13	2.00	0.55	0.09	-0.03
Apr-16	5.08	133.5	2.3	10.4	1.07	1.93	0.52	0.05	0.00
May-16	5.17	72	2.1	10.2	1.07	1.95	0.51	0.07	-0.04
Jun-16	5.25	185	2	8.1	0.98	1.84	0.47	0.00	-0.02
Jul-16	5.33	24.5	1.6	5.9	0.94	1.85	0.45	0.01	-0.02
Aug-16	5.42	401	2	10.5	0.90	1.79	0.43	0.02	-0.02
Sep-16	5.50	347	1.4	6.9	0.86	1.76	0.42	0.04	0.00
Oct-16	5.58	32	1.6	8.4	0.86	1.75	0.41	0.04	-0.02
Nov-16	5.67	52.5	1.8	8	0.81	1.70	0.39	0.07	0.01
Dec-16	5.75	46	2.1	11.5	0.83	1.70	0.40	0.07	N/A

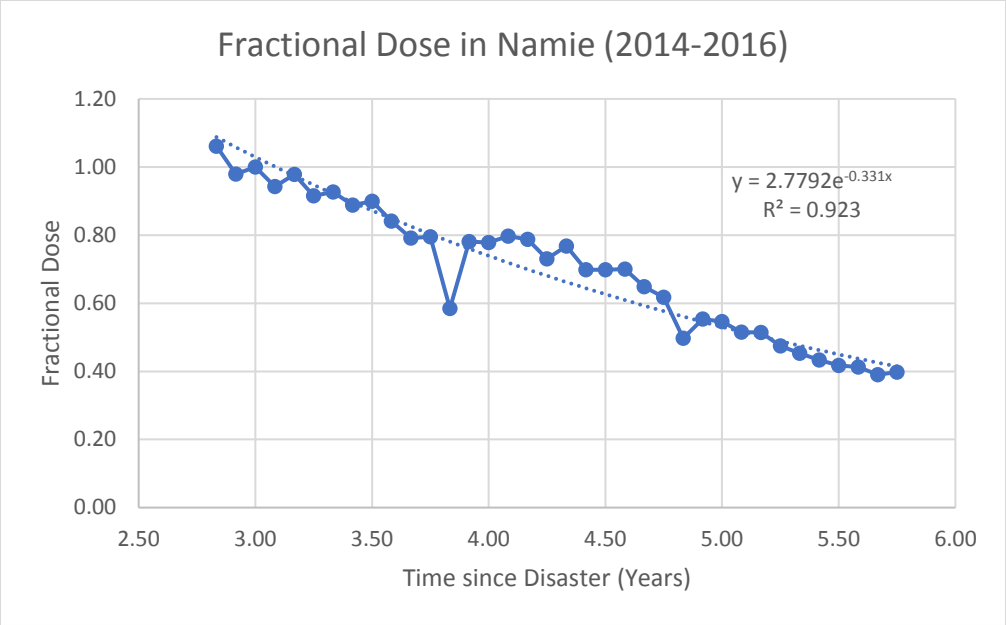

Figure 4.1.7: Fractional Dose in Namie from 2014-2016, Monthly

For estimating dose risk to returning residents, the reference levels for existing exposures are used, keeping with current International Atomic Energy Agency (IAEA) standards, which Japan has adopted. Based on the derived exponential equations from each town, the time to reach 1 mSv per year (~0.11 µSv/h), was calculated since protections considered "unlikely to be justifiable" (UJ) by the IAEA and the International Commission on Radiation Protection (ICRP). The median, approximating the amount of time necessary for 50% of the respective township to be below the reference level, was chosen as the default measurement. Additionally, the time until the dose rate was below 20 mSv per year (~2.28 µSv/h) was calculated since rates above almost always justify (AJ) protection efforts. Table 4.1.6 shows these estimates:

Table 4.1.6: Median Dose Rate Decay to Limit

Town	Fractional Model Equation	Median Dose Rate (µSv/h)	Time until below UJ reference level (Years)	Time until below AJ reference level (Years)
Okuma	$1.277e^{-0.296x}$	5.37 (2012)	13.95	3.72
Futaba	$1.267e^{-0.251x}$	2.45 (2012)	13.31	1.23
Namie	$2.7792e^{-0.331x}$	1.48 (2014)	10.94	Already Below

Where:

$$X\ (Years) = \frac{\ln\left(\frac{0.11\ \mu\frac{Sv}{h}}{\frac{Dose\ Rate}{A_0}}\right)}{-\lambda}$$

The time for the dose rate to fall below always justifiable action is significantly lower, and has been below that threshold in Namie since 2012.

For the most contaminated areas, the maximum dose rate was used to estimate the longest time before measurements fall below reference levels is in Table 4.1.7:

Table 4.1.7: Maximum Dose Rate Decay to Limit

Town	Fractional Model Equation	Maximum Dose Rate (μSv/h)	Time until below UJ reference level (Years)	Time until below AJ reference level (Years)
Okuma	$1.277e^{-0.296x}$	41.31 (2012)	20.86	8.96
Futaba	$1.267e^{-0.251x}$	24.70 (2012)	22.52	8.55
Namie	$2.7792e^{-0.331x}$	18.55 (2014)	18.60	6.65

So, assuming current trends continue (a large assumption), then it will be 22.52 years (October 2034) before a member of the public could live full time at the most contaminated site in Futaba without radiation exposure above reference levels which might suggest protective measures. However, on average (13.4 years from 2012), half of all the exposed townships should be below limits by August 2025. It should be noted that using the occupational limits, the average time in maximally contaminated areas is 8.74 years from 2012, which would be in November 2020.

4.1.4 Climate Effects (Namie data)

The dips occurring in Fig. 4.1.7 are a result of winter snows attenuating the gamma emissions from cesium. These dips only occur during January/February when the region is most likely to have lasting snow.

Directly plotting precipitation against the difference in fractional dose from month to month does not elicit a strong relationship. Fig. 4.1.8 shows a linear relationship with a slope of only a 0.00007:

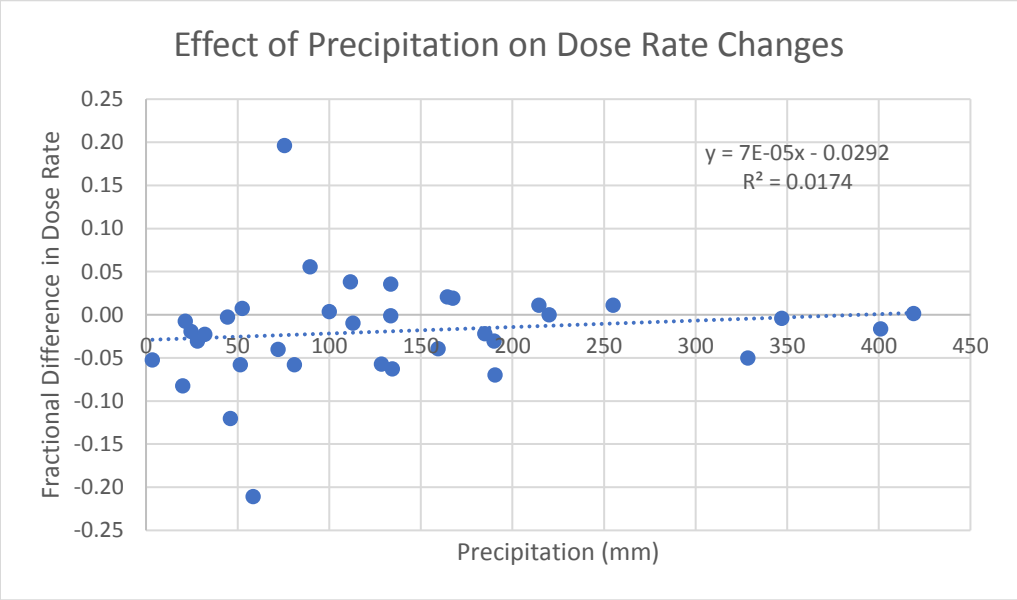

Figure 4.1.8: Effect of Precipitation on Fractional Dose Rate Changes in Namie. The relationship between precipitation and dose rate differences is largely not distinguishable based on these data, with minimal slope.

The Pearson correlation for these factors is 0.132; detectable but not a strong measure of change.

Wind speeds tell a very similar story in Figure 4.1.9, albeit with a more pronounced slope:

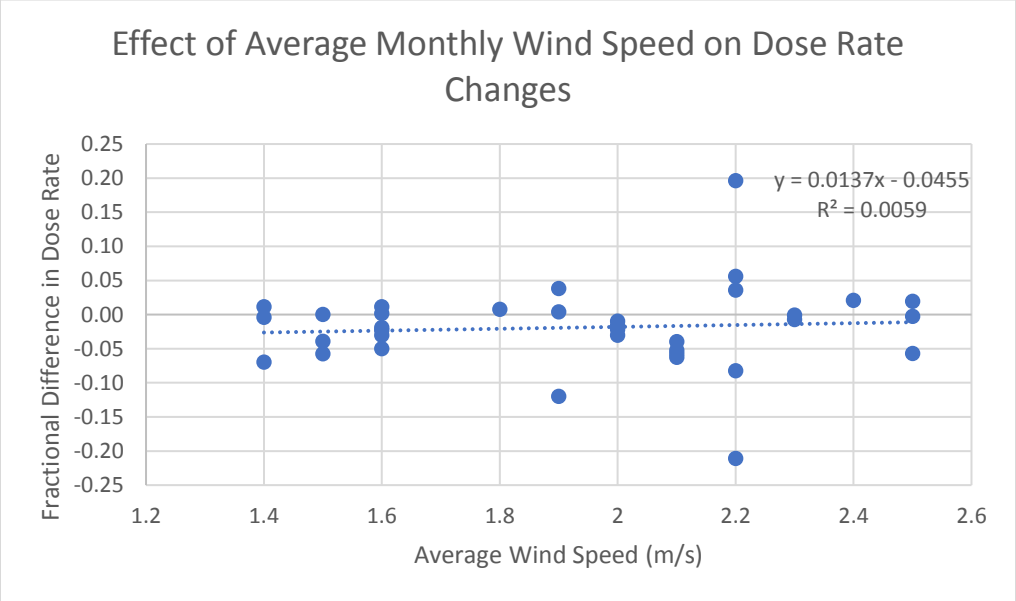

Figure 4.1.9: Effect of Average Wind Speed on Fractional Dose Rate Changes in Namie. While the slope of the relationship is more pronounced than in precipitation, the correlation is less significant.

Average wind speed has a lower Pearson correlation of 0.077 than precipitation. However, maximum recorded wind speeds have an opposite, but still mild, correlation of -0.11 and can be seen graphically in Fig. 4.1.10:

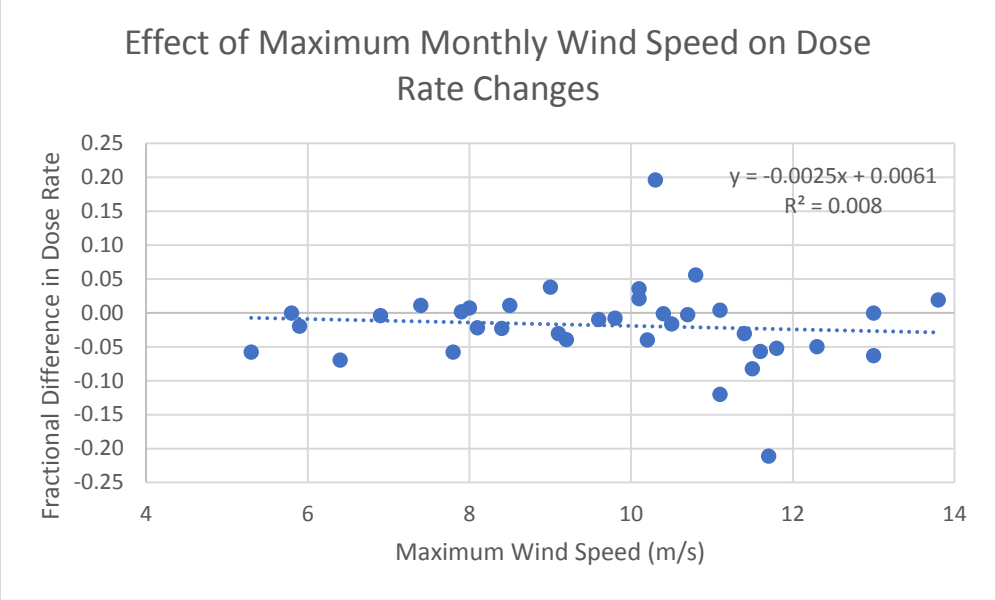

Figure 4.1.10: Effect of Maximum Monthly Wind Speed on Dose Rate Changes. In contrast to average wind speeds, the maximums have an inverse relationship with dose rate differences. Potential reasons for this change in relationship could be the association with maximum wind speeds and precipitation.

When wind and precipitation are compared together, similar trends appear, as seen in Figures 4.1.11 and 4.1.12, where the more precipitation occurs, the lower typical wind speeds:

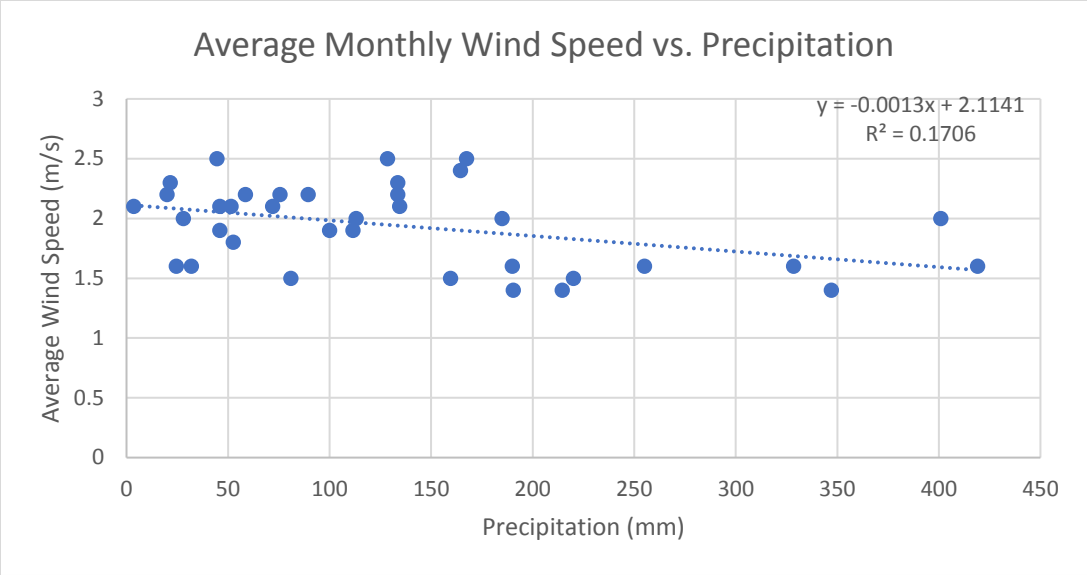

Figure 4.1.11: Average Monthly Wind Speed vs. Precipitation. This inverse relationship is due to the wind speeds peaking in the winter months whereas precipitation peaks in the summer months.

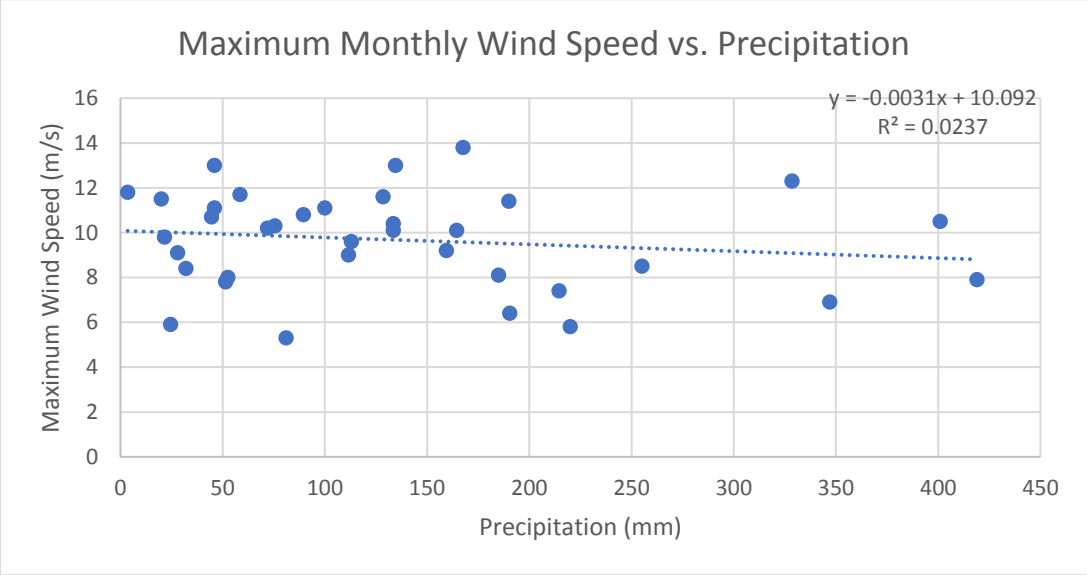

Figure 4.1.12: Maximum Monthly Wind Speed vs. Precipitation. As with average wind speeds, there are seasonal factors which influence maximum wind speeds. However, there is a much weaker correlation between these factors, which based on previous literature, is due to storm events bringing higher maximum speeds during the summer months as well.

Precipitation and average wind speed have a stronger negative correlation at -0.413. Maximum wind speeds have a weaker correlation though, calculated at -0.154. Seasonal variation is the dominant driver of the negative correlation since the higher average wind speeds occur during the winter months, while greater precipitation occurs during the summer months. Due to the impact of summer tropical storms and

typhoons, this would likely be the cause of the lower correlation of maximum wind speeds versus average wind speeds since the maximum values are more sensitive to single events. These seasonal patterns might also play a role in the low correlations between dose rate differences and either precipitation or wind. Rain/Snow effects are inverse to those of wind, with water dampening soil and preventing wind associated suspension of particles. None of these factors were found to be statistically significant at the 0.05 level against the change in dose rate, with p-values of 0.496, 0.425, and 0.172, respectively. (Appendix D).

However, precipitation does influence the deviation of dose rates over time which can be seen in Figure 4.1.13:

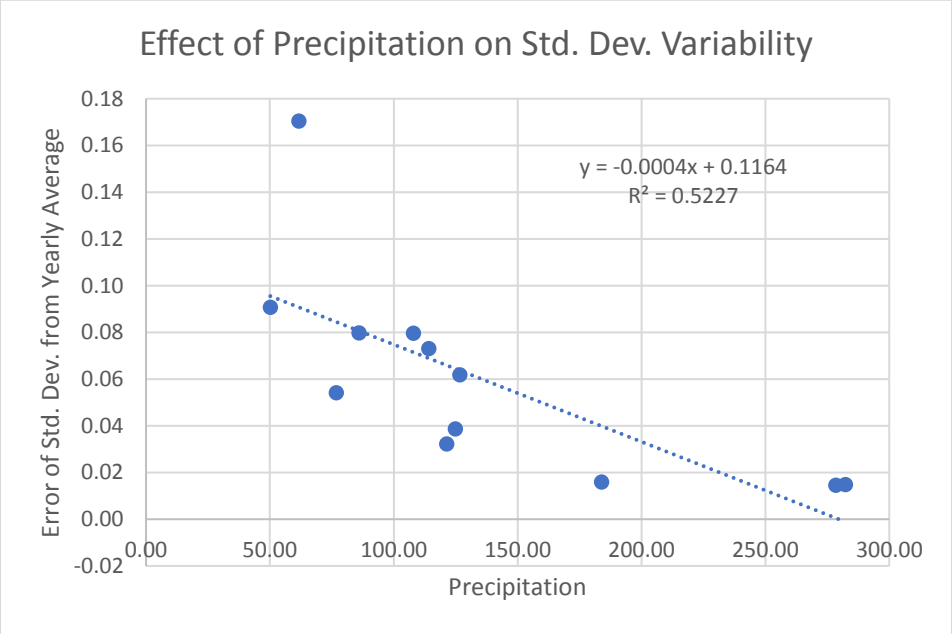

Figure 4.1.13: Effect of Precipitation on the Variability of Dose Rate Standard Deviations. This linearity is hypothesized to be related to precipitation dampening confounding sources of dose rate such as radon gas emission.

Precipitation has a strong correlation of -0.723 when compared to how the standard deviation of the dose rate changes over time. By comparing the variability of the standard deviation each month against the yearly average, precipitation seems to significantly dampen the bounds of the dose rate across Namie.

Although there are several hypotheses which could explain this, the mostly likely is that the precipitation is lowering radon emissions which influence the measurements at the remote stations.

4.2 Vehicle-Borne Surveys

Vehicle surveys have the benefit of being able to generate dense data over a large section of land, with much lower costs than the installation of remote sensing stations or airborne studies. Fig. 4.2.1 illustrates the visualization of vehicle-borne data in Google Maps:

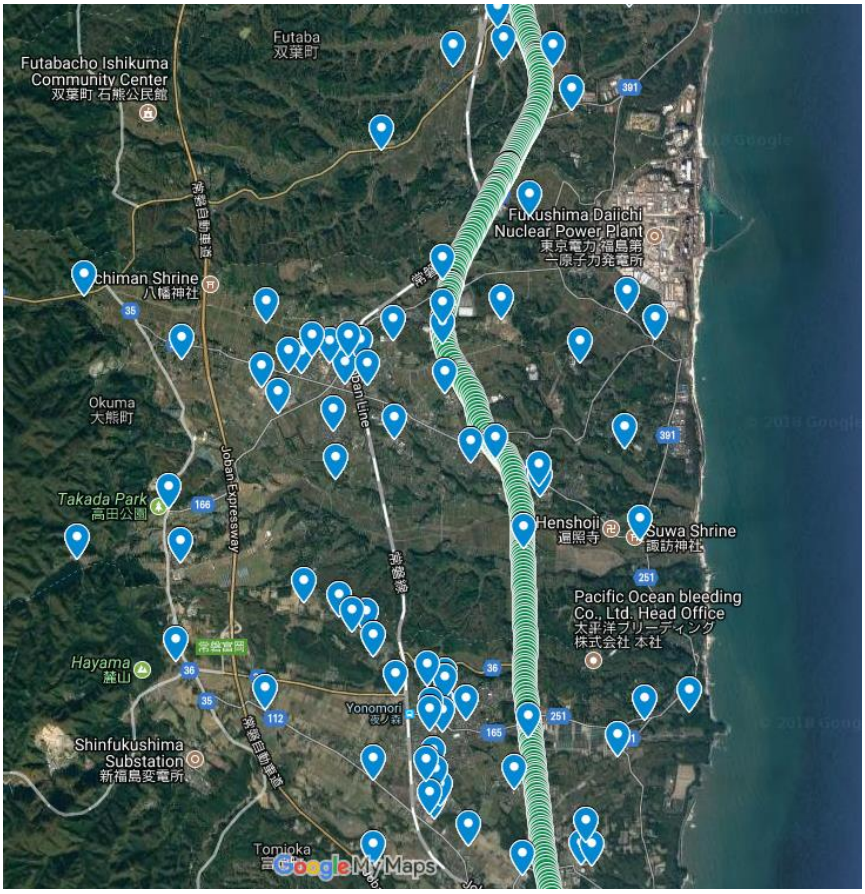

Figure 4.2.1: Vehicle Survey (Green) and Remote Stations (Blue) Mapped. The vehicle survey data points are much more densely located than station data points.

However, challenges arise from the literature-common placement of detectors within vehicles, as opposed to externally, and the narrow band of focus offered by the general restriction to roads. To correct the former, vehicle measurements can be compared to other types of references to try and generate a means to

predict ambient dose equivalent rate based on sheltered detectors. Graphing the vehicle measurements against stations dose rates within 100 m resulted in the equations in Figure 4.2.2:

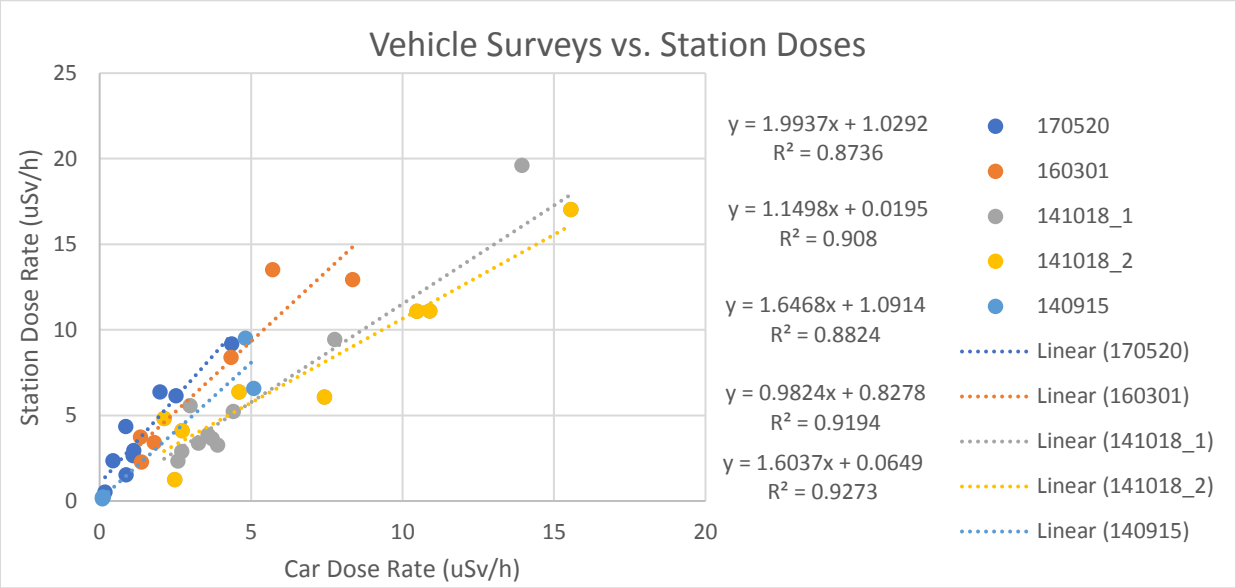

Figure 4.2.2: Vehicle Survey Correction Models when Compared to Remote Stations. These linear models are a direct means of correcting recorded car dose to ambient dose equivalent rate via the monitoring stations.

Equations and data series are ordered by most recent survey to least. Linear equations were chosen as the correction was desired to be as simple and straightforward as possible, per researcher request. Each survey was found to have a unique correction despite similar geometries in each situation. Using the average equation value for the five surveys yields the equation 1.425x +0.606. A separate vehicle survey was conducted on August 4th, 2017 to specifically try and match vehicular data to station data. Figure 4.2.3 shows the car vs. station dose rate for that survey:

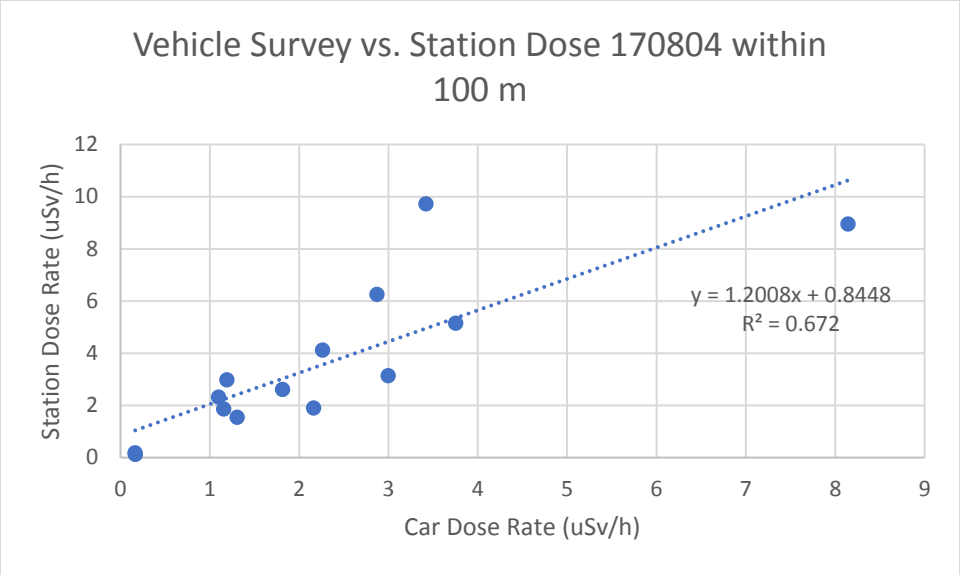

Figure 4.2.3: Vehicle Survey versus Station Data within 100 m from August 4th, 2017.

This equation represents a 15% and 28% deviation of slope and intercept from the first average equation, respectively. Since this survey specifically sought to collect vehicle data near the stations, it was directly averaged with the first equation, equaling 1.31x + 0.725. Based on the data collected, this is the best linear approximation of dose rate inside of a vehicle and externally from a station.

Primarily, these models are meant to act as a simple and straightforward mechanism for correction of vehicular measurements to reflect the ambient dose equivalent rate. This allows for the simplest and most accurate conveyance of potential radiation dose risk while utilizing vehicle surveys, if an individual. To improve the model's usefulness at low dose rates, the y-intercept was excluded, since it would have made the minimum dose rate be 0.725 μSv/h. As a comparison for the utility of vehicular data, airborne surveys offer a more generalized comparison. Un-modeled data plotted alongside the eleventh airborne survey are seen in Figure 4.2.4, while the overlaid model appears in Figure 4.2.5. In making a comparison, the vehicle data would be expected to be somewhat lower than the airborne data since the road surfaces have greater runoff than plant covered roadside curtilage, which are averaged in air surveys. While the model only acts to shift the data by a factor 1.3, this brings the measurement more in line with the assumed ambient dose equivalent rate.

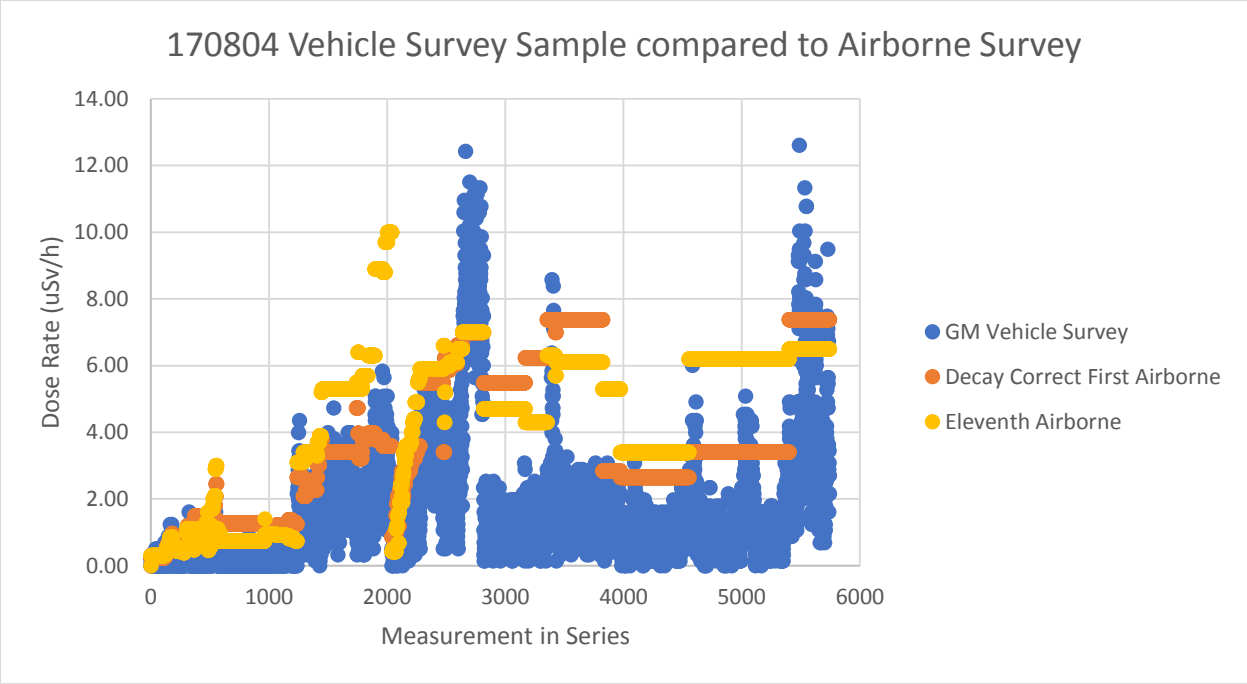

Figure 4.2.4: Vehicle Survey Sample compared to Airborne Survey. The vehicle surveys are comparable to airborne surveys in how they follow spatial radiation patterns, but possess greater resolution. However, the measurements are distinguishably lower than the airborne survey.

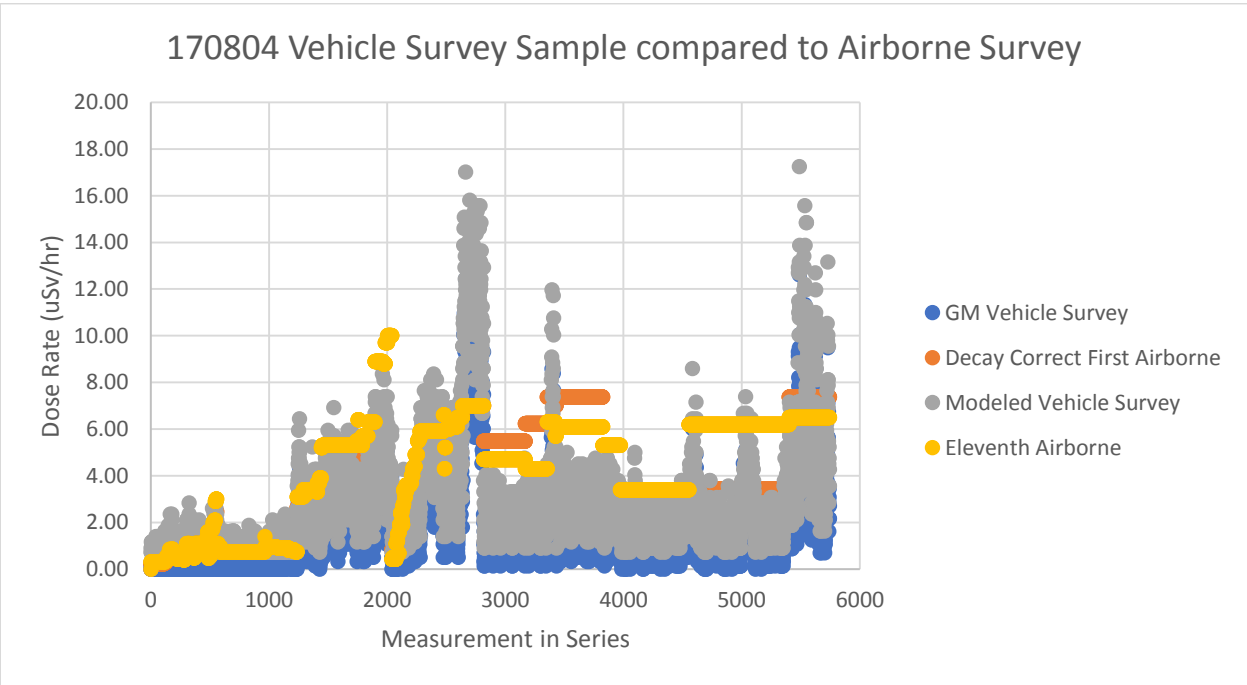

Figure 4.2.5: Modeled Vehicle Survey Sample compared to Airborne Survey. The modeled data shows a closer adherence to the airborne data, and is a visible shift from the GM survey data. It would still be expected to be lower due to road surface runoff.

In its simplicity, the linear model is not able to provide more information other than more accurate exposure than the unmodeled vehicular data. However, strengths of the vehicle survey are apparent in the greater amount of geographic resolution available. While the airborne surveys can convey averages across the region, the vehicle surveys can readily show which locations measured pose greater dose risk, and with the model, a better understanding of the exact amount of contamination present is possible.

4.3 Airborne Analysis

Data from the Eleventh and First Airborne surveys were combined in ArcMap 10.5.1 alongside the environmental classification, and the data trimmed to meet mutual boundaries in the data, which can be seen in how the data present on the map in Figure 4.3.1:

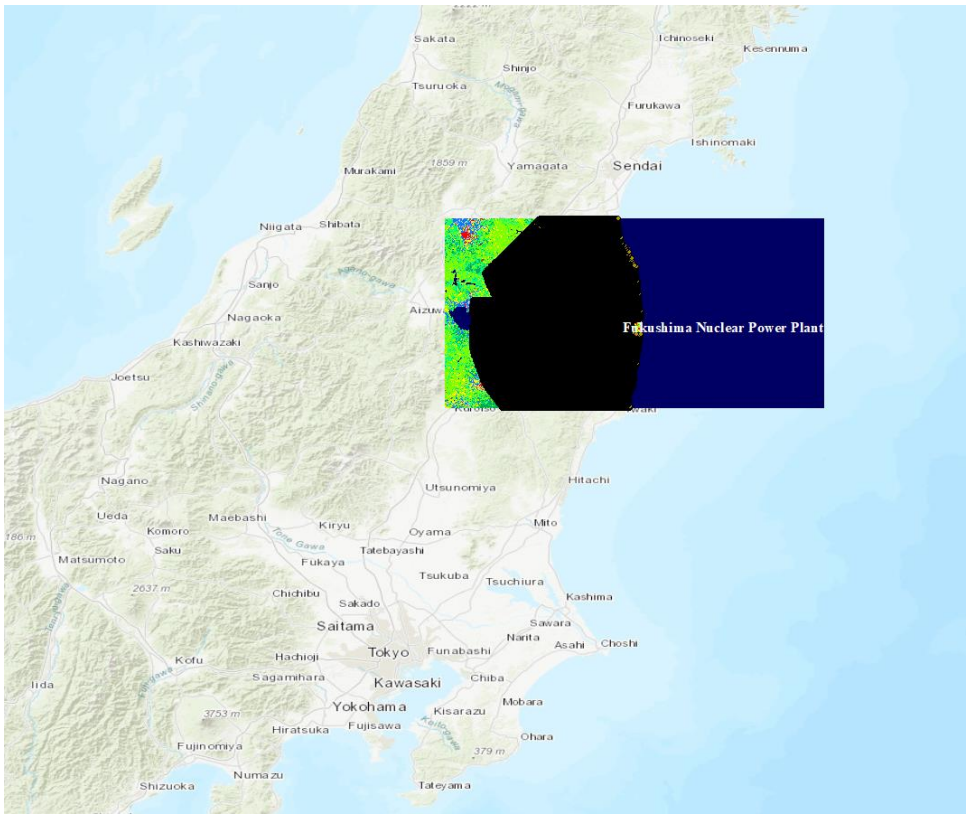

Figure 4.3.1: GIS Data in ArcMap 10.5.1 – Context in Japan (1:3,000,000 scale). This image shows the visible coverage of the analytical data, with the airborne data obscuring the environmental data

to the left of the FDNPP label. Tokyo can be seen in the lower portion of the map and Sendai immediately north of the ROI.

Over a terrain base map of Japan, the environmental data encompasses the region from 139E to 142E and 37N to 38N. The airborne surveys (with data recorded only over land) covered a much larger region, and a subset of each survey was created to adhere to the environmental data, seen in the black cover over the environmental map. With the above figure set at 1:3,000,000 scale, moving down to a 1:125,000 in Figure 4.3.2 allows for a visualization of individual data points:

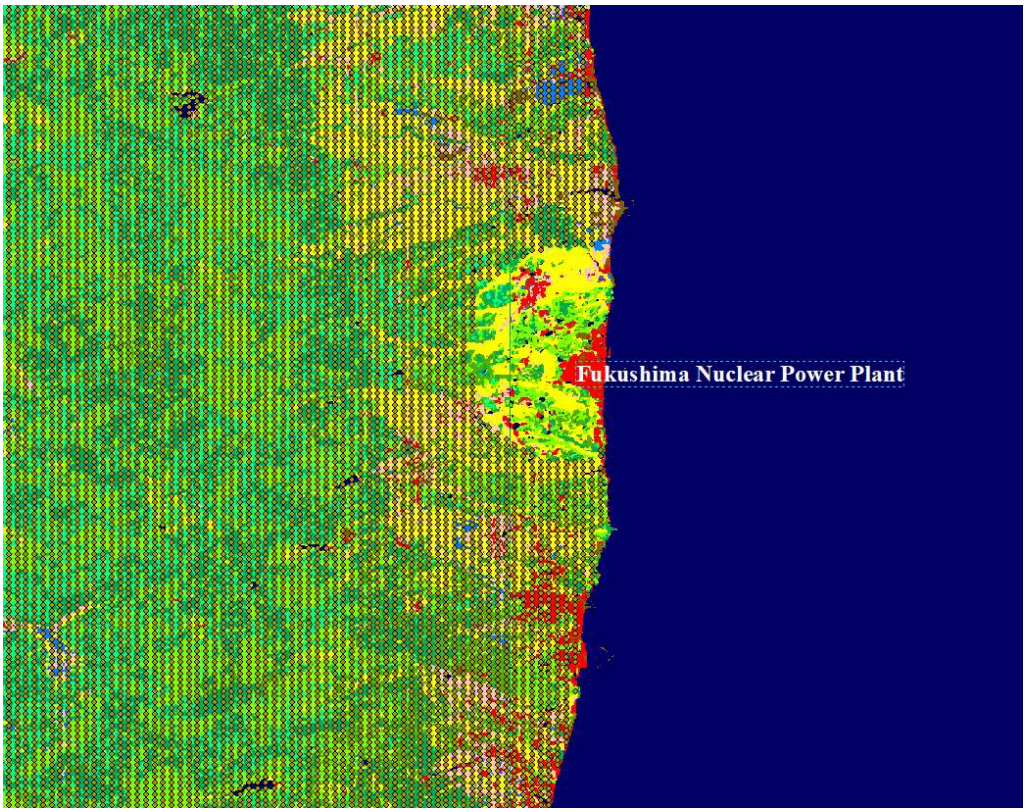

Figure 4.3.2: Close-in Visual of GIS Data – Immediately above FDNPP (1:125,000 scale). The shading over the environment data are the individual measurements from the airborne survey, resolvable at this scale. The exclusion zone had no data recorded in the published air results.

With the data in one frame in ArcMap, comparisons could be made between different environmental factors, with the selected variables of environmental class, elevation, aspect, and slope. Dose Rate Change is used as the primary marker of environmental effects and is defined by:

$$Dose\ Rate\ Change = \left(1.1865 * e^{-(0.158 * 5.55\ years)} * Dose\ Rate\ from\ First\ Airborne\ Survey\right) - (Dose\ Rate\ from\ Eleventh\ Airborne\ Survey$$

Using this equation accounts for the physical decay of the radioisotopes since the first airborne survey and then measures the change from other factors. The time 5.55 years is from the end of the first airborne survey (April 29th, 2011) until the end of the eleventh (November 18th, 2016). With radioactive decay accounted for, further decrease in dose rate must be due to the removal of radioisotopes from the environment. The sample area comprised 116,078 data points, each with attached corrected dose rates, environmental classification (2015 and 2008), elevation, slope, and aspect. For the entire data set, the environment classes are distributed heavily towards forested landscapes, with the other approximately 40% predominantly grass, crop, and rice paddy land (refer to methods for acronym meaning):

Table 4.3.1: Gross Environment Class Counts. These are the descriptive environmental counts for the entire sampled data.

	Unclassified	Water	Urban	Paddy Field	Crop	Grassland	DBF	DNF	EBF	ENF	Bareland	No Data	Total
Counts	0	550	3869	10930	7382	13857	30415	22007	4277	21550	1241	0	**116078**
Percentage	0.00	0.47	3.33	9.42	6.36	11.94	26.20	18.96	3.68	18.57	1.07	0.00	**100**

Graphically, this can best be seen in percentages in a pie graphic like Figures 4.3.3 and 4.3.4:

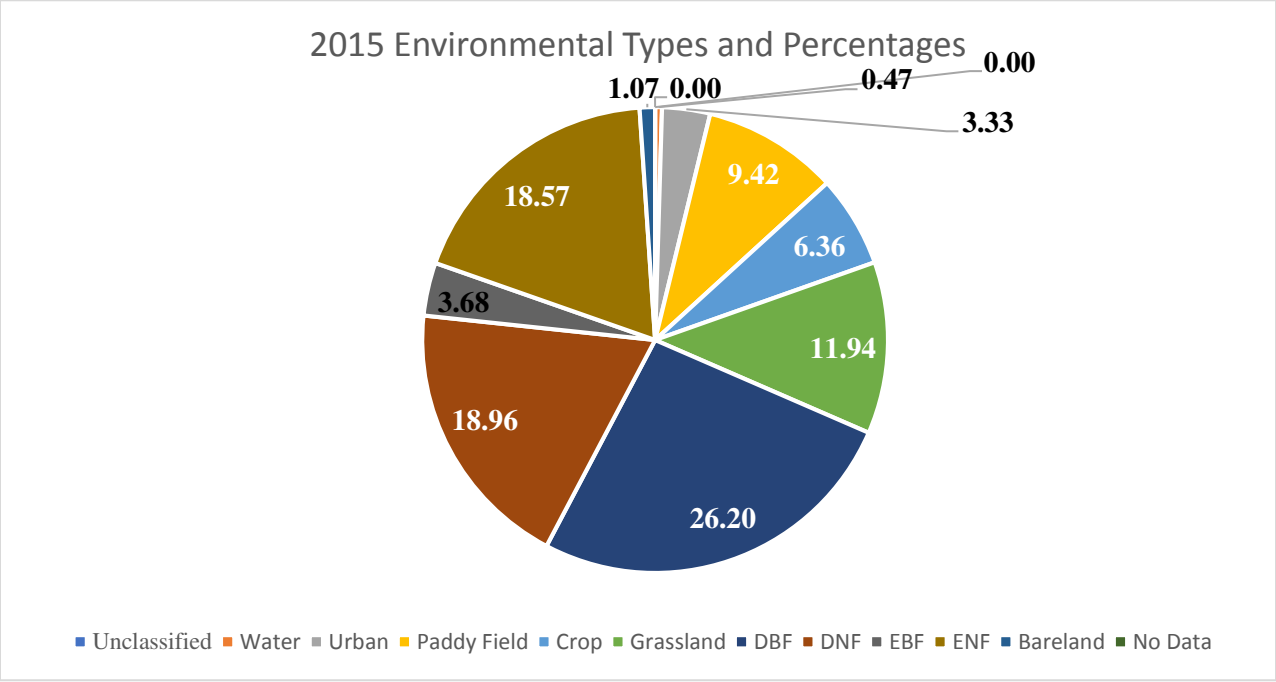

Figure 4.3.3: Environment Types in Sample Area. This represents the environmental breakdown for the entire sample area showing that a majority of the region is covered in forests.

However, considering that most of the contamination was relegated to the initial plume, a subset of the data was created with initial deposition rates above 5 µSv/h. For those regions the environmental characteristics are:

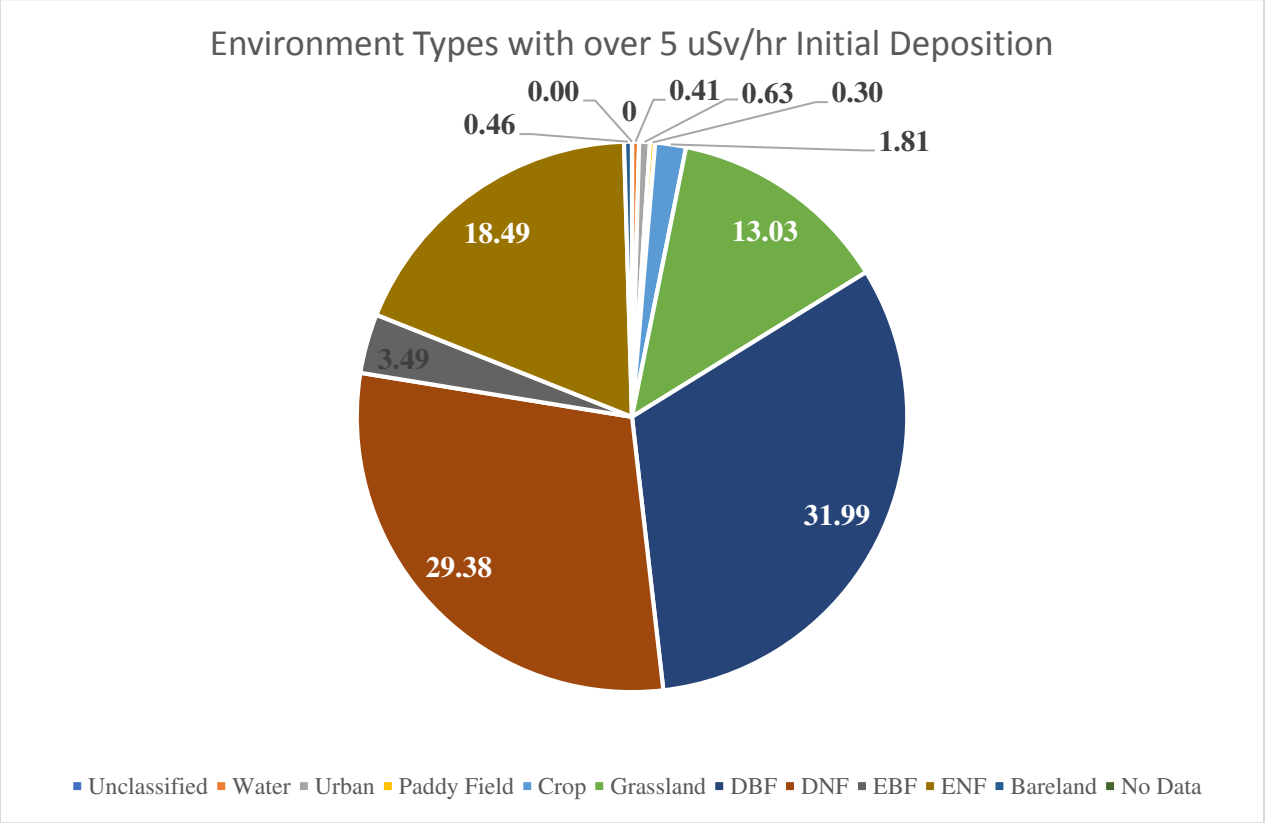

Figure 4.3.4: Environment Types in Area with over 5 µSv/h initial deposition. Due to the plume direction, a greater amount of the land cover, which experienced high deposition, was forested. Urban areas in particular were in reduced proportion.

Since there were no plots of land, which were unclassified or lacking data, those values were excluded from the rest of the analysis. Forests account for over 83% of the analytical area above 5 µSv/h, due to the plume occurring over the mountains in between the FDNPP and the city of Fukushima. This is further seen in a median elevation and slope of 362 m/11 degrees and 437 m/13 degrees for the full and above 5 µSv/h sets, respectively. ANOVA tests were applied to the data (Appendix D) which found Aspect to not impact the mean of the data at the 0.05 alpha level, but found significance in environmental class, elevation, slope, and their interactions.

So, plotting out elevation and slope reveal moderate correlations with changes in dose rate where Fig. 4.3.5 visualizes elevation, 4.3.6 does slope, and 4.3.7 examines their interaction:

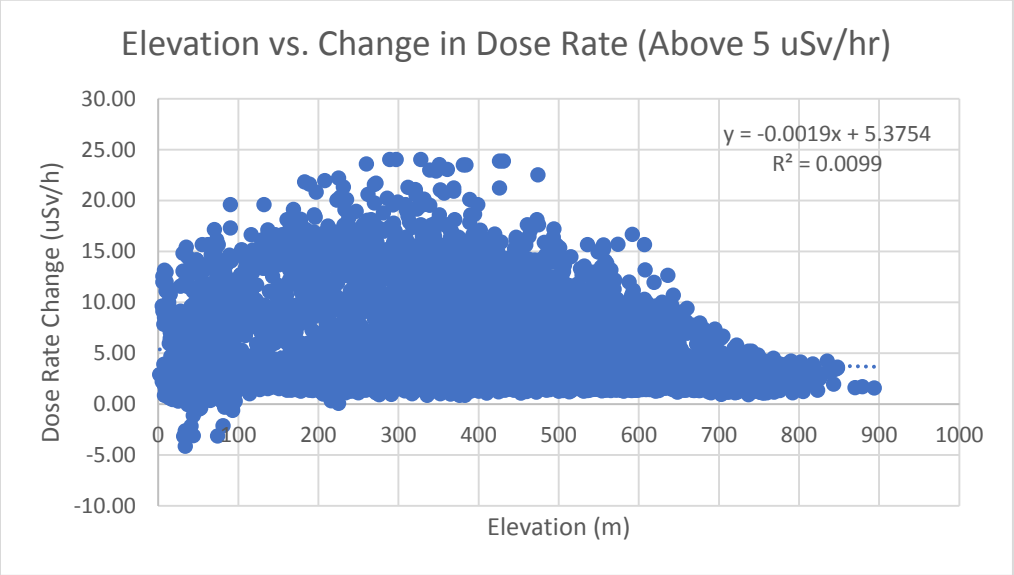

Figure 4.3.5: Elevation effects on Dose Rates above 5 µSv/h. Generally higher radiation doses were found at lower elevation due to both more area at lower elevations and the movement of radioisotopes down slope. The effects of isotope mobility are most directly visualized at the low end of the elevation spectrum, where negative dose rate differences imply an accumulation of radioactive materials through erosive effects.

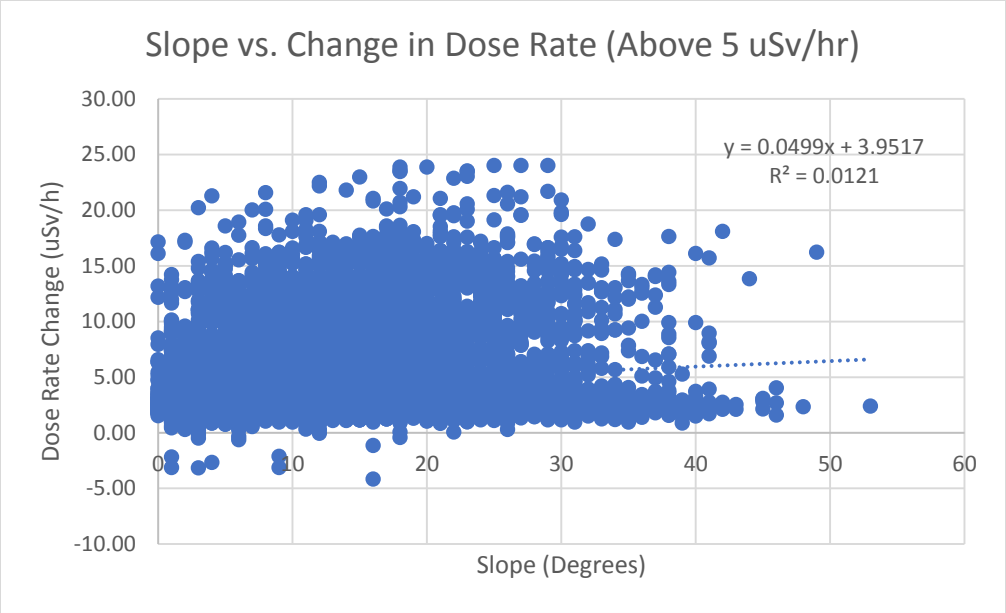

Figure 4.3.6: Slope effects on Dose Rates above 5 µSv/h. Slope varies opposite of elevation, with increasing changes in dose rate with increases in slope, denoting the effect of erosivity in radioisotope movement. Two distinct linear relationships can be discerned at the high end of slope, suggesting confounding factors on slope and dose rate difference.

While slight in overall changes, they are nonetheless statistically significant at the 0.05 level.

Characteristic patterns of radioisotope movement can be seen in the negative values at low elevations and low-grade slopes, indicating deposition from steeper and higher locations.

Slope and elevation have a statistically significant interaction with one another as well, and this has to be controlled as well:

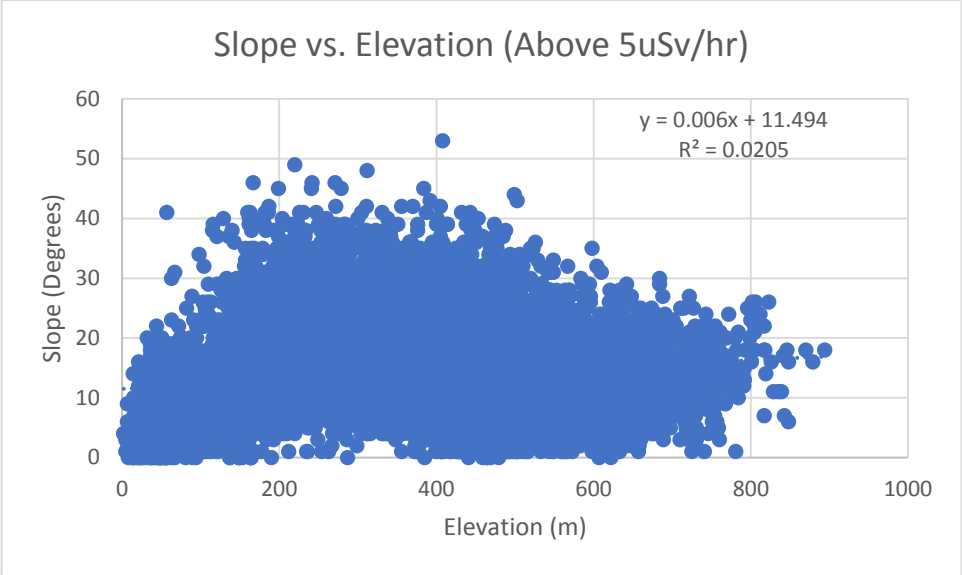

Figure 4.3.7: Slope versus Elevation in regions with initial deposition above 5 µSv/h. As would be expected, slope tends to increase with elevation. There are higher slopes in the 200-400 m elevation range, which could be the result of water ways having greater erosive capacity at those heights.

With these conditions in mind, examining environment types and their relative influence is the focus of this methodological examination. Figure 4.3.8 shows the macroscopic view of radiation dose rate changes by environment type without controlling for other factors:

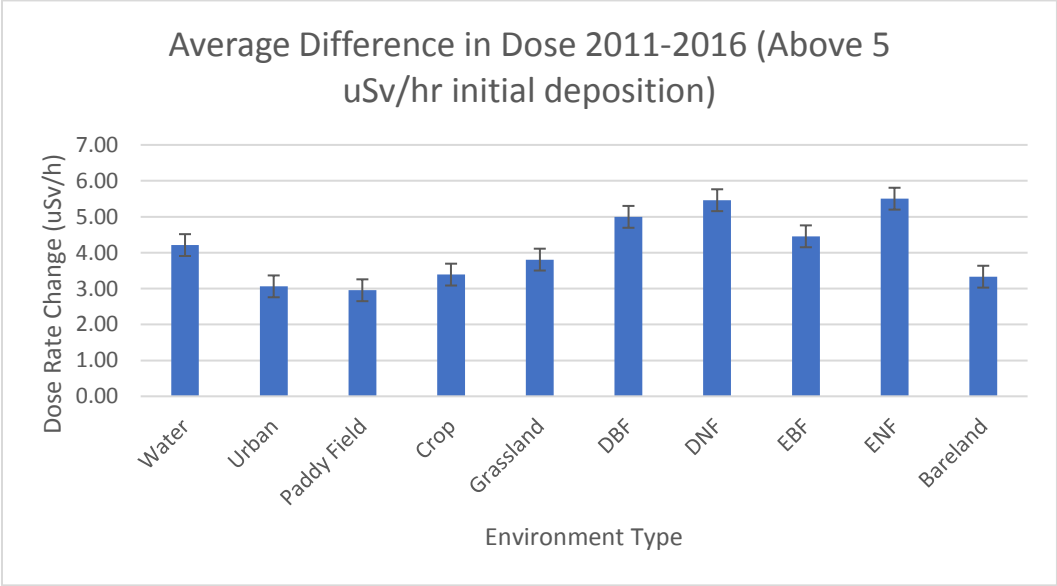

Figure 4.3.8: Average Change in Dose Rates above 5 µSv/h by Environment Type. In regions with high initial dose deposition, and without controlling for various influences, forests show the highest rate of dose rate difference, with paddy fields and urban areas experiencing the lowest. Given that

urban areas have greater runoff potential, and forests are usually retentive, other factors are suggested as influencers.

In totality, for those regions with high initial deposition, Fig. 4.3.8 demonstrates the differences in dose rate by environment type, not controlling for elevation or slope. This represents the macroscopic changes in the Fukushima area for high dose rate conditions. The summary for these data is found in Table 4.3.2, and vy stratifying the data, an understanding of how environmental class particularly affects dose movement can be discerned, given in Table 4.3.2. Given, the available information, points within 95-105 m in elevation, 0-5 degrees slope, and 1.5 μSv/h or less in dose rate were used:

Table 4.3.2: Environment Statistics with Dose Rates above 5 μSv/h. In high initial deposition regions, these are the dose rate differences and other significant environmental factors for each environment type.

	Water	Urban	Paddy	Crop	Grassland	DBF	DNF	EBF	ENF	Bareland
Average	4.21	3.06	2.95	3.39	3.81	5.00	5.46	4.45	5.50	3.33
Std. Dev.	4.50	1.17	1.93	2.23	2.66	4.23	4.19	3.63	4.25	3.07
Median	2.50	2.69	2.61	2.78	2.92	3.05	3.56	2.95	3.67	2.48
Counts	42	64	31	184	1326	3255	2989	355	1881	47
Percentage	0.41	0.63	0.30	1.81	13.03	31.99	29.38	3.49	18.49	0.46
Elevation	190.67	92.00	117.00	216.74	262.24	434.26	439.35	191.39	376.54	268.47
Slope	9.33	3.22	5.71	6.14	6.98	16.32	14.16	14.12	15.20	8.02

Table 4.3.3: Environmentally Stratified Data. The controlled factors are now nearly identical for elevation and within 2 degrees of slope.

	Water	Urban	Paddy Field	Crop	Grassland	DBF	DNF	EBF	ENF	Bareland	Median
Average	0.24	0.31	0.25	0.28	0.26	0.18	0.15	0.25	0.20	0.30	0.25
Std. Dev.	0.11	0.11	0.12	0.12	0.10	0.12	0.10	0.06	0.14	0.13	0.11
Counts	12.00	75.00	65.00	65.00	60.00	18.00	22.00	11.00	16.00	12.00	20.00
Elevation	99.00	99.53	100.32	100.05	99.85	100.56	99.14	98.82	98.63	100.00	99.69
Slope	2.00	1.73	2.58	2.45	2.97	4.06	3.27	3.82	3.31	2.17	2.78

Using the median as the reference point, the classes were compared based on a fractional comparison in Figure 4.3.9, and as a percent deviation from median in Figure 4.3.10:

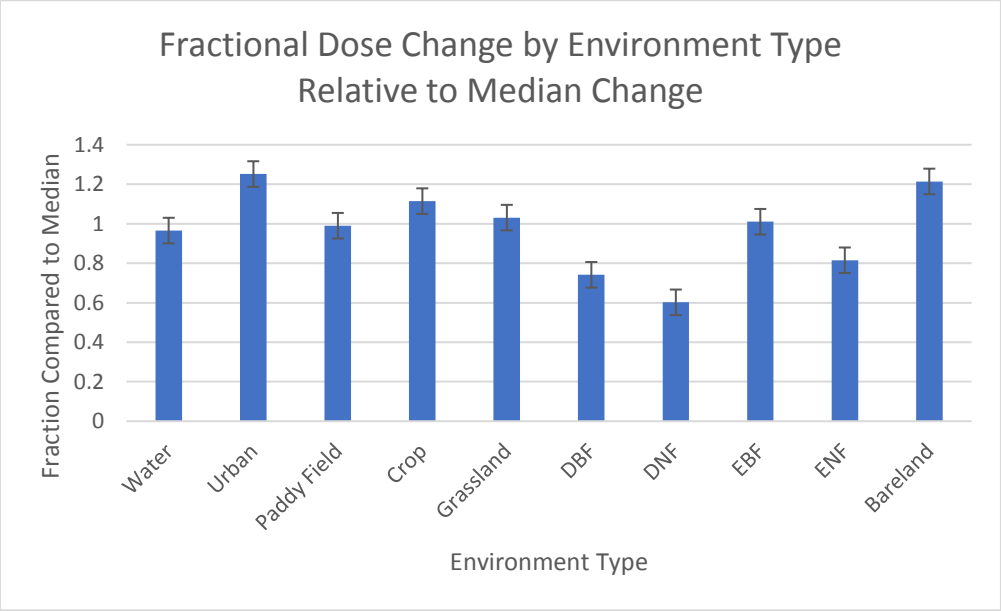

Figure 4.3.9: Fractional Dose Change from Median Change by Environment Type. Here the relative impact of runoff and plant cover becomes apparent. Urban areas now top the list in terms of relative loss of dose rate while the forests, excluding EBF types, retain radioisotopes relative to the median.

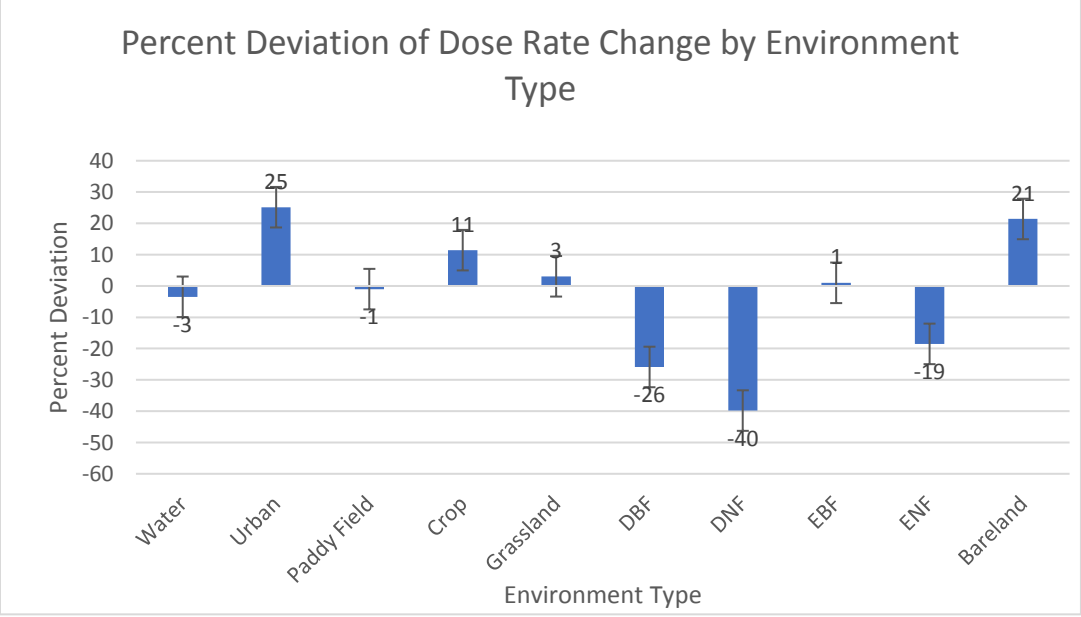

Figure 4.3.10: Percentage Deviation by Environment Type from Median Dose Rate Change. Water, Paddy fields, Grasslands, and EBF's are not significantly distinguishable from the median. Urban,

Cropland, and Bareland all see increased dose rate differences, while DBF, DNF, and ENF forests all seen retention of dose.

These data demonstrate the vastly different rates of radioisotope loss by environment type, when elevation, slope, and dose rate are mitigated. The forests are generally much less erosive and subsequently see a greater retention of radiation relative to urban and bare land areas which lack substantial plant cover.

5 Discussion

Each type of data fills a unique spatial and temporal niche for the purposes of radioecology and risk analysis. Remote sensing offers the greatest consistency in terms of temporal measurements, at the expense of spatial generalizability. Using remote sensing data made the most sense for constructing models on what dose rate reduction over time would look like since it could easily incorporate data from fixed points in time. This makes the exponential models generated for each township have significant predictive value, but necessitates caution when extrapolating outside of the stations' areas. Station density can provide a certain means for interpolating points, but lower data density makes extrapolations more uncertain than with vehicle and airborne surveys. Vehicle surveys have much greater uncertainty in both spatial and temporal data collection. Each of the surveys utilized in this study had differing paths traveled, for different amounts of time, with slightly modified geometries. In examining the correction factors, the intention was to produce a simple method for modeling ambient dose equivalent rates for any vehicle survey. One hope is that with a well-modeled correction, dosimeters could be used in the security vehicles which patrol the exclusion zone to test for vehicular effectiveness with consistent regions and schedules. Airborne surveys have the greatest scope of all, but costs and time limit the availability of these datasets. Further, due to the increased altitude, the potential resolution is minimized as compared with both previous options. Encompassing GIS data presents ample opportunity for the exploitation of airborne surveys for generalizable and thorough analyses of ecologic-radiation interactions.

5.1 Remote Sensing

Based on the data, the station results are best used for tracking long-term temporal trends in very specific regions. Despite being known factors in the movement of radioisotopes, the lack of statistical significance for both precipitation and wind makes it difficult to understand climate impacts on radiation measurements. Based on previous research which demonstrated soil erosivity from storm events, it is unknown why neither precipitation nor wind speed were significantly correlated with dose rate reduction

(Laceby et al., 2016). However, based on the results and the consistent data, the focus was on creating a model to estimate when the towns would be suitable for year-round habitation again. For this reason, the ICRP recommendation of 1 mSv effective dose in one year was chosen as the reference level at which protection measures are likely not justifiable. In line with ICRP recommendations, the reference levels were assumed to be for an existing exposure situation, since under the IAEA safety standards, this is "a nuclear or radiological emergency, after an emergency has been declared to be ended. . ." (IAEA, 2014). The reference levels act to provide operational boundaries for when protective measures may be considered "justifiable." Above 20 mSv/y, actions are always justifiable, but anything below that could provide a situation in which residents chose to return. Japan's scientists should engage in public discourse with the government and citizens about what levels returning members of the public would find appropriate. Joint work with international organizations like the IAEA or ICRP could help assuage the distrust which has formed between the public and government/TEPCO officials as well.

While the accelerated decrease in dose rate is statistically significant relative to physical decay alone, it is not possible to determine causality based on these data. There is no manner to separate out intervention tactics unless specific days of work in the immediate vicinity of the stations could be found.

Other potential sources of uncertainty in using publicly available data are detector maintenance. Since the detectors are maintained by the Japanese Nuclear Regulatory Agency, it would likely be safe to assume that at least yearly calibration was conducted to ensure continuity of measurement. Since the days used in the calculation of the models was the same across each year and included all stations, the detectors should be in at least similar points of functioning for each time point. Further, the mix of stations overall should help maintain a steady average, even if individual measurements vary. In the absence of calibration dates, measurement uncertainty cannot be explicitly excluded, however, and the models provided are merely strong estimates as to the progression of dose rate loss in the region. Total regional weather data sets like what NOAA provides for the United States would be ideal. Precipitation and wind data are both subpar for use in this analytical framework but were the best found for this study. Both are based on monthly

averages for Namie weather station. Stations were excluded in the Namie area that were not in the same general ecological area, predominantly being below the foothills of the surrounding mountains, around the township itself. This was done to control for the variation in precipitation based on the environmental types. Since the consistency of rain patterns cannot be understood without significant amounts of data, the assumption was made that the average among all the stations in the town would be comparable to the weather station. As with precipitation, mean wind speed is not able to properly account for the impact of extreme weather events like cyclones which likely contribute a significant portion of soil transport effects. Maximum wind speed somewhat shows the impact of cyclones by having a greater correlation with precipitation and having more similar seasonality. However, given the visible relationship in these data, precipitation would be acting against wind effects during storms, potentially mitigating this confounding factor. Further research is suggested into these interactions.

5.2 Vehicle-Borne Surveys

Vehicle survey results were kept to the most conservative outcomes due to continuing concern about the potential to correct the data to outside dose rates. Model variability is still the greatest challenge in accounting for the shielding impacts of the car. The variation implies some inherent uncertainty that is not controlled for in the data, and a lack of consistent documentation for the vehicle surveys is a weakness in the analysis. As could be expected, the correction is not large, increasing the measured dose rate by 31% (1.31x) in the averaged model. For practical use, the y-intercept was excluded for two reasons: given the units, 0.715 represents μSv/h and setting that as a minimum would skew the low dose values too high for accurate surveys, and second, that leaving 1.31 as a single factor would make a simple “rule of thumb.” Simplicity is a strength when trying to disseminate information for the use of lay citizens, workers, and government officials. While lacking in some accuracy of other numerical models, there are few more understandable equations than linear ones.

In including air survey results, comparisons as seen in previous research were attempted to relate vehicle data to more generalized measurements (Wainwright et al., 2017, 2018). Similar effects were seen where

the vehicle results generally trend exactly along with airborne results, and the average of the vehicle survey corresponds to the airborne survey. Since the airborne surveys are the average of 100x100 m^2 squares, it would be expected for the vehicle data to follow this trend. Greater variation is seen in the vehicle, which is its relative strength of doing those kinds of surveys, which can better target areas of concern for potential treatment and happen at a much greater velocity than walking surveys, which have the greatest resolution.

Developing a more consistent methodology in placement of detectors and more consistent surveys times for the vehicle surveys will be a critical advancement in this evaluation. Determining the relative benefits of simple versus more complex models should be investigated as well, both at a technical and end-user level. Further, the last survey was weighted more heavily than the other surveys due to the distance from stations in the other studies. Previous studies were evaluated after being conducted, while the last study on August 4th, 2017 was conducted for the express purpose of evaluating the similarity between vehicle measurements and the stations. Other surveys were included due to the similarity in corrections and to the increase the overall amount of data used in analysis to reduce standard error in measurements.

5.3 Airborne Analysis

Establishing a methodology for combining environmental data was the essential component of the last phase of analysis. Measurements based on the airborne dose rates were intended to be compared to environmental factors since this offered the largest and most generalizable set of data for comparison. While other methods have looked at dose rate reductions in GIS format, they usually are done with a focus only on dose rate, or with a smaller set of data (Saito et al., 2015; Wainwright et al., 2018). This allows for the visual analysis of data in terms of data availability and easy accessibility when exported into a spreadsheet. Any number of factors with data available could be incorporated into the analysis, but slope, elevation, aspect, and environment type were hypothesized as the dominant potential variables. Measurements focusing on initial dose rates in 2012 of above 5 μSv/h to look within the deposition plume. Due to the many variables, stratification was chosen as the means to separate variables from one

another. These first analyses effectively separated by location, visible in the environmental composition of the total set versus those above 5 µSv/h, the latter being more heavily forested and mountainous. This was one factor which helped reduce concerns for immediate and long-term doses to residents. In this subset, elevation, slope, and their interaction were found to have significant effects on the dose rate mean based on ANOVA, which while difficult to discern in graphic form was statistically measurable. Through the graphs, the general trend of radioisotopes to trend from high to low elevation is apparent, especially in the negative (therefore increasing) values below 100 m in elevation. However, based on the correlation, dose rate loss increases as elevation changes, so another factor must be confounding. Slope displays the expected trend, with greater differences in dose rates with steeper slopes, denoting increased rates of soil movement. Slope and elevation are themselves related, with steeper slopes as elevation changes. Looking at the high dose rate data without any further stratification, the forested regions have the highest rate of radiation dose loss. Given previous research about plant uptake of radiation and the reduced rates of erosivity in areas with plant cover, environmental data was stratified from other factors. Initial analysis of the summary statistics for the regions above 5 µSv/h to the confluence of environmental factors on reducing dose rates. All of the forested regions have an average of 10 more degrees of slope and, excluding EBF forest types, are above 100 m in elevation.

Stratifying for dose rate, elevation, and slope resulted in the ability to examine each type of environment by dose rate difference from 2012 to 2016. This produced expected differences based on unique class differences when compared to the median dose difference. Urban and Bareland (a broad term, but critically, lacking major plant cover) showed the greater decreases in dose rate, as the radioisotopes should be most mobile without plant uptake and in poor or hard substrates. Forests, showed a general trend towards retention of isotopes, most likely though a myriad of factors including soil retention, greater soil depth, and uptake. It is unknown why the broad-leafed evergreens (EBF) displayed a noticeably distinct retention from other forests. Water, Paddy Fields, Grasslands, and EBF's were not significant in their deviations from the median. Cropland differences, while variable by plants, would likely differ from

grasslands by effort placed into decontamination. Due to the need to have flooded paddies, the environmental similarities between water and paddy field locations could explain the nearly indistinguishable difference values, with any contaminated soil retention likely due to sedimentation of eroded particles. This value would be expected to be variable throughout the year with changing erosivity rates, but further data will be required to separate these conditions.

One of the major challenges with these data sets is the difference in resolution in the data sets. The airborne survey data was averaged in a 100 x 100 m^2 square, slope, aspect, and elevation were 30 x 30 m^2, and the environment class was 10 x 10 m^2. Dose rates are representative of a much larger area than the other data since they are from airborne data, and this introduces uncertainty about the relation between dose rate changes and other factors more so than other measures. As detailed in Appendix C, the environmental class data are based on satellite data quantified through computer algorithms and are not perfect. The most recent data set had a measured accuracy of 80% based on a sample of sites, manually checked by teachers and other trained individuals. While this is better than the previous classification, 55% of sites changed classification from the 2008 data set to the 2015 version. While not inherently a flaw in the data, the variability between these two versions implies caution about the generalizability of this data over a period beyond several years. Research into why these environmental changes occurred is recommended. While many dominant factors in the environment which could affect dose rate changes are included, this is certainly not a comprehensive list and further research expanding into potential variables is suggested. This research lacks the ability to confer causality for these factors on the differences in dose rates and is meant to suggest avenues of further research or inform about current conditions.

6 Conclusion

The accident at the Fukushima Dai-Ichi Nuclear Power Plant will linger in the Japanese psyche for many years to come, and will persist among the residents for decades until the dose rate increases are immeasurable. However, even without detection, memories of the disaster will persist. Improving the understanding of how current means of measurements can be used to better create models and produce accurate information is essential for scientific research and maintaining public trust and comfort. Remote sensing stations have the greatest temporal consistency and should be expanded in regions with low information to allow for better long-term tracking of dose rates as they present an excellent opportunity for localized analysis of changes and creating strong temporal models. Vehicle surveys offer great potential in terms of long-term data collection with little investment cost and higher spatial variability. More work must be done to accurately understand the shielding impact of vehicle sidings on detectors, but based on this research, easy-to-use models are within reach which could offer a simple means of providing accessible information. Finally, GIS offers the most expansive and analytical means of evaluating multiple factors on radiation dose rate changes over time. Airborne surveys proved to be the most useful across the entire region, but any type of data could be paired with these methods. This could allow analysis of a multitude of resolutions based on available data and present future opportunities for more granular examinations. For the sake of former residents, and for maintaining high standards for the measurement of radiation, research must continue to be conducted in the Fukushima area, and education provided to citizens based on the results to help increase the understanding of radiation from academia, to the government, and most importantly, to the public.

References

Andoh, M., Nakahara, Y., Tsuda, S., Yoshida, T., Matsuda, N., Takahashi, F., … Saito, K. (2015). Measurement of air dose rates over a wide area around the Fukushima Dai-ichi Nuclear Power Plant through a series of car-borne surveys. *Journal of Environmental Radioactivity*, *139*, 266–280. https://doi.org/10.1016/J.JENVRAD.2014.05.014

Braun, M. (2011). *The Fukushima Daiichi Incidient*.

Evrard, O., Laceby, J. P., Onda, Y., Wakiyama, Y., Jaegler, H., & Lefèvre, I. (2016). Quantifying the dilution of the radiocesium contamination in Fukushima coastal river sediment (2011–2015). *Scientific Reports*, *6*(1), 34828. https://doi.org/10.1038/srep34828

GE. (2011). *ENCLOSURE 2 BWR MARK I AND MARK II CONTAINMENT REGULATORY HISTORY*. Washington, D.C. Retrieved from https://www.nrc.gov/docs/ML1232/ML12326A344.pdf

Hasegawa, A., Tanigawa, K., Ohtsuru, A., Yabe, H., Maeda, M., Shigemura, J., … Chhem, R. K. (2015). Health effects of radiation and other health problems in the aftermath of nuclear accidents, with an emphasis on Fukushima. *The Lancet*, *386*(9992), 479–488. https://doi.org/10.1016/S0140-6736(15)61106-0

IAEA. (2014). *IAEA Safety Standards*. Vienna. Retrieved from http://ec.europa.eu/dgs/communication/services/visual_identity/index_en.htm

Ishihara, M. (2014). Time Variation and Strength Distribution of Air Dose Rate in Fukushima. *Health Physics*, *106*(5), 558–564. https://doi.org/10.1097/HP.0000000000000043

Konoplev, A. V., Golosov, V. N., Yoschenko, V. I., Nanba, K., Onda, Y., Takase, T., & Wakiyama, Y. (2016). Vertical distribution of radiocesium in soils of the area affected by the Fukushima Dai-ichi nuclear power plant accident. *Eurasian Soil Science*, *49*(5), 570–580. https://doi.org/10.1134/S1064229316050082

Laceby, J. P., Chartin, C., Evrard, O., Onda, Y., Garcia-Sanchez, L., & Cerdan, O. (2016). Rainfall erosivity in catchments contaminated with fallout from the Fukushima Daiichi nuclear power plant accident. *Hydrol. Earth Syst. Sci*, *20*, 2467–2482. https://doi.org/10.5194/hess-20-2467-2016

NEI. (2016). *National Public Opinion Survey - Nuclear Energy 2016*. Chevy Chase. Retrieved from https://www.nei.org/CorporateSite/media/filefolder/resources/reports-and-briefs/national-public-opinion-survey-nuclear-energy-201610.pdf

NPA. (2018). *Police Countermeasures and Damage Situation associated with 2011Tohoku district - off the Pacific Ocean Earthquake*. Tokyo. Retrieved from https://www.npa.go.jp/news/other/earthquake2011/pdf/higaijokyo_e.pdf

NRC. (2011). *Mark I Containment Report PURPOSE PERFORMANCE OF MARK I CONTAINMENTS AT FUKUSHIMA DAIICHI*. Retrieved from http://files.gereports.com/wp-content/uploads/2011/10/NEI-Mark-1-White-Paper.pdf

Povinec, P. P., Hirose, K., & Aoyama, M. (2013). Introduction. In *Fukushima Accident: Radioactivity Impact on the Environment* (pp. 1–30). Waltham, MA: Elsevier. https://doi.org/10.1016/B978-0-12-408132-1.00001-2

Reconstruction Agency. (n.d.). The Status in Fukushima. Retrieved June 21, 2018, from http://www.reconstruction.go.jp/english/topics/2013/03/the-status-in-fukushima.html

Saito, K., Tanihata, I., Fujiwara, M., Saito, T., Shimoura, S., Otsuka, T., … Shibata, T. (2015). Detailed deposition density maps constructed by large-scale soil sampling for gamma-ray emitting radioactive nuclides from the Fukushima Dai-ichi Nuclear Power Plant accident. *Journal of Environmental Radioactivity*, *139*, 308–319. https://doi.org/10.1016/J.JENVRAD.2014.02.014

Satoh, D., Furuta, T., Takahashi, F., Endo, A., Lee, C., & Bolch, W. E. (2014). *Calculation of dose conversion coefficients for external exposure to radioactive cesium distributed in soil*. https://doi.org/10.11484/JAEA-RESEARCH-2014-017

Steinhauser, G., Brandl, A., & Johnson, T. E. (2014). Comparison of the Chernobyl and Fukushima nuclear accidents: A review of the environmental impacts. *Science of The Total Environment*, *470–471*, 800–817. https://doi.org/10.1016/J.SCITOTENV.2013.10.029

Takahara, S., Watanabe, M., Hirouchi, J., Iijima, M., & Munakata, M. (2018). Dose-reduction Effects of Vehicles against Gamma Radiation in the Case of a Nuclear Accident. *Health Physics*, *114*(1), 64–72. https://doi.org/10.1097/HP.0000000000000729

Tanabe, F. (2012). Analyses of core melt and re-melt in the Fukushima Daiichi nuclear reactors. *Journal of Nuclear Science and Technology*, *49*(1), 18–36. https://doi.org/10.1080/18811248.2011.636537

Tanaka, K., Sakaguchi, A., Kanai, Y., Tsuruta, H., Shinohara, A., & Takahashi, Y. (2013). Heterogeneous distribution of radiocesium in aerosols, soil and particulate matters emitted by the Fukushima Daiichi Nuclear Power Plant accident: retention of micro-scale heterogeneity during the migration of radiocesium from the air into ground and rive. *Journal of Radioanalytical and Nuclear Chemistry*, *295*(3), 1927–1937. https://doi.org/10.1007/s10967-012-2160-9

Wainwright, H. M., Seki, A., Chen, J., & Saito, K. (2017). A multiscale Bayesian data integration approach for mapping air dose rates around the Fukushima Daiichi Nuclear Power Plant. *Journal of Environmental Radioactivity*, *167*, 62–69. https://doi.org/10.1016/J.JENVRAD.2016.11.033

Wainwright, H. M., Seki, A., Mikami, S., & Saito, K. (2018). Characterizing regional-scale temporal evolution of air dose rates after the Fukushima Daiichi Nuclear Power Plant accident. *Journal of Environmental Radioactivity*, *189*, 213–220. https://doi.org/10.1016/J.JENVRAD.2018.04.006

Yoshida, N., & Kanda, J. (2012). Geochemistry. Tracking the Fukushima radionuclides. *Science (New York, N.Y.)*, *336*(6085), 1115–1116. https://doi.org/10.1126/science.1219493

Appendix A

Stations used for Remote Sensing and Vehicle Analysis:

Okuma Stations

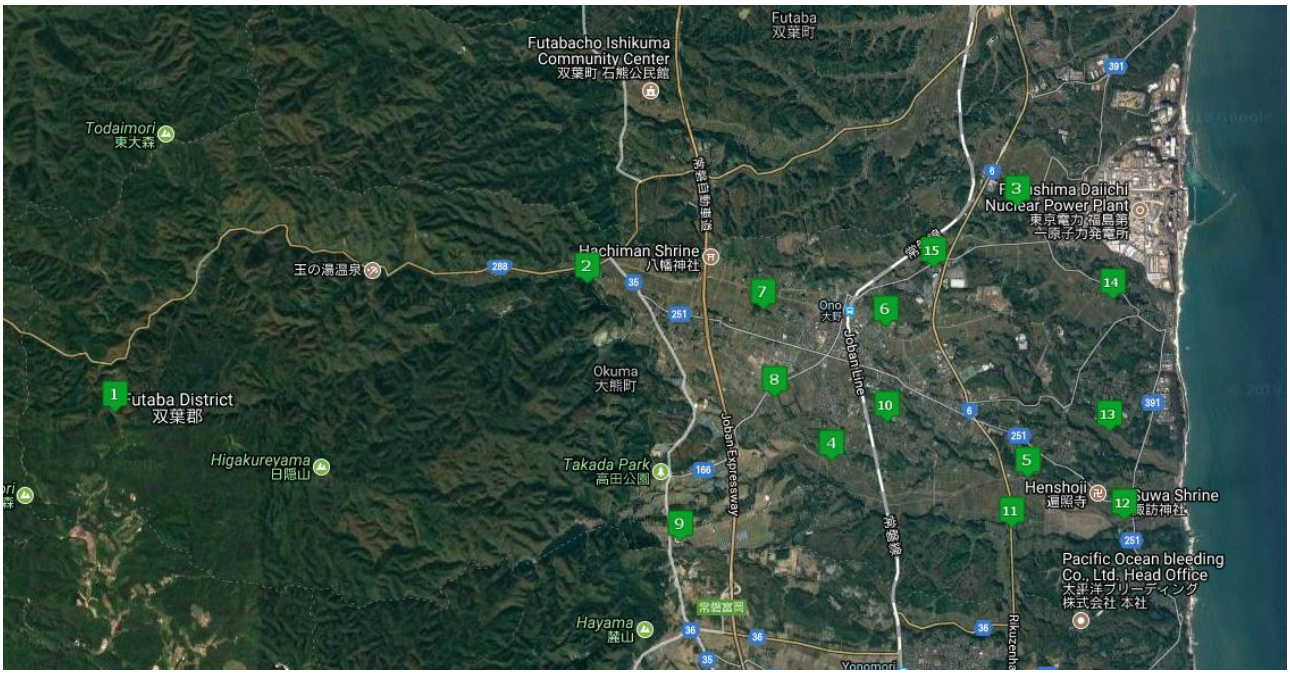

Figure A.1: Okuma Stations on April 1st, 2012

Table A.1: GIS Coordinates of Okuma Stations

Station	Latitude	Longitude
1	37.408833	140.997067
2	37.40667	140.98048
3	37.383912	140.943535
4	37.399025	140.873147
5	37.414508	140.94467
6	37.423708	141.009657
7	37.39319	140.981448
8	37.391198	141.011293
9	37.40928	140.989802
10	37.411318	140.971233
11	37.400883	140.972908
12	37.383523	140.95867
13	37.397872	140.989943
14	37.385143	141.008842
15	37.386183	141.02588
16	37.396798	141.023583

17	37.412535	141.024005
18	37.416338	140.996933

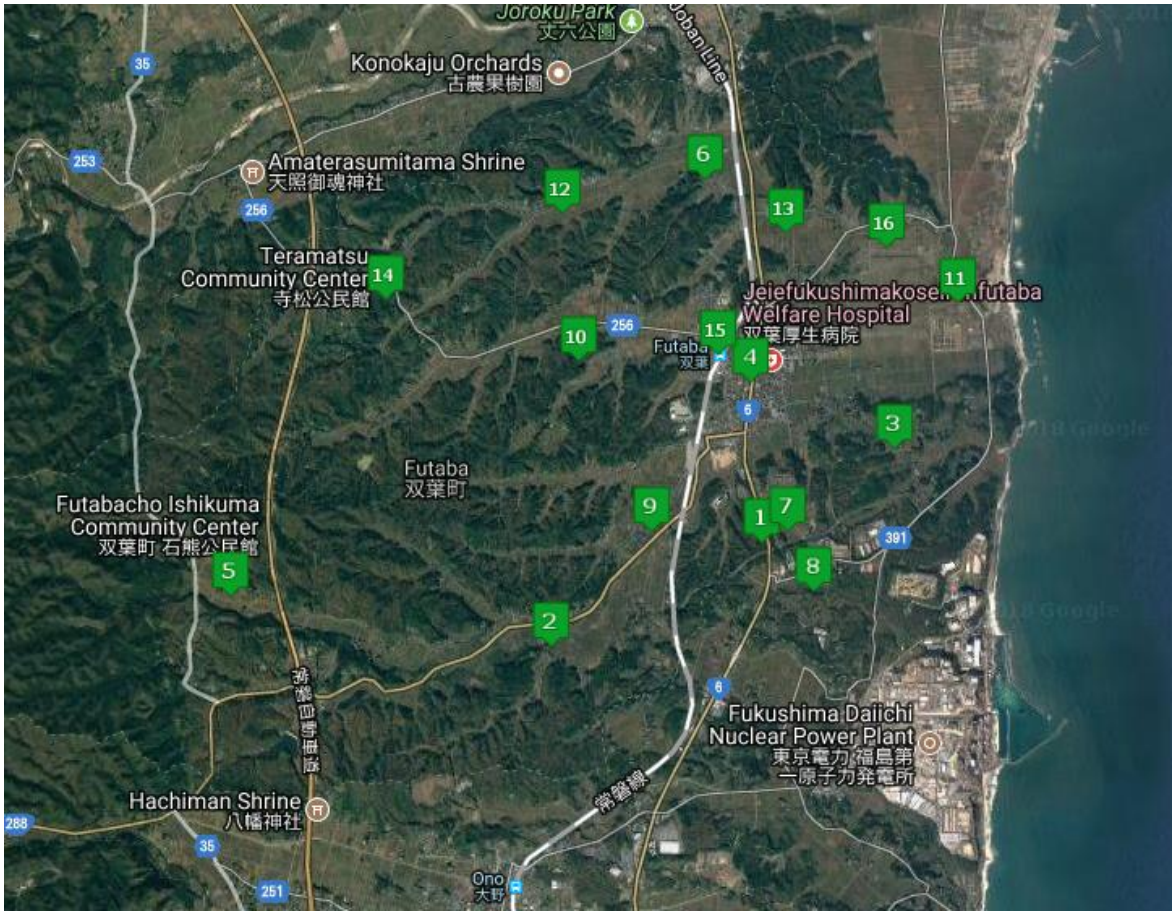

Figure A.2: Futaba Stations on April 1st, 2012

Table A.2: GIS Coordinates of Futaba Stations

Station	Latitude	Longitude
1	37.4401	141.0103
2	37.43139	140.988
3	37.44806	141.0244
4	37.45361	141.0091
5	37.43568	140.954
6	37.47061	141.0044
7	37.44101	141.0131
8	37.43605	141.0159
9	37.44111	140.9986
10	37.45541	140.991
11	37.46032	141.0311
12	37.46784	140.9893

13	37.46609	141.0129
14	37.46056	140.9705
15	37.45598	141.0057
16	37.46494	141.0235

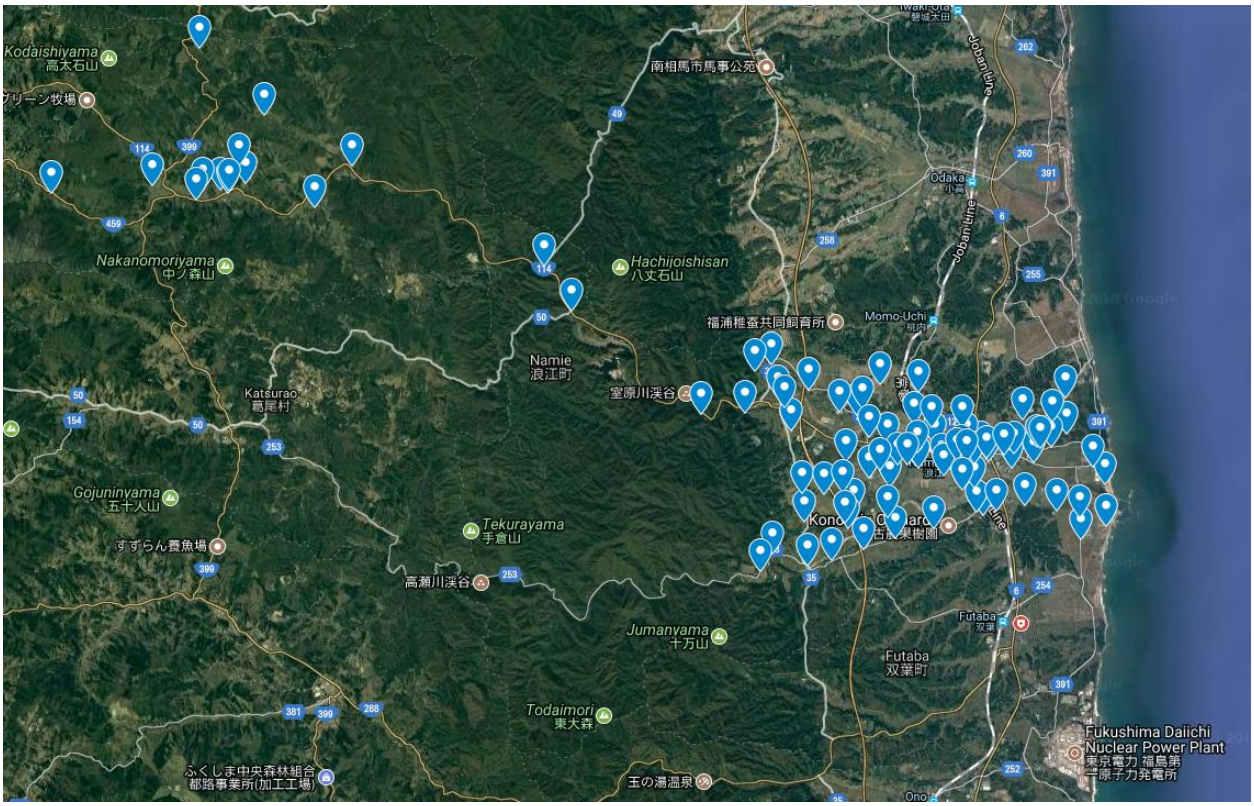

Figure A.3: All Namie Stations on February 1st, 2014

Note: The Namie stations were not numbered due to the technical limitations of Google Maps for icon placement and the much higher number of stations making visual determination difficult.

Figure A.4: Namie Stations used for Analysis, on February 1st, 2014

Table A.3: GIS Coordinates of Namie Stations

Station	Latitude	Longitude
1 (excluded)	37.5609	140.7605
2 (excluded)	37.56267	140.7685
3	37.48022	140.9992
4 (excluded)	37.56093	140.7553
5	37.49565	140.9987
6	37.48137	141.0223
7	37.49773	140.994
8	37.47427	141.0298
9	37.47963	141.0293
10	37.49243	140.9904
11	37.49355	141.0009
12	37.4977	140.984
13	37.49335	141.0151
14	37.4786	140.9433
15	37.5012	140.9392
16	37.50942	140.9349
17	37.50943	141.025
18	37.47075	140.9333
19	37.48567	140.9425
20	37.47472	140.9719
21	37.51775	140.9329
22	37.51275	140.9669
23	37.50293	140.9776
24	37.50207	140.9926
25 (excluded)	37.56005	140.7629
26 (excluded)	37.5585	140.753
27	37.48955	140.9635
28	37.49252	140.9861
29	37.49473	140.9924
30	37.49195	140.9789
31	37.49207	141.0083
32	37.50203	140.983
33 (excluded)	37.50557	140.9246
34	37.48265	141.0124
35	37.49022	140.987
36	37.49778	140.9692
37	37.5005	141.0253
38	37.48152	140.9588
39	37.49553	141.0089
40	37.4971	141.0207
41	37.48122	140.9972
42 (excluded)	37.56693	140.7665
43	37.48788	141.0372
44	37.51597	140.9277
45	37.48752	140.9701

46	37.47177	140.9617
47	37.50522	140.9599
48	37.47987	140.9695
49	37.48722	140.9965
50	37.49597	140.9786
51	37.4932	140.9965
52	37.50397	141.0118
53	37.49277	140.9723
54	37.4854	140.9495
55	37.49389	140.991
56	37.49722	141.016
57	37.49362	140.9562
58 (excluded)	37.59614	140.7542
59 (excluded)	37.531	140.8705
60 (excluded)	37.50528	140.911
61 (excluded)	37.56699	140.8018
62	37.47693	140.9572
63	37.50586	140.9542
64	37.49457	141.0002
65	37.46654	140.9296
66 (excluded)	37.56071	140.7632
67 (excluded)	37.54209	140.8621
68	37.49368	140.9942

69	37.49282	140.9756
70	37.48662	140.9928
71	37.48135	141.0034
72	37.49518	141.0057
73	37.49689	141.0169
74	37.50334	141.0208
75	37.49233	141.0335
76	37.47766	141.0376
77	37.4914	140.9668
78	37.469	140.952
79	37.48614	140.9551
80	37.47851	140.956
81	37.47697	140.9836
82	37.50706	140.9371
83	37.51127	140.9448
84	37.5067	140.9614
85	37.49976	140.9634
86	37.51068	140.9791
87 (excluded)	37.56012	140.7076
88 (excluded)	37.56188	140.7394
89 (excluded)	37.55654	140.79
90 (excluded)	37.57932	140.7744
91	37.46769	140.9442

Table A.4: 140915 Stations

Car Dose Rate	Lat/Long of Station	Outside Dose Rate
5.089	37.38485, 141.00865	6.586
4.815	37.46103, 141.01022	9.522
0.122	37.52071, 140.99768	0.225
0.09	37.52377, 140.99862	0.222
0.0865	37.58457, 141.00901	0.131

Table A.5: 141018_1 Stations

Car Dose Rate	Lat/Long of Station	Outside Dose Rate
2.586	37.40711, 140.95868	2.341
2.712	37.4039, 140.97055	2.893
2.988	37.40566, 140.9745	5.577
3.577	37.40502, 140.97653	3.869
3.717	37.40736, 140.97786	3.656

4.416	37.40681, 140.98495	5.244
2.474	37.40426, 140.9828	1.263
2.724	37.4042, 140.98597	4.118
3.26	37.40766, 140.98325	3.388
4.601	37.38514, 141.00884	6.378
3.894	37.39556, 141.00464	3.284
2.129	37.41115, 140.99693	4.828
10.899	37.40674, 141.01732	11.11
10.476	37.4237, 141.00965	11.096
15.555	37.40928, 141.028	17.04
13.939	37.41625, 140.99698	19.618
7.765	37.41173, 141.00551	9.454
7.425	37.39233, 141.01108	6.08

Table A.6: 141018_2 Stations

Car Dose Rate	Lat/Long of Stations	Outside Dose Rate
2.474	37.40426, 140.9828	1.263
2.724	37.4042, 140.98597	4.118
4.601	37.38514, 141.00884	6.378
2.129	37.41115, 140.99693	4.828
10.899	37.40674, 141.01732	11.11
10.476	37.4237, 141.00965	11.096
15.555	37.40928, 141.028	17.04
7.425	37.39233, 141.01108	6.08

Table A.7: 160301 Stations

Car Dose Rate	Lat/Long of Stations	Outside Dose Rate
5.70667	37.41642, 140.997086	13.523
1.34833	37.411213, 140.99707	3.744
1.801667	37.409, 140.997009	3.419
1.376667	37.395706, 141.004654	2.277
4.34	37.406723, 141.017441	8.406
8.355	37.409248, 141.028168	12.937

Table A.8: 170520 Stations

Car Dose Rate	Lat/Lon	Outside Dose Rate
4.36	37.409462, 141.027	9.177
0.865	37.385109, 141.008636	4.359
1.1025	37.408985, 140.996948	2.653
1.99	37.4067,141.0173	6.382

2.523	37.409,141.03185	6.163
0.18	37.41951, 141.01958	0.52
0.44	37.363239, 141.009506	2.356
0.875	37.395626, 141.004761	1.535
1.122	37.41135, 140.99757	2.948

Appendix B

Methods for Google Earth Engine Data Acquisition

Produced by Danielle Davis

1. In ***Google Chrome***, go to the Google Earth Engine (GEE) Coders web page and log in.
    a. The screen should look similar to what is shown below. We will be using the **SRTM** script

Copy the script into your own GEE folder: (image below)

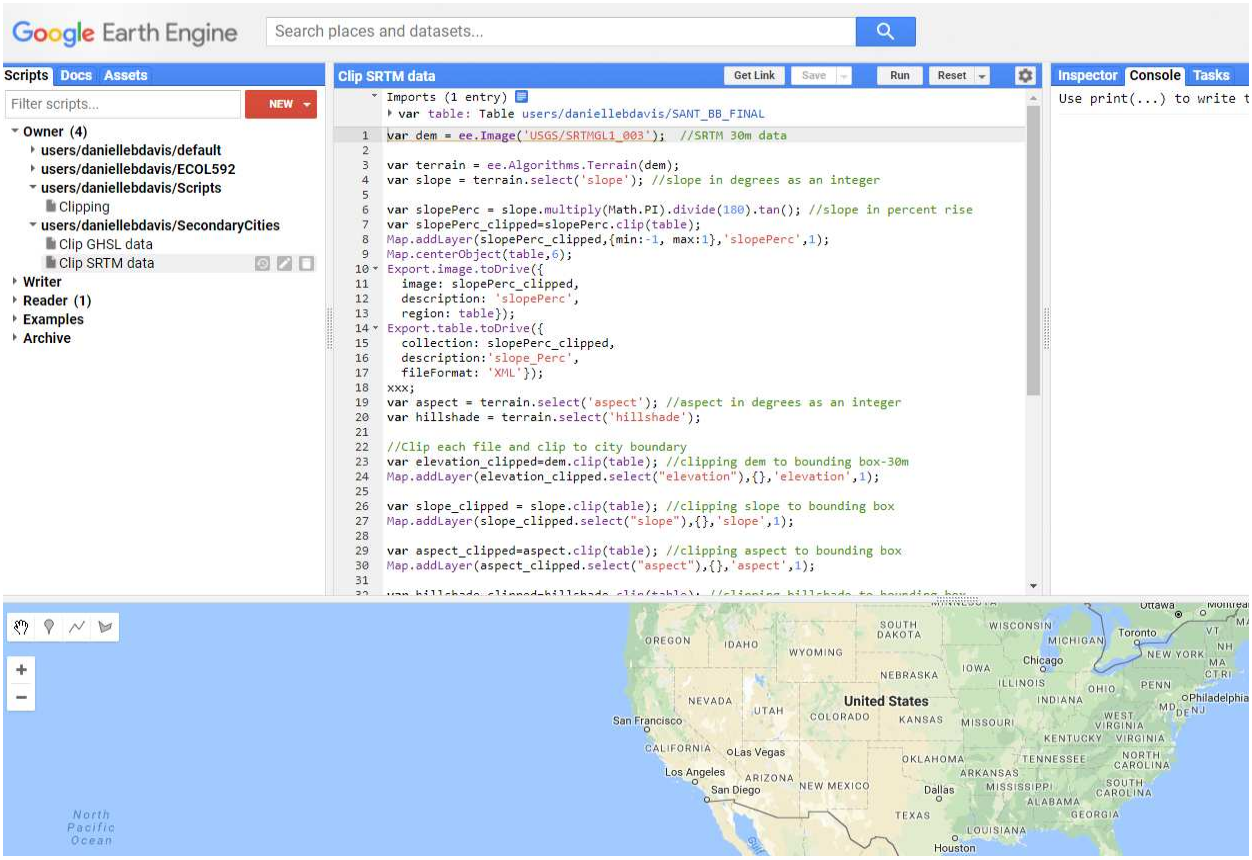

Figure B.1: Screenshot of GEE Page on Initiation

2. In the left panel, be sure the "Scripts" tab is highlighted → click "NEW" → "Repository". Name this repository something relating the 2C

    a. For organizing data in GEE, a folder goes in a repository. Essentially, a repository is a fancy word for folder, but folder is already an option, so Google came up with another term.

b. Right now, the script is under the "Reader" repository in your GEE account as you are pulling it from my GEE account.

3. Copy the script by *clicking and dragging* the script from my repository to YOUR new repository (see image below)

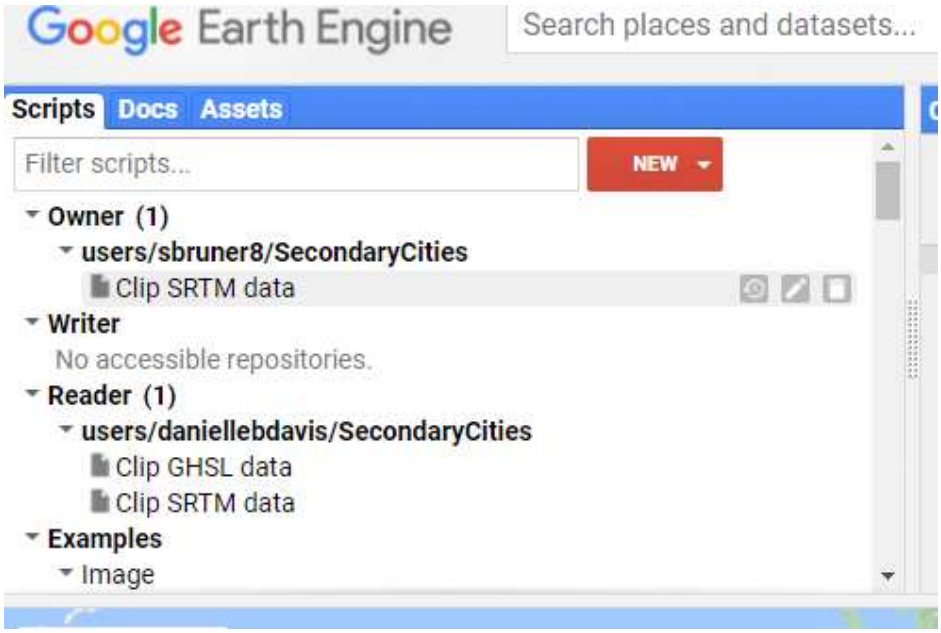

Figure B.2: Script Transfer into own Repository

Import bounding boxes: (see image below)

4. In the left panel, click the "Assets" tab
5. Click "NEW" → choose "Table upload"
    a. In GEE, vector data is called *tables*, and raster data is called *images*
6. Click "Select" → navigate in browser to location of bounding box shapefile → select all the files that create the shapefile → "Open"
7. Rename the file if you wish under "Asset ID" → Click "OK"
    a. It will take 4 to 5 minutes to upload each bounding box. You will see the progress of the upload in the right panel under the "tasks" tab

*After completing this one time, you DO NOT need to reload the bounding box every time. It will permanently exist in your GEE account until you delete it.

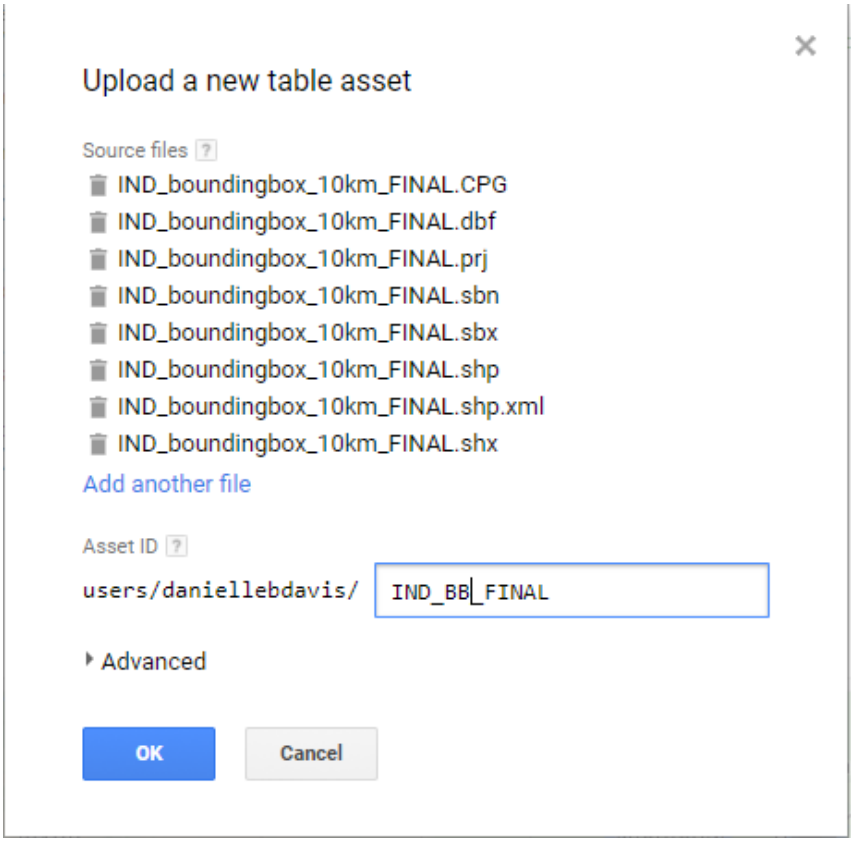

Figure B.3: Bounding Box Import

Clip data types to bounding box:

8. In the scripting panel (the middle panel with the programming), in the very top part of the panel under "Imports", remove any current tables → hover over "**var** table:" → click on the *trash can* to the left

9. In the "Asset" tab in the left panel, hover over bounding box → click to the grey arrow that says "Import into script"

10. In the scripting panel, change the variable name to "table" if the asset imports as something else. See image below for reference of what the window will look like before you run the script

Run the script and export to Google Drive:

11. Push “Run” in the upper right corner of the scripting panel

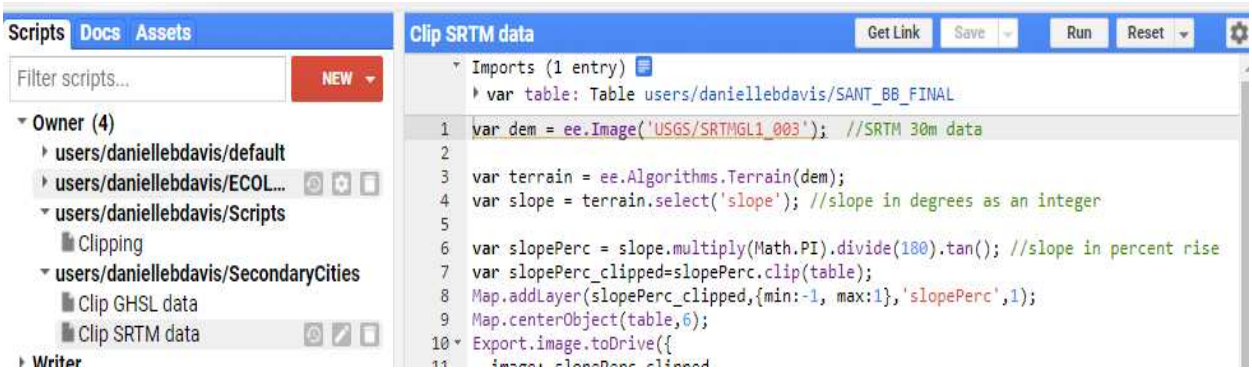

Figure B.4: Initiating Script

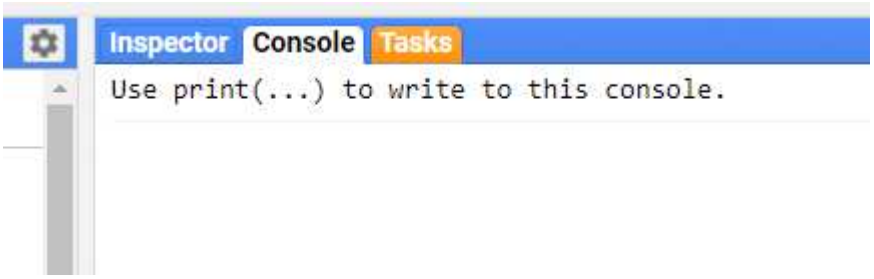

Figure B.5: Active Tasks Tab

a. After the script runs, the “Tasks” tab in the right panel will highlight orange.

12. Click the “Tasks” tab in the right panel
13. Click “RUN” → Change “Resolution” to 30 → type “2C data” in “Data Folder” box → change filename to include the city

14. Repeat step 13 for all SRTM files
15. Go to Google Drive folder and download files

Appendix C

Accuracy of Environmental Classification Data

Table C.1: Confusion Matrix for the 18.03 Data

		Validation											User's accuracy (%)
		1	2	3	Four	Five	6	7	8	9	Ten	TOTAL	
Classified	1	276	1	1	0	0	0	0	1	3	0	282	97.9
	2	3	247	2	7	1	0	0	0	0	35	295	83.7
	3	0	Five	284	Five	1	1	1	0	0	1	298	95.3
	Four	1	3	31	218	26	Four	3	1	1	6	294	74.1
	Five	0	2	6	14	240	14	0	8	0	Five	289	83.0
	6	0	0	0	0	9	236	29	13	11	0	298	79.2
	7	0	0	0	1	Four	twenty four	252	Four	14	0	299	78.6
	8	0	1	0	1	2	15	7	207	49	0	282	73.4
	9	0	0	0	0	1	6	Four	twenty four	264	0	299	88.3
	Ten	15	43	6	14	twenty three	8	3	6	7	161	286	56.3
	TOTAL	295	302	330	260	307	308	299	264	349	208	2,922	- -
Producer's accuracy (%)		93.6	81.8	86.1	83.8	78.2	76.6	84.3	78.4	75.6	77.4	- -	Overall accuracy: 81.6%

Table C.2: Confusion Matrix for the 16.09 Data

		Validation											User's accuracy (%)
		1	2	3	Four	Five	6	7	8	9	Ten	TOTAL	
Classified	1	193	1	1	0	0	0	0	0	0	2	197	98.0
	2	2	222	2	1	0	0	0	0	0	2	229	96.9
	3	1	2	260	18	6	2	0	1	0	1	291	89.3
	Four	1	2	28	76	41	Four	1	9	1	Five	168	45.2
	Five	0	0	Ten	14	42	Four	2	8	0	1	81	51.9
	6	0	1	2	8	Five	74	13	15	13	0	131	56.5
	7	0	0	0	0	1	1	11	0	1	0	14	78.6
	8	0	0	0	0	1	Five	1	32	16	0	55	58.2
	9	1	0	0	1	0	11	Four	30	167	0	214	78.0
	Ten	0	2	1	1	3	0	0	0	0	twenty two	29	75.9
	TOTAL	198	230	304	119	99	101	32	95	198	33	1,409	- -
Producer's accuracy (%)		97.5	96.5	85.5	63.9	42.4	73.3	34.4	33.7	84.3	66.7	- -	Overall accuracy: 78.0%

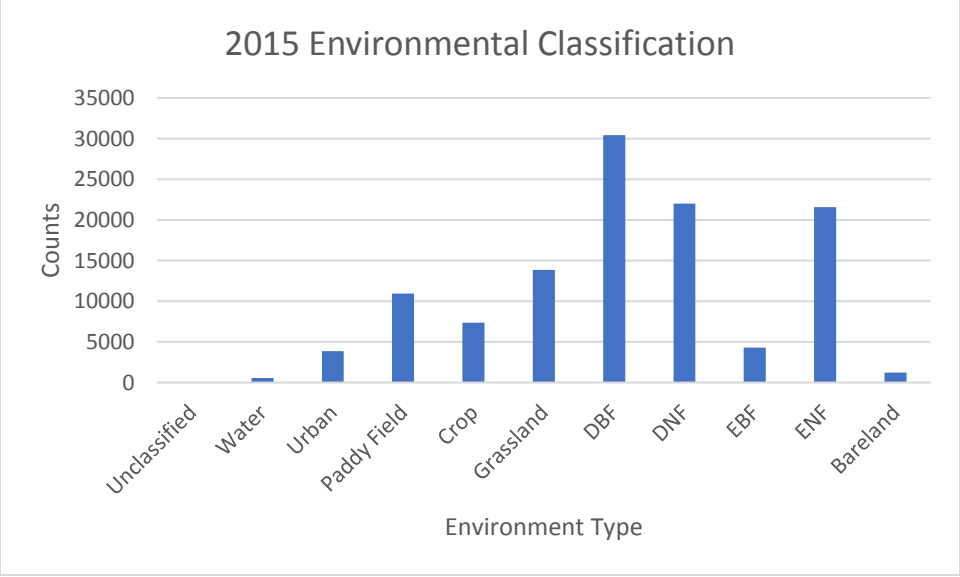

Figure C.1: 2015 Environmental Classification Counts in ROI

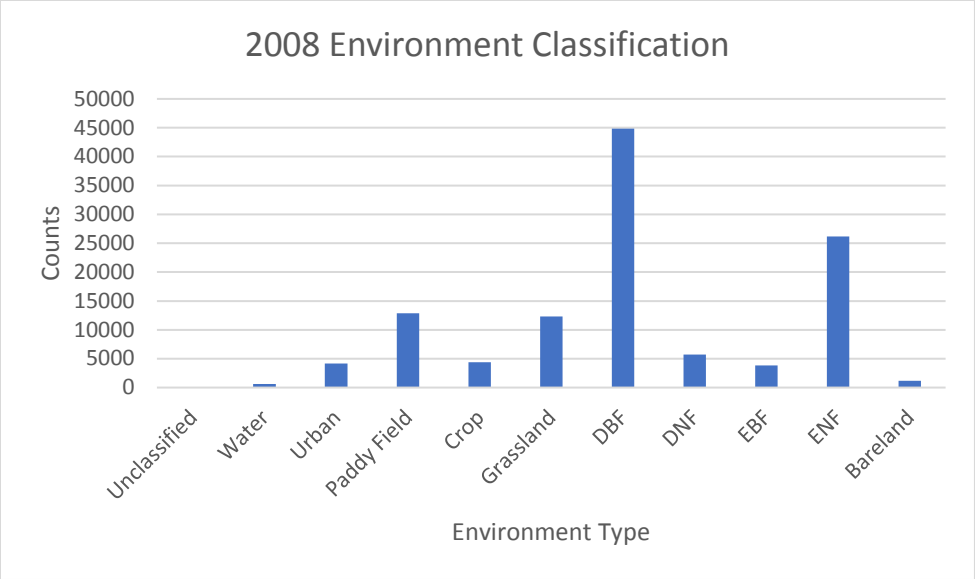

Figure C.2: 2008 Environmental Classification Counts in ROI

Appendix D

Anova Tables

Table D.1 Precipitation and Wind ANOVA Results in R

	Df	Sum Sq	Mean Sq	F value	Pr(>F)
precip	1	0.00198	0.001977	0.477	0.496
avwind	1	0.00272	0.002715	0.656	0.425
maxwind	1	0.00816	0.008163	1.971	0.172
precip:avwind	1	0.00019	0.000190	0.046	0.832
precip:maxwind	1	0.00033	0.000326	0.079	0.781
avwind:maxwind	1	0.00111	0.001111	0.268	0.609
precip:avwind:maxwind	1	0.00554	0.005536	1.337	0.258
Residuals	27	0.11181	0.004141		

Above 5uSv/hr

	Df	Sum Sq	Mean Sq	F value	Pr(>F)
New.Env	1	1762	1762.5	131.189	< 2e-16
Aspect	1	45	45.3	3.369	0.06645
Elevation	1	1803	1802.8	134.190	< 2e-16
Slope	1	1583	1583.0	117.831	< 2e-16
New.Env:Aspect	1	80	80.2	5.966	0.01460
New.Env:Elevation	1	104	103.7	7.717	0.00548
Aspect:Elevation	1	11	11.0	0.815	0.36658
New.Env:Slope	1	11	10.9	0.811	0.36791
Aspect:Slope	1	220	220.0	16.378	5.23e-05
Elevation:Slope	1	1128	1128.5	83.998	< 2e-16
New.Env:Aspect:Elevation	1	5	5.2	0.384	0.53560
New.Env:Aspect:Slope	1	2	1.5	0.115	0.73429
New.Env:Elevation:Slope	1	30	30.4	2.263	0.13252
Aspect:Elevation:Slope	1	1	1.1	0.084	0.77212
New.Env:Aspect:Elevation:Slope	1	31	30.6	2.279	0.13114
Residuals	10158	136470	13.4		

Table D.2: All GIS Data

	Df	Sum Sq	Mean Sq	F value	Pr(>F)
New.Env	1	2065	2064.7	919.13	< 2e-16
Slope	1	807	807.4	359.43	< 2e-16
Elevation	1	757	757.3	337.13	< 2e-16
New.Env:Slope	1	166	165.5	73.69	< 2e-16
New.Env:Elevation	1	126	126.1	56.14	6.81e-14
Slope:Elevation	1	1089	1088.8	484.73	< 2e-16
New.Env:Slope:Elevation	1	60	60.0	26.72	2.35e-07
Residuals	116070	260729	2.2		

Appendix E

Results from Water Sampling

Methods:

I. Environmental Sample Collection

Soil/Sediment samples were collected at the following locations:

Sample collection consisted of using clear LDPE plastic containers to collect media either with the container itself or with gloved hands. The upstream and downstream locations were selected by judgment and accessibility from the roadside. The control locations were selected at random within the bounds of where remote sensing stations were located.

Once returned to the lab, the samples were qualitatively analyzed for dominant soil composition and then measured using a Canberra GC2518 Standard Electrode Coaxial Ge Gamma detector.

Upstream Slope Sample:

γ線核種分析結果 20170807_upstraem_slope_samples

スペクトル

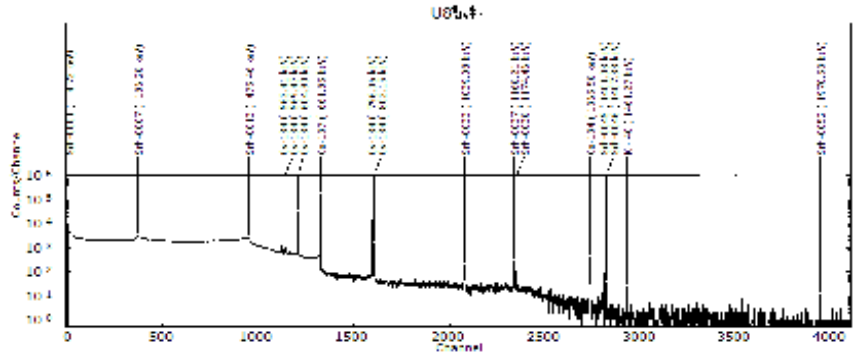

測定コード	測定コード	20170807_upstream_slope_samples	試料コード	20170807_UPSTRAEM_SLOPE_SAMPLES
試料情報	試料区分	U8汎用	地域	–
	試料種類	–	地点	–
	採取開始	2017年08月04日 15時00分	緯度・経度	
	採取終了	2017年08月04日 15時00分	試料コメント	2017/8/4 collected soil Fukushima, Ohkuma
	試料容器	U－8容器	目的	その他
	供試料量	2.26E-02 kg		
	回収率	100.00 %	母材	海底土, 土壌, 灰化物
	充填高さ	4.10 cm	元素組成式	
	密度	0.311 g/cm3	AMP比	0.00 %
測定情報	検出器番号	No. 1	測定位置	密着
	測定開始	2017年08月07日 12時04分	測定者	小豆川
	測定時間	LT 14681 秒 RT 14735 秒	測定コメント	U8試料
付加情報				
分析条件	核データ	食品主要	減衰補正	採取開始～採取終了、採取終了～測定開始、測
	BG補正	する(結果利用)	エネルギー校正	DET01_ENE_0710_20140325
	BG1:B120170501113747	BG2:	効率校正	DET01_EFF_U8_Group_20140327

No.	核種名	エネルギー (keV)	半減期	放射能濃度 (Bq/kg)	荷重平均放射能濃度 (Bq/kg)	検出限界値 (Bq/kg)	マーク
1	I -131	364.48	8.04E+00 D	N D		8.3614E+01	N
2	Cs-134	604.66	2.06E+00 Y	1.2648E+04 ± 4.8793E+01	1.2604E+04 ± 3.4697E+01	5.0372E+01	
3	Cs-137	661.64	3.02E+01 Y	9.3734E+04 ± 1.3635E+02	9.3734E+04 ± 1.3635E+02	4.3086E+01	
4	K - 40	1460.75	1.28E+09 Y	1.9926E+02 ± 3.4458E+01	1.9926E+02 ± 3.4458E+01	9.4947E+01	

20170807_upstraem_slope_samples.txt

マークについて A:注意ピーク L:2σ以上ロの未満) C:積算法で計算 X:レンジ外
積算法での複合処理 N:近接処理 D:分割処理 S:寄与差引 E:同一核種処理 W:和処理
減衰補正に関する注意 T:試料保存期間が半減期×64を超えた為、試料保存中の減衰補正をOFF

1 / 1

Upstream River Sample:

γ線核種分析結果 — Upstream_River_Sample

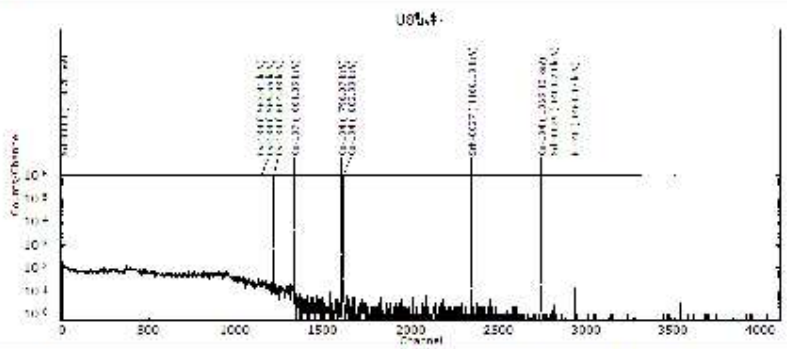

測定コード	測定コード	Upstream_River_Sample	試料コード	UPSTREAM_RIVER_SAMPLE
試料情報	試料区分	U8汎用	地域	-
	試料種類	-	地点	-
	採取開始	2017年08月04日 12時50分	緯度・経度	
	採取終了	2017年08月04日 12時50分	試料コメント	2017/8/4 collected soil Fukushima, Ohkuma
	試料容器	U－8容器	目的	その他
	供試料量	1.54E-01 kg		
	回収率	100.00 %	母材	海底土、土壌、灰化物
	充填高さ	3.15 cm	元素組成式	
	密度	2.754 g/cm3	AMP比	0.00 %
測定情報	検出器番号	No. 1	測定位置	密着
	測定開始	2017年08月07日 16時14分	測定者	小豆川
	測定時間	LT 735 秒 RT 737 秒	測定コメント	U8試料
付加情報				
分析条件	核データ	食品主要	減衰補正	採取開始～採取終了、採取終了～測定開始、測
	BG補正	する(結果利用)	エネルギー校正	DET01_ENE_0710_20140325
	BG1:B120170501113747	BG2:	効率校正	DET01_EFF_U8_Group_20140327

No.	核種名	エネルギー (keV)	半減期	放射能濃度 (Bq/kg)	荷重平均放射能濃度 (Bq/kg)	検出限界値 (Bq/kg)	マーク
1	I -131	364.48	8.04E+00 D	N D		4.7821E+01	
2	Cs-134	604.66	2.06E+00 Y	8.6913E+02 ± 2.3128E+01	8.4903E+02 ± 1.6223E+01	2.7787E+01	
3	Cs-137	661.64	3.02E+01 Y	6.6675E+03 ± 6.4630E+01	6.6675E+03 ± 6.4630E+01	2.5694E+01	
4	K - 40	1460.75	1.28E+09 Y	4.9519E+02 ± 7.3254E+01	4.9519E+02 ± 7.3254E+01	1.1700E+02	

Upstream_River_Sample マークについて A:注意ピーク L:2σ以上(3σ未満) C:積算法で計算 X:レンジ外 1 / 1
積算法での複合処理 N:近接処理 D:分割処理 S:等号無引 E:同一核種処理 W:和処理
減衰補正に関する注意 T:試料保存期間が半減期×6を超えた為、試料保存中の減衰補正をOFF

Downstream Slope Sample:

γ線核種分析結果 Downstream_Slope_Sample

スペクトル

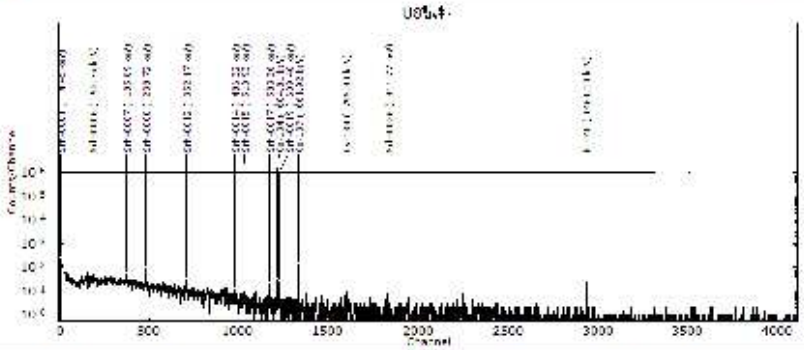

測定コード	測定コード	Downstream_Slope_Sample		試料コード	DOWNSTREAM_SLOPE_SAMPLE
試料情報	試料区分	U8汎用		地域	-
	試料種類	-		地点	-
	採取開始	2017年08月04日 13時35分		緯度・経度	
	採取終了	2017年08月04日 13時35分		試料コメント	2017/8/4 collected soil Fukushima, Ohkuma
	試料容器	U－8容器		目的	その他
	供試料量	7.84E-02 kg			
	回収率	100.00 %		母材	海底土、土壌、灰化物
	充填高さ	4.95 cm		元素組成式	
	密度	0.894 g/cm3		AMP比	0.00 %
測定情報	検出器番号	No. 1		測定位置	密着
	測定開始	2017年08月07日 16時29分		測定者	小豆川
	測定時間	LT 5377 秒 RT 5382 秒		測定コメント	U8試料
付加情報					
分析条件	核データ	食品主要		減衰補正	採取開始～採取終了、採取終了～測定開始、測
	BG補正	する(結果利用)		エネルギー校正	DET01_ENE_0710_20140325
	BG1:B120170501113747	BG2:		効率校正	DET01_EFF_U8_Group_20140327

No.	核種名	エネルギー (keV)	半減期	放射能濃度 (Bq/kg)	荷重平均放射能濃度 (Bq/kg)	検出限界値 (Bq/kg)	マーク
1	I -131	364.48	8.04E+00 D	ND		6.2186E+00	
2	Cs-134	604.66	2.06E+00 Y	9.7011E+00 ± 1.4430E+00	8.8092E+00 ± 1.1535E+00	4.2419E+00	
3	Cs-137	661.64	3.02E+01 Y	6.6675E+01 ± 3.7630E+00	6.6675E+01 ± 3.7630E+00	4.6445E+00	
4	K - 40	1460.75	1.28E+09 Y	2.1796E+02 ± 3.0287E+01	2.1796E+02 ± 3.0287E+01	6.4078E+01	C

Downstream_Slope_Sampleマークについて A:注意ピーク L:2σ以上D<σ未満) C:積算法で計算 X:レンジ外 1 / 1
積算法での複合処理 N:近接処理 D:分割処理 S:寄与差引 E:同一核種処理 W:和処理
減衰補正に関する注意 T:試料保存期間が半減期×6を超えた為、試料保存中の減衰補正をOFF

Downstream River Sample:

γ線核種分析結果 Downstream_River_Sample

スペクトル

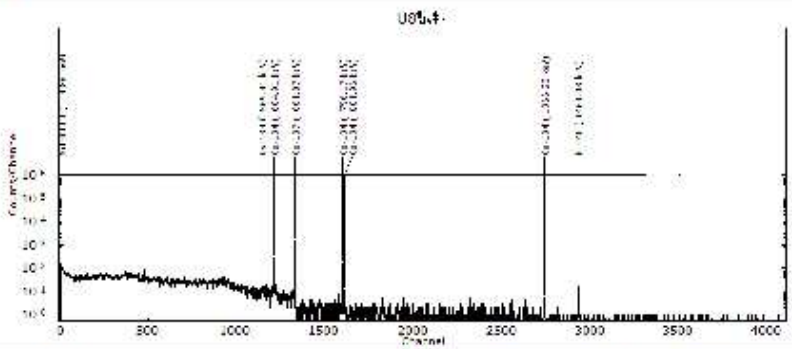

測定コード	測定コード	Downstream_River_Sample		試料コード	DOWNSTREAM_RIVER_SAMPLE
試料情報	試料区分	U8汎用		地域	-
	試料種類	-		地点	-
	採取開始	2017年08月04日 13時30分		緯度・経度	
	採取終了	2017年08月04日 13時30分		試料コメント	2017/8/4 collected soil Fukushima, Ohkuma
	試料容器	U－8容器		目的	その他
	供試料量	1.86E-01 kg			
	回収率	100.00 %		他材	海底土、土壌、灰化物
	充填高さ	4.88 cm		元素組成式	
	密度	2.156 g/cm3		AMP比	0.00 %
測定情報	検出器番号	No. 1		測定位置	密着
	測定開始	2017年08月07日 18時02分		測定者	小豆川
	測定時間	LT 2126 秒 RT 2128 秒		測定コメント	U8試料
付加情報					
分析条件	核データ	食品主要		減衰補正	採取開始～採取終了、採取終了～測定開始、測
	BG補正	する(結果利用)		エネルギー校正	DET01_ENE_0710_20140325
	BG1:B120170501113747	BG2:		効率校正	DET01_EFF_U8_Group_20140327

No.	核種名	エネルギー (keV)	半減期	放射能濃度 (Bq/kg)	荷重平均放射能濃度 (Bq/kg)	検出限界値 (Bq/kg)	マーク
1	I -131	364.48	8.04E+00 D	N D		1.2837E+01	
2	Cs-134	604.66	2.06E+00 Y	1.3197E+02 ± 5.6005E+00	1.2664E+02 ± 4.0244E+00	8.2115E+00	
3	Cs-137	661.64	3.02E+01 Y	9.9027E+02 ± 1.5164E+01	9.9027E+02 ± 1.5164E+01	7.0032E+00	
4	K - 40	1460.75	1.28E+09 Y	2.4684E+02 ± 3.2181E+01	2.4684E+02 ± 3.2181E+01	4.9561E+01	

Downstream_River_Sampleマークについて A:注意ピーク L:2σ以上3σ未満 C:複算法で計算 X:レンジ外
複算法での複合処理 N:近接処理 D:分割処理 S:寄与差引 E:同一放種処理 W:和処理
減衰補正に関する注意 T:試料保存期間が半減期×64を超えた為、試料保存中の減衰補正をOFF

1 / 1

Kuma River Slope Sample:

γ線核種分析結果 Kuma_Slope_Sample

スペクトル

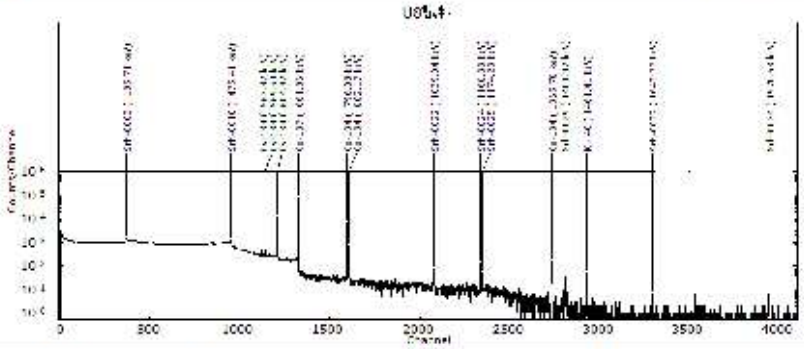

測定コード	測定コード	Kuma_Slope_Sample		試料コード	KUMA_SLOPE_SAMPLE
試料情報	試料区分	U8汎用		地域	-
	試料種類	-		地点	-
	採取開始	2017年08月04日 14時10分		緯度・経度	
	採取終了	2017年08月04日 14時10分		試料コメント	2017/8/4 collected soil Fukushima, Ohkuma
	試料容器	U－8容器		目的	その他
	供試料量	5.18E-02 kg			
	回収率	100.00 %		母材	海底土, 土壌, 灰化物
	充填高さ	2.73 cm		元素組成式	
	密度	1.071 g/cm3		AMP比	0.00 %
測定情報	検出器番号	No. 1		測定位置	密着
	測定開始	2017年08月07日 18時40分		測定者	小豆川
	測定時間	LT 6980 秒 RT 7003 秒		測定コメント	U8試料
付加情報					
分析条件	核データ	食品主要		減衰補正	採取開始～採取終了、採取終了～測定開始、測
	BG補正	する(結果利用)		エネルギー校正	DET01_ENE_0710_20140325
	BG1:B120170501113747	BG2:		効率校正	DET01_EFF_U8_Group_20140327

No.	核種名	エネルギー (keV)	半減期	放射能濃度 (Bq/kg)	荷重平均放射能濃度 (Bq/kg)	検出限界値 (Bq/kg)	マーク
1	I -131	364.48	8.04E+00 D	N D		4.4466E+01	
2	Cs-134	604.66	2.06E+00 Y	4.0151E+03 ± 2.4702E+01	4.0059E+03 ± 1.7576E+01	2.7197E+01	
3	Cs-137	661.64	3.02E+01 Y	3.0291E+04 ± 6.8720E+01	3.0291E+04 ± 6.8720E+01	2.2948E+01	
4	K - 40	1460.75	1.28E+09 Y	3.9062E+02 ± 3.3751E+01	3.9062E+02 ± 3.3751E+01	5.9474E+01	

Kuma_Slope_Sample マークについて A:注意ピーク L:2σ以上Oの未満) C:積算法で計算 X:レンジ外 1 / 1
積算法での複合処理 N:近接処理 D:分割処理 S:寄与差引 E:同一核種処理 W:和処理
減衰補正に関する注意 T:試料保存期間が半減期×6Hを超えた為、試料保存中の減衰補正をOFF

Kuma River Sediment Sample:

γ線核種分析結果 Kuma_River_sample

スペクトル

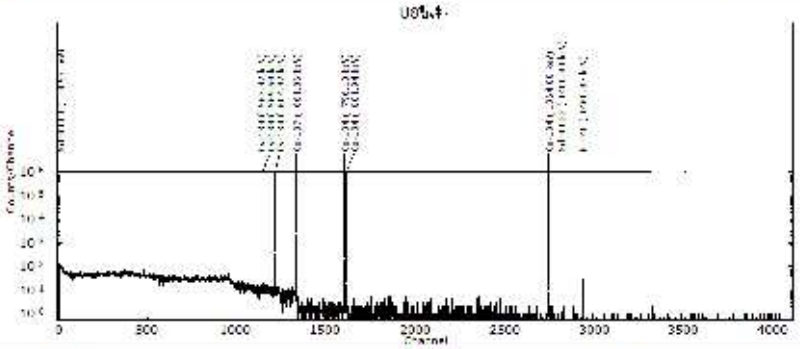

測定コード	測定コード	Kuma_River_sample	試料コード	KUMA_RIVER_SAMPLE	
試料情報	試料区分	U8汎用	地域	-	
	試料種類	-	地点	-	
	採取開始	2017年08月04日 14時07分	緯度・経度		
	採取終了	2017年08月04日 14時07分	試料コメント	2017/8/4 collected soil Fukushima, Ohkuma	
	試料容器	U－8容器	目的	その他	
	供試料量	1.71E-01 kg			
	回収率	100.00 %	母材	海底土, 土壌, 灰化物	
	充填高さ	4.66 cm	元素組成式		
	密度	2.073 g/cm3	AMP比	0.00 %	
測定情報	検出器番号	No. 1	測定位置	密着	
	測定開始	2017年08月07日 20時38分	測定者	小豆川	
	測定時間	LT 1380 秒 RT 1381 秒	測定コメント	U8試料	
付加情報					
分析条件	核データ	食品主要	減衰補正	採取開始～採取終了、採取終了～測定開始、測	
	BG補正	する(結果利用)	エネルギー校正	DET01_ENE_0710_20140325	
	BG1:B120170501113747	BG2:	効率校正	DET01_EFF_U8_Group_20140327	

No.	核種名	エネルギー (keV)	半減期	放射能濃度 (Bq/kg)	荷重平均放射能濃度 (Bq/kg)	検出限界値 (Bq/kg)	マーク
1	I -131	364.48	8.04E+00 D	N D		2.1115E+01	
2	Cs-134	604.66	2.06E+00 Y	2.5307E+02 ± 9.7977E+00	2.5697E+02 ± 6.9796E+00	1.3766E+01	
3	Cs-137	661.64	3.02E+01 Y	2.0844E+03 ± 2.7910E+01	2.0844E+03 ± 2.7910E+01	1.2357E+01	
4	K - 40	1460.75	1.28E+09 Y	6.5335E+02 ± 6.3581E+01	6.5335E+02 ± 6.3581E+01	7.5442E+01	

Kuma_River_sample マークについて A:注意ピーク L:2σ以上0σ未満) C:積算法で計算 X:レンジ外 1 / 1
積算法での複合処理 N:近接処理 D:分割処理 S:寄与重引 E:同一核種処理 W:和処理
減衰補正に関する注意 T:試料保存期間が半減期×6を超えた為、試料保存中の減衰補正をOFF

Control Soil Sample:

γ線核種分析結果 — Non_river glass sample

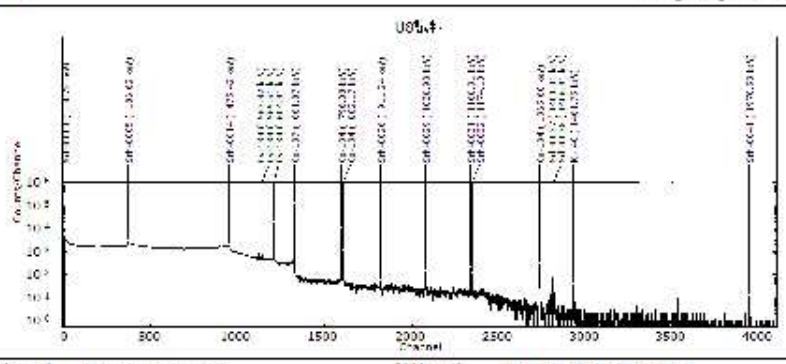

測定コード	測定コード	Non_river glass sample		試料コード	NON_RIVER GLASS SAMPLE
試料情報	試料区分	U8汎用		地域	-
	試料種類	-		地点	-
	採取開始	2017年08月04日 14時57分		緯度・経度	
	採取終了	2017年08月04日 14時57分		試料コメント	2017/8/4 collected soil Fukushima, Ohkuma
	試料容器	U－8容器		目的	その他
	供試料量	5.66E-02 kg			
	回収率	100.00 %		母材	海底土，土壌，灰化物
	充填高さ	3.18 cm		元素組成式	
	密度	1.005 g/cm3		AMP比	0.00 %
測定情報	検出器番号	No. 1		測定位置	密着
	測定開始	2017年08月07日 21時03分		測定者	小豆川
	測定時間	LT 7315 秒 RT 7350 秒		測定コメント	U8試料
付加情報					
分析条件	核データ	食品主要		減衰補正	採取開始～採取終了，採取終了～測定開始，測
	BG補正	する(結果利用)		エネルギー校正	DET01_ENE_0710_20140325
	BG1:B120170501113747	BG2:		効率校正	DET01_EFF_U8_Group_20140327

No.	核種名	エネルギー (keV)	半減期	放射能濃度 (Bq/kg)	荷重平均放射能濃度 (Bq/kg)	検出限界値 (Bq/kg)	マーク
1	I -131	364.48	8.04E+00 D	N D		5.5178E+01	
2	Cs-134	604.66	2.06E+00 Y	6.4009E+03 ± 3.0195E+01	6.3618E+03 ± 2.1433E+01	3.3336E+01	
3	Cs-137	661.64	3.02E+01 Y	4.8189E+04 ± 8.4209E+01	4.8189E+04 ± 8.4209E+01	2.7832E+01	
4	K - 40	1460.75	1.28E+09 Y	2.1898E+02 ± 2.6577E+01	2.1898E+02 ± 2.6577E+01	6.0880E+01	

Non_river glass sample　マークについて A:注意ピーク L:3σ以上(3σ未満) C:積算法で計算 X:レンジ外　1 / 1

積算法での複合処理 N:近接処理 D:分割処理 S:等ヶ重引 E:同一核種処理 W:和処理

減衰補正に関する注意 T:試料保存期間が半減期×64を超えた為、試料保存中の減衰補正をOFF